THERMOCHRONOLOGY OF EARLY JURASSIC EXHUMATION OF THE YUKON-TANANA TERRANE, WEST-CENTRAL YUKON

by

ELEANOR KNIGHT

B. Sc., Simon Fraser University – Vancouver, British Columbia, 2005

A THESIS SUBMITTED IN PARTIAL FULFILMENT OF THE REQUIREMENT FOR THE DEGREE OF

MASTER OF SCIENCE

in

THE FACULTY OF GRADUATE STUDIES

Department of Earth Sciences

We accept this thesis as conforming to the required standard

THE UNIVERSITY OF OTTAWA

June 2012

Thermochronology of Early Jurassic exhumation of the Yukon-Tanana terrane, west-central Yukon

E. Knight
Department of Earth Sciences, University of Ottawa, Ottawa, K1N 6N5 Canada

ABSTRACT

This study utilised U-Pb geochronology, and $^{40}Ar/^{39}Ar$ and (U-Th)/He thermochronology to delineate arc magmatism, metamorphism, and exhumation of the pericratonic Yukon-Tanana terrane in the McQuesten map area of west-central Yukon, Canada. SHRIMP U-Pb ages delineate Mid to Late Paleozoic arc magmatism and fit key units into the regional lithotectonic framework of the terrane. The juxtaposition of unmetamorphosed and predominantly undeformed Devono-Mississippian rocks in the northwest of the study area with polydeformed and up to amphibolite facies metamorphosed rocks in the southwest suggests a crustal-scale discontinuity, the Willow Lake fault, bounds the two domains. The asymmetric distribution of $^{40}Ar/^{39}Ar$ ages across the fault suggest it is extensional, and was active in the Early Jurassic. Zircon (U-Th)/He ages delineate erosion of rocks in the northwest through the upper crust during the Late Triassic and Late Jurassic to Early Cretaceous followed by Middle Cretaceous erosion of the southwestern domain and possibly fault reactivation.

Keywords: Cordillera, Yukon-Tanana terrane, geochronology, thermochronology, Jurassic, exhumation, extension

Word count (without references): 12,695
Word count (references): 16,005
Tables: 2
Figures: 10
Appendices: Petrology, methods and data repository (4 data tables)

TABLE OF CONTENTS

LIST OF TABLES

LIST OF FIGURES

ACKNOWLEDGMENTS

This has been a fruitful and immensely rewarding journey filled with many highs and some lows. I have many people to thank for getting me through to the end. This project was kindly funded by the Geological Survey of Canada under the auspices of the Geomapping for Energy and Minerals – Multiple Metals Northwest Canadian Cordillera program, and included a bursary through the Research Affiliate Program. I would also like to thank the Yukon Geological Survey for employing me during fieldwork in the summer of 2009.

I have many colleagues to thank at the Geological Survey of Canada for their leadership and technical support. Ron Christie, Ray Chung, and Greg Case guided me through sample preparation and ensured I obtained the highest quality mineral separates. I would like to thank Pat Hunt in the SEM lab for imaging my wonky zircon mounts, and for accommodating my last-minute requests. Thanks to Stephen Williams for guiding me through my frantic GIS issues. Bill Davis, Nicole Rayner and Tom Pestaj are thanked immensely for their assistance in the SHRIMP lab at the GSC, and never-ending patience and willingness to answer a barrage of questions. Simon Jackson, Arthur Wong, and John Chapman are thanked for their assistance with LA-ICP-MS analytical work and data processing. Very special thanks go to Mike Villeneuve, Nancy Joyce, and Dawn Kellett for educating me in the complex world of argon. Mike has supported me and stood by me through good times and bad, and I am eternally grateful for his mentorship. Nancy has been both a great friend and teacher, and I truly couldn't have gotten to where I am today without her guidance and unfaltering patience. My deepest gratitude is extended to Jim Ryan for his willingness to be a last-minute addition to my supervisory committee. Jim's eagerness to answer the phone led to many insightful and thought-provoking geological discussions, all of which have helped to greatly improve the caliber of this thesis.

I would also very much like to thank Isabelle Coutand, Keith Taylor, and Kyle Landry for leading me through zircon picking and helium extraction at Dalhousie University. Matt Heizler is thanked for overseeing efficient and timely data collection of my samples at the New Mexico Institute of Mining and Technology.

I have a huge amount of friends all across the country to thank for their contribution to this journey, too may to name, but in particular I would like to thank Mélanie Mercier, Danielle Thomson, and Thomas Mumford for offering me the grad-student advice I so desperately needed. Reid Staples at Simon Fraser University also provided stimulating geological discussions and ideas, and I wish him the very best of luck completing his Ph. D.. I'm a better person for having Ween in my life; they inspired many great trips during my time out east, kept me entertained during intense writing sessions, and always help me remember my place in the universe. I'll miss you guys, thanks for all the good times. My wonderful and caring parents, brothers, and extended family are thanked for their love, support and encouragement. Mum and Dad, remember when I didn't want to go to university at all? Multiple family visits to Ottawa kept my spirits high, and provided me with fond and amazing memories to last a lifetime.

Penultimately, my sincerest gratitude goes to my supervisor, David Schneider at the University of Ottawa, for pushing me in all the right directions, despite my resistance, and for continued support through geological and analytical discussions, beers, eagerness to laugh, and mutual admiration for all things Star Wars.

Last but most certainly not least, I would like to thank my partner, Jeff Auston, for his relentless support, patience, and love and insightful geological discussions. He made this journey so much more fun and bearable, and I am indebted to him for being my rock and moving 4500 km across the country to be with me.

INTRODUCTION

The northern Canadian Cordillera is composed of a series of parautochthonous to allochthonous terranes that were episodically accreted to the western margin of North America between the Late Paleozoic to Cenozoic (Monger et al., 1972; Coney et al., 1980). The Yukon-Tanana terrane is a pericratonic terrane which has been thrust over miogeoclinal rocks of the ancestral continent, and underlies a widespread region of central Yukon, eastern Alaska, and northwestern British Columbia (**Fig. 1**). The terrane is comprised of Mid to Late Paleozoic polydeformed and metamorphosed igneous and sedimentary rocks and is considered pericratonic due to provenance and isotopic linkages with North America (Mortensen, 1992; Colpron et al., 2006*a*).

The McQuesten area of this study straddles the Klondike Plateau and Willow Lowland physiographic regions of west-central Yukon, and is underlain predominantly by Mid to Late Paleozoic rocks of the Yukon-Tanana terrane, with a lesser component of Mesozoic to recent igneous rocks. The domain of Yukon-Tanana terrane rocks in the study area is divided into a northern belt of little-deformed and unmetamorphosed plutonic and volcanic rocks termed the Reid Lakes complex (Colpron and Ryan, 2010; Ryan et al., 2010). This belt is juxtaposed against a central belt of more typical polydeformed Yukon-Tanana terrane rocks that are metamorphosed to a maximum of amphibolite facies. The discordance of metamorphism and deformation between the two domains indicates they are fault bounded. Through the regional mapping of the McQuesten area, the Willow Lake fault was delineated (Ryan et al., 2010), and interpreted as an extensional structure (Colpron and Ryan, 2010).

Exhumation of mid-crustal rocks is thought to be accommodated by three processes: normal faulting, erosion, and ductile thinning (e.g. Ring et al., 1999). Normal faulting and erosion are the dominant mechanisms and operate at the fastest rates; ductile thinning con-

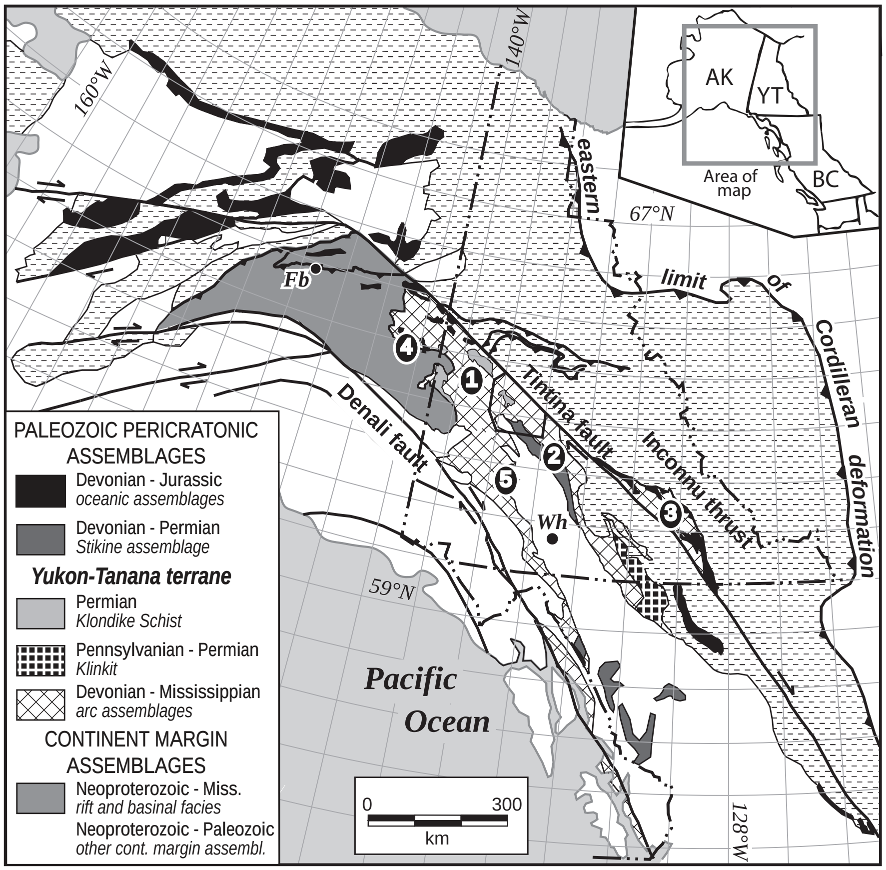

Figure 1. Generalised map of the northern Cordillera showing the distribution of Paleozoic arc and oceanic assemblages (modified from Wheeler and McFeely, 1991; Siberling et al., 1992; Foster et al., 1994; Murphy et al., 2006; and Colpron et al., 2006a). Study area is outlined in black. Areas mentioned in the text and shown as black ellipses are: 1-Stewart River; 2-Glenlyon; 3-Finlayson; 4-Yukon-Tanana Upland; 5-Aishihik batholith. Location names shown in italics: Fb-Fairbanks; Wh-Whitehorse.

tributes to uplift only in conjunction with other exhumation processes, and at a much slower rate. Crustal-scale extensional faults in continental collision zones typically juxtapose medium to high-grade metamorphosed and penetratively deformed footwall rocks from middle to lower crustal depths with predominantly lesser metamorphosed hanging-wall rocks from shallow levels (Davis and Coney, 1979; Lister and Davis, 1989; Ring et al., 1999; Rosenbaum et al., 2005; Stockli, 2005). Moreover, tectonic exhumation is characterised by rapid cooling and an asymmetric distribution of cooling ages across a structural discontinuity (e.g. Wheeler and Butler, 1994; Ring et al., 1999). In regimes dominated by low-angle normal faults, cooling ages are markedly younger in footwall rocks, which have been exhumed through their respective thermochronometer closure temperature after structurally higher rocks in the hanging-wall (Ring et al., 1999; Stockli, 2005).

The purpose of this investigation is to resolve the tectonic history of these two apparently disparate domains by conducting strategic and comprehensive geochronology and thermochronology across this purported crustal-scale structure, and define its role in the development of the Yukon-Tanana terrane in the northern Canadian Cordillera. In this paper zircon U-Pb, hornblende and mica $^{40}Ar/^{39}Ar$ and zircon (U-Th)/He ages are presented to elucidate the tectonothermal history of the Yukon-Tanana terrane in the McQuesten area of central Yukon. Rolling topography and a lack of good bedrock exposure through thick forest and colluvium cover hinder the observation of geological field relationships in the region. Utilising geo- and thermochronology is therefore a critical aid in deciphering complex tectonic relationships. Despite a paucity of rock exposure, the results of this study define a unique evolution of the Yukon-Tanana terrane: Mid to Late Paleozoic arc magmatism and metamorphism and subsequent exhumation associated with syn- to post-collisional Jurassic extensional orogenic collapse.

PREVIOUS AND ONGOING WORK

The McQuesten map area was mapped in 2009 as part of a large-scale reconnaissance bedrock geology project to further our understanding of the mineral endowment of the area and tectonic evolution of terrane accretion in the northern Cordillera (Colpron and Ryan, 2010; Ryan et al., 2010). The mapping project, of which this study is a component, was conducted as part of the Geomapping for Energy and Minerals (GEM) program of the Geological Survey of Canada in collaboration with the Yukon Geological Survey. Prior to that project, the area had not been mapped since the 1940s (Bostock, 1964). Other studies in the area conducted under the GEM program include a Ph. D. study examining the pressure, temperature, and metamorphic evolution of the Yukon-Tanana terrane (Staples, 2012, in preparation), and an investigation into the Late Cretaceous tectonics and metallogeny of west-central Yukon and east-central Alaska (Ciolkiewicz, in prep). A previous study in the center of the McQuesten area focused on the tectonic setting of ultramafic rocks underlying the White Mountains (**Fig. 2**; Erdmer, 1982).

TECTONIC SETTING

Regional Geology

Phanerozoic parautochthonous and allochthonous terranes of various geodynamic environments accreted onto the margin of ancestral North America since the Mesozoic constitute the Canadian Cordillera (Monger et al., 1972). The Mid to Late Paleozoic pericratonic Yukon-Tanana terrane is exposed in eastern Alaska, southwest Yukon Territory, and northern British Columbia (**Fig. 1**). In Yukon, northwestern Canada, the Yukon-Tanana terrane consists of a series of variably metamorphosed and deformed arc, back-arc and continental margin assemblages and associated basinal rocks classified by four assemblages: the Snowcap,

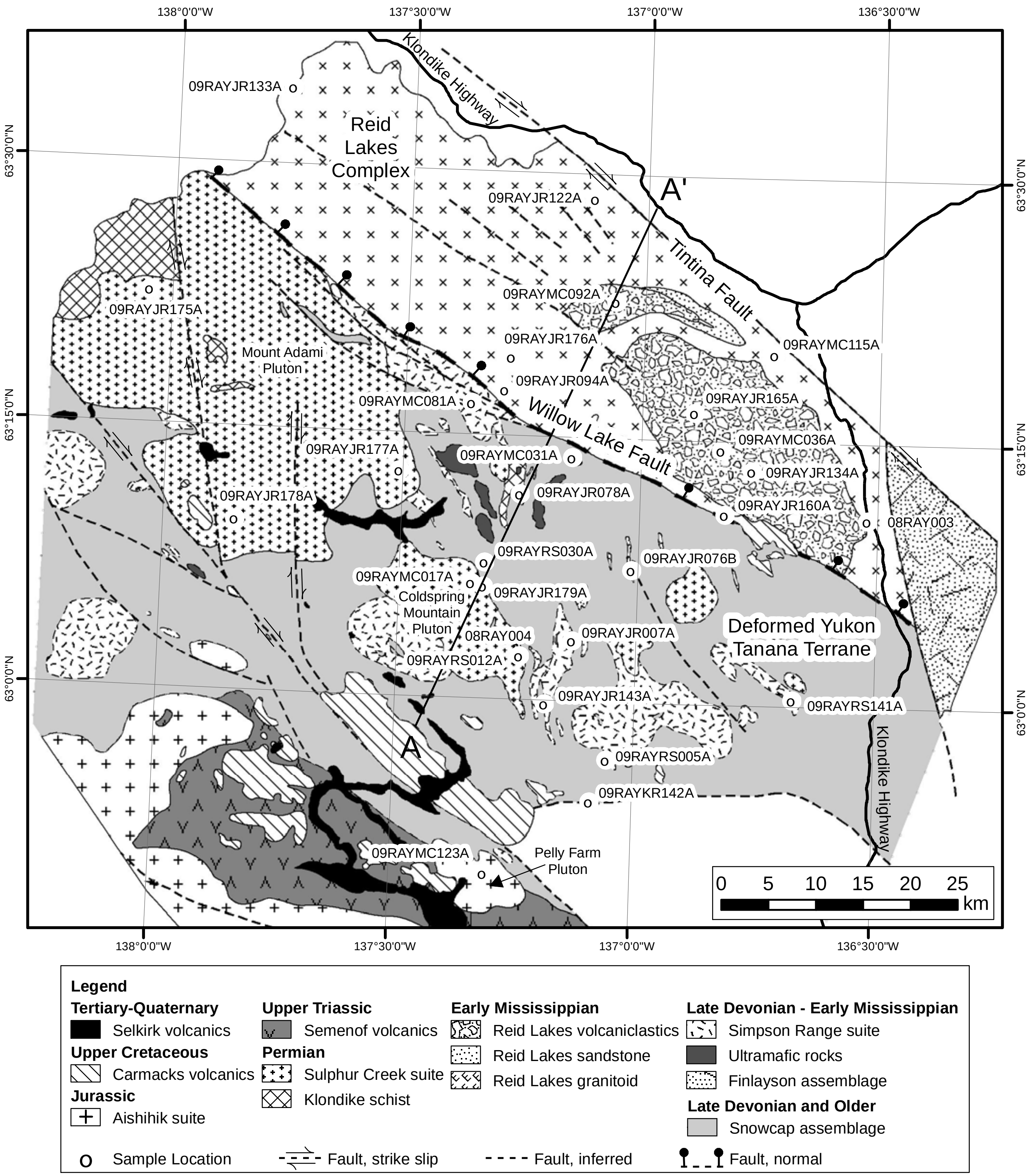

Figure 2. Bedrock geology of the McQuesten map area (modified from Ryan et al., 2010) showing location of samples investigated in this study. Position of cross-section (Figure 7) shown by line A-A′.

Finlayson, Klinkit, and Klondike (Mortensen, 1992; Colpron et al., 2006*a*; Nelson et al., 2006; Colpron et al., 2007). The Snowcap assemblage is comprised of polydeformed siliciclastic rocks derived from a continental margin setting, metamorphosed under greenschist to amphibolite facies conditions, and is interpreted as the pre-Late Devonian basement to the Yukon-Tanana terrane. The overlying Finlayson assemblage is Late Devonian to Early Mississippian in age, and consists of metavolcanic and metasedimentary rocks of a continental arc and back-arc setting. Coeval granitic rocks of the Simpson Range suite intrude both the Snowcap and Finlayson assemblages. The Klinkit assemblage unconformably overlies the Finlayson, and is comprised of limestones and intermediate to mafic volcanic and volcaniclastic rocks deposited in a Middle Mississippian to Early Permian island arc setting. A felsic volcanic package derived from a Middle to Late Permian continental arc constitutes the Klondike assemblage. The coeval Sulphur Creek orthogneiss suite is likely the granitic plumbing system to the Klondike arc (Colpron et al., 2006*a*). Late Devonian to Permian marginal basin and oceanic rocks of the Slide Mountain assemblage were deposited in a back-arc to the Yukon-Tanana arc system outboard of the North American margin (Colpron et al., 2006*a*).

Six magmatic cycles with distinct geochemical and isotopic signatures are defined for the Mid to Late Paleozoic duration of arc and back-arc activity of the Yukon-Tanana terrane. Cycle 1, the Ecstall, spanned ca. 390-365 Ma, corresponding to incipient arc magmatism. Rocks of the Finlayson assemblage were formed during the second and third Finlayson and Wolverine cycles, spanning 365-357 Ma and 357-342 Ma, respectively. The fourth cycle, Little Salmon, from 342-314 Ma and the fifth cycle, Klinkit, from 314-269 Ma represent magmatism associated with the Klinkit assemblage. The final period of Yukon-Tanana arc magmatism is the Klondike cycle, spanning 269-253 Ma. Magmatism due to rifting of the

Slide Mountain Ocean is thought to have occurred throughout the Finlayson to Klinkit cycle (Colpron et al., 2006*a*; Nelson et al., 2006; Piercey et al., 2006).

As the west-facing Devono-Mississippian Yukon-Tanana arc rifted away from North America, the Slide Mountain Ocean progressively widened (Colpron et al., 2006*a*; Murphy et al., 2006). In the Middle Permian, the polarity of subduction reversed, leading to consumption of Slide Mountain oceanic lithosphere in a westward dipping subduction zone, overridden by the Yukon-Tanana arc (Nelson et al., 2006; Berman et al., 2007; Beranek and Mortensen, 2011). It is a generally accepted model that Early Mesozoic contraction in the northern Cordillera accompanied Late Triassic to Jurassic accretion of the Yukon-Tanana terrane to the North American miogeocline via the post Late Triassic Inconnu thrust fault in the Finlayson region (**Fig. 1**; Murphy et al., 2002; Murphy et al., 2006) and other equivalent thrust faults throughout the Yukon and northern BC (Nelson et al., 2006). New evidence by Beranek and Mortensen (2011), however, suggests the Yukon-Tanana arc was shedding detritus onto ancestral North America ca. 251 to 235 Ma, leading them to conclude that Latest Permian arc-continent collision had occurred prior to deposition of ca. 235-200 Ma assemblages that overlap both the Yukon-Tanana terrane and North American strata.

Late Triassic and Early Jurassic igneous and sedimentary rocks of the Quesnellia and Stikinia arcs intrude and overlap the Yukon-Tanana terrane (Mortensen, 1992; Nelson and Friedman, 2004; Colpron et al., 2007). Although once thought to be independent, exotic terranes, increasing evidence suggests the Yukon-Tanana terrane may serve as the basement onto which they were built (Simard et al., 2003; Nelson and Friedman, 2004; Nelson et al., 2006; Roots et al., 2006). In the northern Cordillera, the Late Triassic to Early Jurassic Aishihik suite is likely related to subduction-related arc magmatism of Quesnellia (Johnston et al., 1996).

A complex history of five phases of metamorphism and three phases of deformation were identified in a detailed geothermobarometry study of the Yukon-Tanana terrane in the Stewart River area to the west of the study area (**Fig. 1**; Berman et al., 2007). The first phase of low-pressure metamorphism occurred ca. 365-350 Ma, as determined by metamorphic growth of titanite in an amphibolite facies calc-silicate schist associated with the Finlayson assemblage. The second event, ca. 260-239 Ma, occurred under high-pressure conditions of ca. 9 kbar and 600 ^{o}C. An Early Jurassic metamorphic event occurred ca. 195-187 Ma, with peak conditions reaching 7.8 kbar and 600 ^{o}C. Two subsequent localised contact metamorphic events are constrained at ca. 146 and 114 to 107 Ma (Berman et al., 2007).

In the northern Cordillera, Jurassic and Cretaceous ^{40}Ar/^{39}Ar ages dominate the cooling history of the Yukon-Tanana terrane, and are generally interpreted as the result of regional uplift and exhumation following accretion of the Yukon-Tanana terrane to North America (Hansen et al., 1991; Dusel-Bacon et al., 1995; Johnston et al., 1996; Villeneuve et al., 2003; Dusel-Bacon et al., 2006; Berman et al., 2007). A suite of Early Jurassic mica ^{40}Ar/^{39}Ar ages from the Glenlyon area (**Fig. 1**) are thought to constrain the timing of ductile deformation related to thrust imbrication of the Yukon-Tanana and Slide Mountain terranes (Oliver, 1996; Colpron et al., 2005). A large dataset of ca. 188-186 Ma hornblende, muscovite, and biotite ^{40}Ar/^{39}Ar ages from Finlayson-age rocks of the outboard Fortymile River assemblage in the Yukon-Tanana upland in eastern Alaska (**Fig. 1**) are interpreted as widespread Early Jurassic metamorphic cooling related to obduction of these rocks onto parautochthonous continental-margin rocks of the Lake George assemblage (Hansen et al., 1991; Dusel-Bacon et al., 2002). Middle Cretaceous ^{40}Ar/^{39}Ar ages ca. 135-108 Ma from the Lake George assemblage are interpreted as the result of exhumation of these structurally deeper rocks (Hansen et al., 1991; Dusel-Bacon et al., 1995; Hansen and Dusel-Bacon, 1998; Dusel-Bacon et al., 2002; Dusel-

Bacon et al., 2006).

Up to 430 km of Eocene dextral displacement on the Tintina fault bisects the Yukon-Tanana terrane in the northern Cordillera (Snyder et al., 2005; Gabrielse et al., 2006). Restoration of fault displacement aligns Yukon-Tanana rocks north of the Tintina fault from the Finlayson Lake area in southeastern Yukon (**Fig. 1**) with the main Yukon-Tanana belt south of the fault that outcrops in west-central Yukon and east-central Alaska (Murphy et al., 2006).

Geology of the McQuesten Area

The geology of the McQuesten area is divided into three northwest-southeast trending belts: an unmetamorphosed and predominantly undeformed northern belt of Devono-Mississippian plutonic and volcanogenic rocks; a central belt of Mid to Late Paleozoic polydeformed and metamorphosed rocks typical of the Yukon-Tanana terrane; and a southern belt primarily underlain by Mesozoic igneous rocks (**Fig. 2**). All four arc assemblages of the Yukon-Tanana terrane are represented in the McQuesten map area. Thin-section and petrographic descriptions of rock samples investigated in this study are presented in **Appendix 1**.

In the central belt of the study area, rocks of the Yukon-Tanana terrane are polydeformed and metamorphosed to greenschist and amphibolite facies. Outcrops of quartzite, quartz-mica ± garnet schist, marble, greenstone and garnet-bearing amphibolite are designated as part of the Snowcap assemblage. These rocks are characterised by at least two phases of isoclinal folding and associated transposition foliations (**Fig. 3A**; Colpron and Ryan, 2010). The Snowcap assemblage is intruded by both the Devono-Mississippian Simpson Range and Mid-Permian Sulphur Creek plutonic suites. The Simpson Range suite in the study area is typically monzogranite to diorite in composition, and moderately to strongly

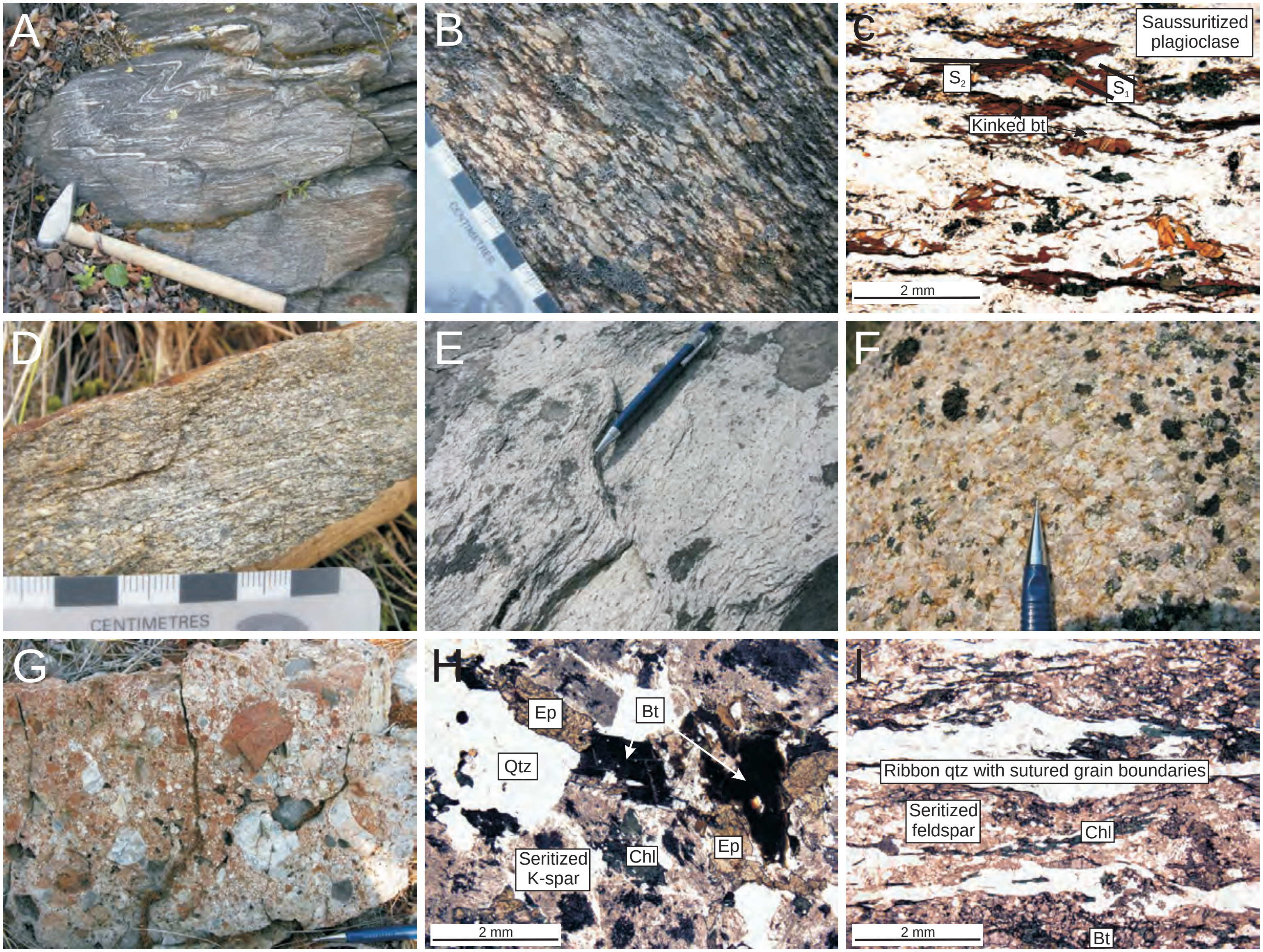

Figure 3. Representative lithologies in the McQuesten map area. (A) Psammitic schist of the Snowcap assemblage showing tight to isoclinal folds. Hammer approximately 50 cm. (B) Strongly foliated granodiorite of the Simpson Range suite. (C) Photomicrograph of granodiorite protolith of the Simpson Range suite. (D) Strong foliation in granodiorite of the Sulphur Creek suite showing characteristic k-feldspar augens. (E) Highly fissile metarhyodacite of the Klinkit assemblage. (F) Typical monzogranite of the Reid Lakes complex showing k-feldspar phenocrysts and smoky grey quartz. (G) Polymict volcaniclastic breccia of the Reid Lakes complex. Pencil used for scale is approximately 14 cm long. (H) Photomicrograph of monzogranite of the Aishihik suite, showing altered feldspar, minor chlorite after biotite, and magmatic epidote. (I) Photomicrograph of highly strained component of the Reid Lakes complex. Note the high degree of strain relative to the Simpson Range sample. Abbreviations used in photomicrographs: Bt-biotite; chl-chlorite; ep-epidote; qtz-quartz.

foliated (**Fig. 3B** and **3C**; Colpron and Ryan, 2010). Sulphur Creek rocks are predominantly monzogranitic, characterised by augen of quartz and K-feldspar (**Fig. 3D**; Colpron and Ryan, 2010). U-Pb ages of the Sulphur Creek suite from an earlier reconnaissance study yielded ca. 263 to 261 Ma ages for the Mount Adami and Coldspring Mountain pluton (**Fig. 2**), respectively (N. Joyce, 2010, personal commun.).

Minor outcrops of metamorphosed mafic to intermediate volcanic and volcaniclastic rocks probably correlate with the Finlayson assemblage (Colpron and Ryan, 2010). The highly-strained Klinkit and Klondike assemblages are represented as lenses of intermediate to mafic schists with a quartz and sericite matrix and associated metamorphosed felsic volcanic rocks (**Fig. 3E**; Colpron and Ryan, 2010).

In the northeast quadrant of the study area (**Fig. 2**), intermediate to felsic rocks of the polyphase Reid Lakes batholith and associated volcanogenic rocks represent a predominantly undeformed component of the Finlayson assemblage and Simpson Range plutonic suite. A local weakly developed foliation is developed in rocks near the Willow Lake fault boundary with the central belt of Yukon-Tanana terrane rocks. The Reid Lakes batholith is predominantly monzogranitic with distinctive blue-grey quartz phenocrysts, in addition to minor granodiorite, quartz monzonite, and gabbroic phases (**Fig. 3F**; Colpron and Ryan, 2010). In thin-section, prolific seritisation and saussuritisation of feldspar is ubiquitous, suggesting fluid alteration in the absence of deformation. The volcanic succession consists of andesite to dacite flows, rhyolite to rhyodacite porphyries, and volcaniclastic sandstone, tuff, conglomerate and breccia (**Fig. 3G**; Colpron and Ryan, 2010). U-Pb ages from an earlier reconnaissance study dated the plutonic phase of the complex between ca. 360 and 342 Ma; one sample from the volcanic succession yielded a ca. 357 Ma age (N. Joyce, 2010, personal commun.). LA-ICP-MS U-Pb ages obtained from the southeastern extent of the batholith in a separate study are 341.5 ± 0.7 Ma and 355.9 ± 0.8 Ma (Mortensen, 2009).

The southwestern region of the study area is predominantly underlain by Mesozoic volcanic and plutonic rocks (**Fig. 2**). Augite-phyric andesitic to dacitic flows and volcaniclastic rocks are interpreted as being part of either the Late Triassic Lewes River Group of Stikinia or the Semenof Formation of Quesnellia. These rocks are intruded by a biotite ± hornblende granodiorite to monzogranite assigned to the Jurassic Aishihik suite (Colpron and Ryan, 2010). The Aishihik suite in the Klondike plateau and elsewhere is generally characterised by minimal deformation and the presence of magmatic epidote (Johnston et al., 1996). Highly strained Aishihik suite rocks, such as those that characterise the Minto Mine to the south of the study area, are anomalous (Tafti and Mortensen, 2004; Tafti, 2005; Hood et al., 2009).

The main belt of deformed Yukon-Tanana terrane rocks southwest of the Willow Lake fault are polydeformed by two or more phases of isoclinal folding and development of transposition foliations. An early phase of deformation occurred at upper greenschist to amphibolite facies metamorphism and is most apparent in the Snowcap assemblage (Colpron and Ryan, 2010). The next generation of pervasive deformation occurred during the Late Permian, imparting a dominant foliation to all Yukon-Tanana terrane assemblages in the region, with the exception of the Reid Lakes complex. Less intense Triassic to Jurassic metamorphism and deformation is characterised by open folding (Colpron and Ryan, 2010). In the northeast of the study area, rocks of the Reid Lakes complex have escaped regional deformation and metamorphism. They are locally deformed, defined by a mild foliation, in proximity to the Willow Lake and Tintina faults (Colpron and Ryan, 2010). The juxtaposition of undeformed and unmetamorphosed rocks of the Reid Lakes complex with polydeformed and greenschist to amphibolite facies metamorphosed rocks suggests a structural break between the two domains. The Willow Lake Fault is the inferred bounding structure, and is delineated by a prominent northwest-southeast trending linear low magnetic anomaly and a topographic valley along much of its length (Colpron and Ryan, 2010).

SAMPLING STRATEGY

In order to define the thermochronologic history of the Yukon-Tanana terrane in the Klondike plateau, we employ multiple dating methods with isotopic systems that span a wide range of temperature sensitivities. Zircon U-Pb dating can provide age determinations of the highest portion of the temperature window (as high as 900 ºC; Lee et al., 1997; Cherniak and Watson, 2000), and is generally interpreted as the primary crystallisation age for magmatic or metamorphic rocks. In order to place lithological assemblages of the McQuesten area within the predefined regional tectonostratigraphic framework of the Yukon-Tanana terrane, rock units selected for U-Pb dating were chosen based on their petrological characteristics and relative structural positions. Widespread sampling coverage ensures that all key units of the terrane in the area are identified and assigned a U-Pb age. We utilise the $^{40}Ar/^{39}Ar$ method to define the ca. 550-300 ºC cooling history of the Klondike plateau (Harrison, 1981; Harrison et al., 1985; Harrison et al., 2009). Target samples for $^{40}Ar/^{39}Ar$ dating were chosen from each of the main geological units in a transect across the area approximately perpendicular to the Willow Lake fault to test whether the thermochronologic history varied across the fault, and attempt to estimate the timing of displacement along this fault. Care was taken to ensure samples were not taken in proximity to presumed younger plutons which could have caused resetting of the $^{40}Ar/^{39}Ar$ cooling age. Finally, the zircon (U-Th)/He dating method was employed to define the low-temperature evolution of the map area. We chose the zircon U-He-

Pb double dating approach to define the complete high to low temperature evolution on the same subset of rocks; both U-Pb and (U-Th)/He dating were completed on the same mineral separates. Zircon He ages serve to further delineate the timing of fault displacement and possible erosional history of the area.

In the discussion that follows, we assign the following nominal closure temperatures: >900 ^{o}C for Pb in zircon (Lee et al., 1997; Cherniak and Watson, 2000); 550 ^{o}C for Ar in hornblende (Harrison, 1981); 405 ^{o}C for Ar in muscovite (Harrison et al., 2009); 300 ^{o}C for Ar in biotite (Harrison et al., 1985); and 180 ^{o}C for He in zircon (Reiners, 2005). The reader should note that these are experimentally derived values, and that actual cooling temperatures may vary by ± 50 ^{o}C depending on parameters such as grain size and cooling rate. A summary of all geochronology conducted as part of this study is presented in **Table 1**.

U-Pb GEOCHRONOLOGY

Methods

Rock samples for U-Pb geochronology were crushed, processed and analysed by standard techniques for zircon U-Pb dating. A detailed description of zircon extraction and analytical procedures is provided in **Appendix 2**. Zircon grains between 500 and 105 μm were hand picked for SEM imaging and SIMS isotopic analysis on the SHRIMP II at the Geological Survey of Canada, Ottawa, Canada. SHRIMP U-Pb data are reported in **Appendix 2**: igneous samples are in **Table A1**, and data for a detrital sample is in **Table A2**. Unless otherwise stated all ages are reported as the ^{207}Pb-corrected ^{206}Pb/^{238}U weighted mean at the 95% confidence level. Tera-Wasserburg and weighted mean plots generated with Isoplot v. 3.66 (Ludwig, 2003) are presented here in **Figure 4**. SEM images of representative zircons are

TABLE 1. AGE COMPILATION

Sample	Location (NAD 83)		Rock type	U-Pb Age	±2σ	$^{40}Ar/^{39}Ar$ Age	±2σ	Mineral*	(U-Th)/He Age	±2σ
	Lat (°N)	Long (°W)		(Ma)		(Ma)			(Ma)	
Reid Lakes Complex										
09RAYMC092A	63° 22' 48.4"	137° 03' 44.1"	Quartz sandstone	< 446.0	3.7					
09RAYJR134A	63° 13' 22.8"	136° 45' 55.6"	Tuff	ca. 360†					216	14
09RAYJR122A	63° 28' 37.8"	137° 06' 48.0"	Granodiorite	ca. 359†		342.8	6.9	Hbl	146	13
						347.7	2.8	Bt		
08RAY003	63° 10' 42.9"	136° 31' 12.9"	Granodiorite	ca. 358†					130	17
09RAYMC036A	63° 14' 32.5"	136° 49' 55.8"	Tuff	ca. 357†					214	17
09RAYJR176A	63° 19' 29.3"	137° 16' 47.3"	Monzogranite	ca. 347†		191.3	1.1	Bt	158	9
09RAYJR165A	63° 16' 37.8"	136° 53' 21.3"	Volcaniclastic breccia	346.4	3.7					
09RAYJR094A	63° 17' 37.7"	137° 17' 29.6"	Foliated monzogranite	346.3	2.8	191.3	0.7	Bt	140	17
09RAYJR160A	63° 10' 52.8"	136° 49' 13.9"	Orthogneiss	346.1	4.5	193.2	0.7	Ms		
09RAYJR133A	63° 34' 21.8"	137° 45' 45.7"	Granodiorite			348.5	2.8	Hbl		
						325.1	2.0	Bt		
09RAYMC115A	63° 20' 02.0"	136° 43' 25.4"	Granodiorite			333.9	3.4	Hbl		
Snowcap Assemblage										
09RAYRS030A	63° 07' 47.7"	137° 19' 19.0"	Pelitic schist			143.2	15.0	Bt		
Simpson Range Suite										
09RAYMC081A	63° 16' 50.6"	137° 21' 37.4"	Metagranodiorite	362.7	4.4	189.4	1.2	Bt		
09RAYRS005A	62° 56' 45.2"	137° 03' 15.8"	Metagranodiorite			188.9	0.7	Bt		
09RAYRS141A	63° 00' 25.7"	136° 40' 12.3"	Metamonzonite			184.6	1.0	Bt		
09RAYKR142A	62° 54' 21.1"	137° 05' 10.6"	Metamonzonite			181.6	0.7	Bt		
09RAYJR007A	63° 03' 29.5"	137° 07' 58.6"	Metagranodiorite			180.1	4.0	Bt		
09RAYJR143A	62° 59' 50.8"	137° 11' 12.4"	Metagranodiorite			177.1	1.9	Bt		
Finlayson Assemblage										
09RAYJR076B	63° 07' 35.0"	137° 00' 44.5"	Quartz-muscovite schist			183.4	1.1	Ms		
Klinkit Assemblage										
09RAYMC031A	63° 13' 54.5"	137° 08' 40.6"	Metafelsite	322.1	2.7	186.5	1.4	Ms		
09RAYJR078A	63° 11' 45.2"	137° 15' 06.7	Metarhyodacite			142.0	4.1	Ms		
						90.0	1.2	Bt		
Sulphur Creek Suite										
09RAYJR175A	63° 22' 34.4"	138° 02' 56.3"	Metamonzogranite	ca. 263†		170.6	1.5	Bt	113	10
09RAYJR177A	63° 12' 50.8"	137° 30' 25.5"	Metagranodiorite	262.7	2.0	168.9	1.9	Ms	90	7
09RAYJR178A	63° 09' 43.5"	137° 50' 55.7"	Metamonzogranite	262.6	2.1				179	14
09RAYJR179A	63° 06' 25.3"	137° 19' 19.9"	Quartz monzonite	262.0	1.9	196.9	1.4	Bt	101	13
08RAY004	63° 02' 32.4"	137° 14' 31.3"	Metagranodiorite	ca. 261†					107	9
09RAYMC017A	63° 06' 34.8"	137° 20' 53.5"	Quartz monzonite			189.9	1.5	Bt		
09RAYRS012A	63° 02' 32.0"	137° 14' 29.9"	Quartz monzonite			165.4	3.0	Bt		
Aishihik Suite										
09RAYMC123A	62° 50' 05.8"	137° 18' 08.7"	Monzogranite	204.9	3.3	195.6	1.5	Hbl		
						204.6	1.3	Bt		

*Refers to mineral analysed for $^{40}Ar/^{39}Ar$ dating: hbl-hornblende, ms-muscovite, bt-biotite.

†Age from unpublished reconnaissance study, provided by N. Joyce (2010, personal commun.).

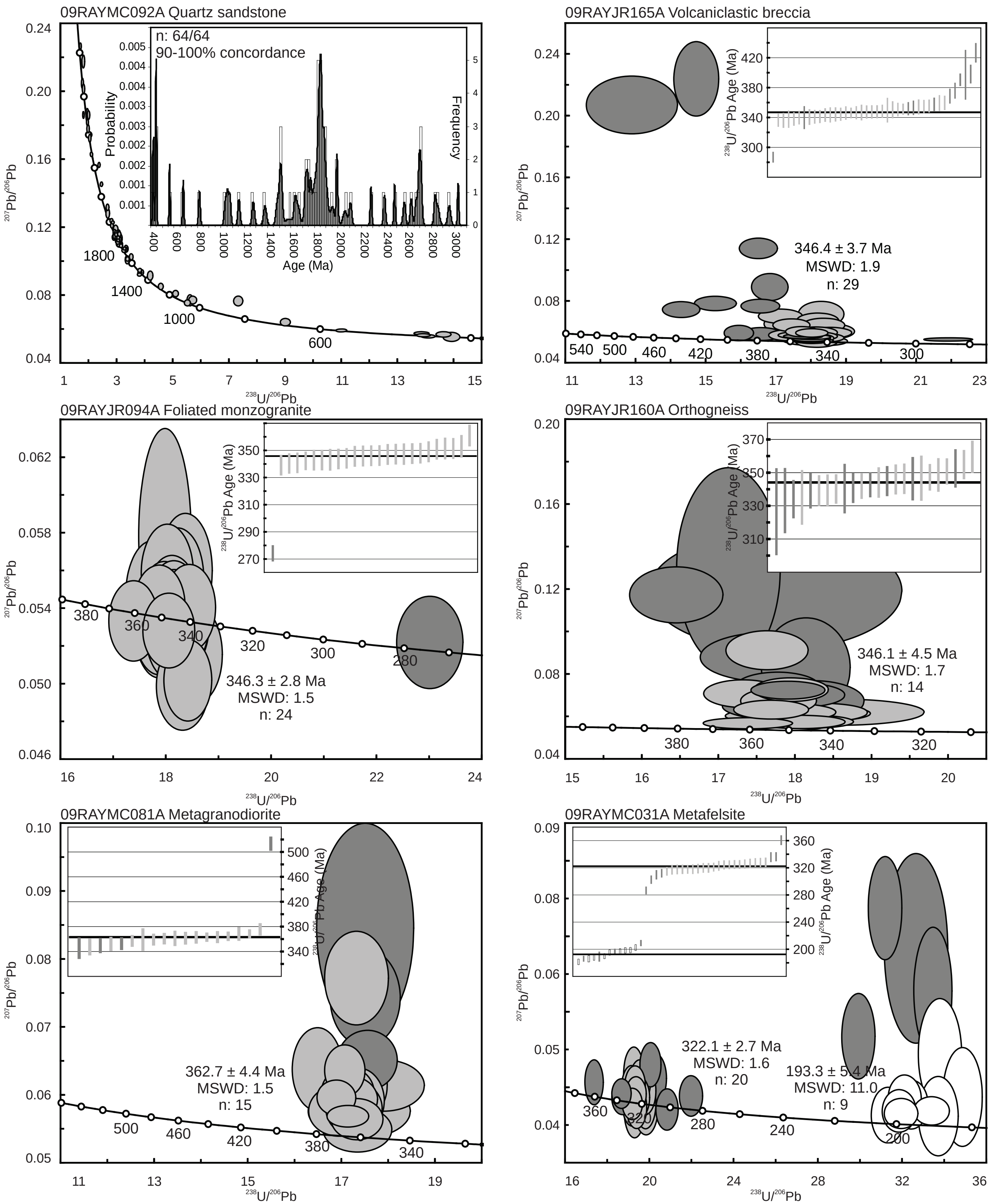
09RAYMC092A Quartz sandstone
n: 64/64
90-100% concordance
Probability
Frequency
Age (Ma)
1800
1400
1000
600
09RAYJR165A Volcaniclastic breccia
346.4 ± 3.7 Ma
MSWD: 1.9
n: 29
09RAYJR094A Foliated monzogranite
346.3 ± 2.8 Ma
MSWD: 1.5
n: 24
09RAYJR160A Orthogneiss
346.1 ± 4.5 Ma
MSWD: 1.7
n: 14
09RAYMC081A Metagranodiorite
362.7 ± 4.4 Ma
MSWD: 1.5
n: 15
09RAYMC031A Metafelsite
322.1 ± 2.7 Ma
MSWD: 1.6
n: 20
193.3 ± 5.4 Ma
MSWD: 11.0
n: 9
$^{207}Pb/^{206}Pb$
$^{238}U/^{206}Pb$
$^{238}U/^{206}Pb$ Age (Ma)

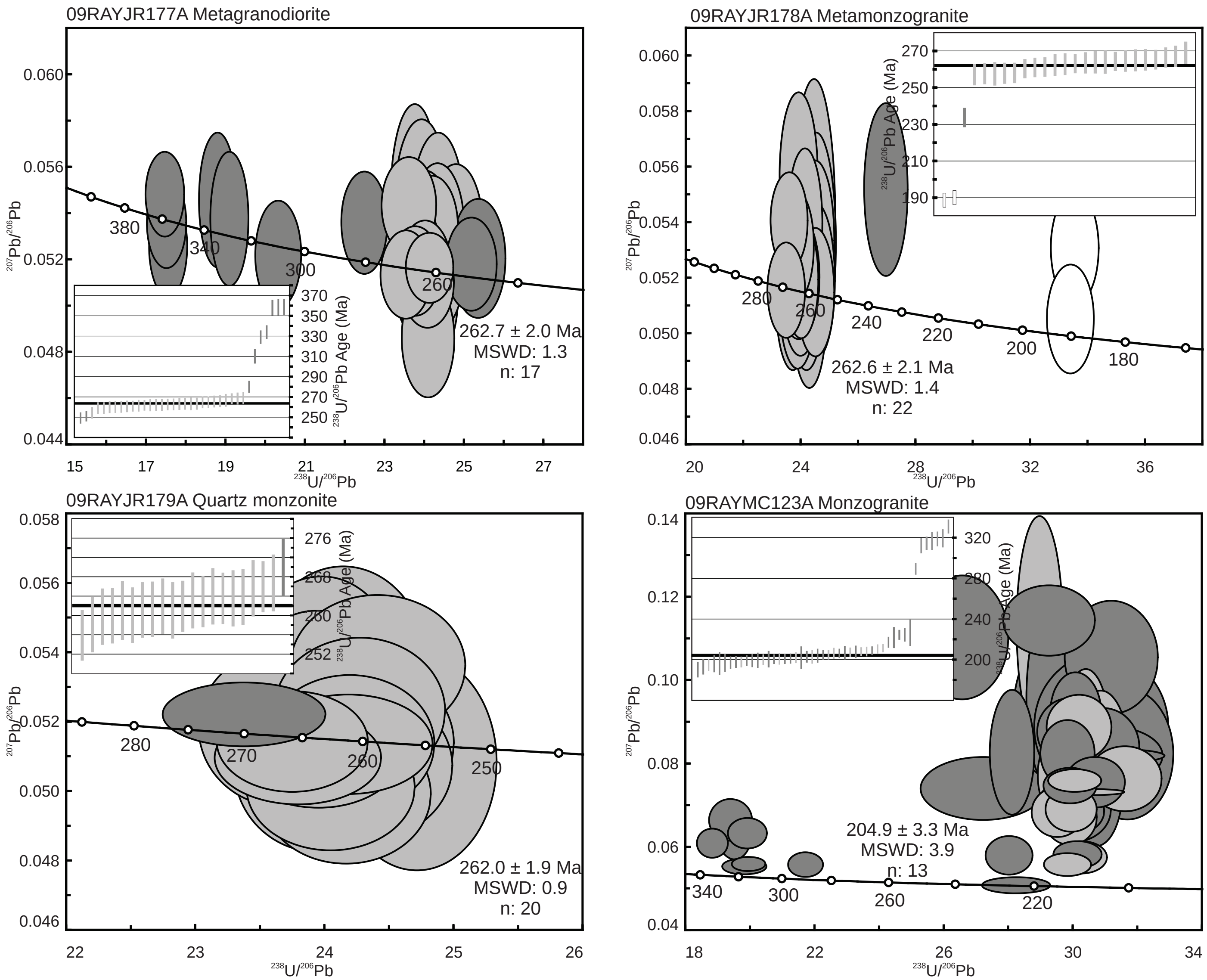

Figure 4. U-Pb Tera-Wasserburg plots for SIMS results from samples from the McQuesten area. Concordia ellipses and weighted mean error bars represent a single spot analysis; error is 2σ. Light grey error ellipses and weighted mean error bars are used to calculate the weighted mean age, dark grey ellipses and error bars are excluded from the age calculation, and white error bars and ellipses are interpreted as metamorphic overgrowths. See Figure 2 for sample locations and Table DR1 and DR2 in Appendix 1 for isotopic data and rationale for data point exclusion.

shown in **Figure 5**.

Analytical issues caused problems with data collection for SHRIMP mount 566 (samples 09RAYJR160A, 09RAYMC081A, 09RAYMC123A, and 09RAYJR165A). High common lead and occasionally incorrect centering on the ^{207}Pb peak were the result of a weak primary beam intensity and small spot size coupled with unscheduled electrical outages to the lab's power supply. Somewhat higher MSWD for these samples is attributed to analytical issues as opposed to having geological significance.

Results

Reid Lakes Complex

Sample 09RAYMC092A is a volcanogenic quartz sandstone collected from a 1 m thick horizon within reworked volcaniclastic rocks of intermediate composition in the northeast of the study area. In transmitted light, zircons extracted from this sample are generally stubby and anhedral, with lesser amounts of subhedral grains. Some grains retain their characteristic zircon morphology, whereas the majority are rounded to spherical with severely abraded surfaces. In cathodoluminescence (CL), subhedral grains have well-defined oscillatory zoning, whereas anhedral grains are homogenous or have broad and irregular internal zoning. Sixty-four grains were analysed, with single spot ages spanning ca. 418 to 3028 Ma. For the purpose of accurately comparing zircons with a broad range of apparent ages, grains older than 1500 Ma are reported and displayed as the ^{204}Pb-corrected ^{207}Pb/^{206}Pb age, whereas grains with a ^{207}Pb/^{206}Pb age less than 1500 Ma are reported and displayed as their ^{207}Pb-corrected ^{206}Pb/^{238}U age. **Figure 4** shows the probability density plot of individual U-Pb grain ages; every grain is less than 10% discordant and is therefore considered concordant. The largest peak occurs at ca. 1870 Ma, in addition to two smaller peaks at ca. 1510 and 2700 Ma. The reader should note that the peaks centered at ca. 450 Ma are unrepresentative-

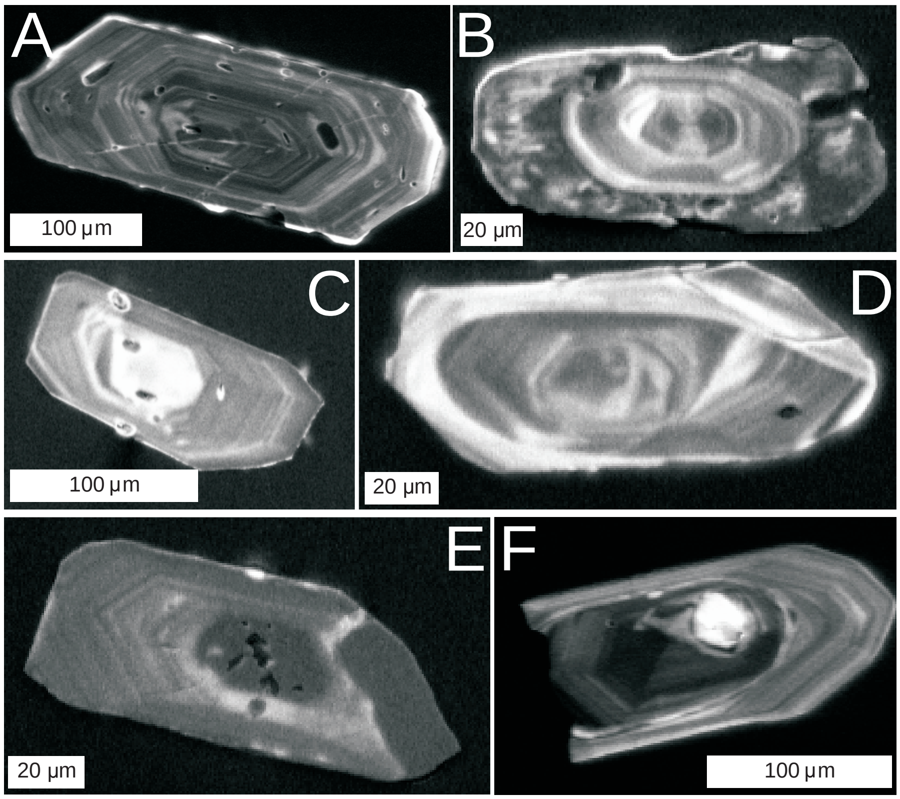

Figure 5. SEM cathodoluminescence images of representative zircons for samples dated by U-Pb and (U-Th)/He methods. Bright areas are low U. (A) Abundant inclusions in sample 09RAYMC081A (Simpson Range suite). (B) Convolute-zoned Jurassic-age rims of sample 09RAYMC031A bordering oscillatory-zoned Devonian cores. (C) Typical zircon of the Reid Lakes batholith, showing moderate abundance of inclusions (sample 09RAYJR094A). (D) Devonian core in Permian metagranodiorite of the Sulphur Creek suite (09RAYJR177A). (E) Jurassic-age recrystallization in the eastern quadrant of the grain. Sample (09RAYJR178A) is a metamonzogranite belonging to the Sulphur Creek suite. (F) Pennsylvanian-age cores bounded by Jurassic mantles of the Aishihik suite (sample 09RAYMC123A).

ly large due to preferentially targeting young grains in order to constrain the maximum age of deposition and do not represent a true statistical probability peak. The youngest grain has a $^{206}Pb/^{238}U$ age of 418 ± 3 Ma, however this age was not reproduced and a more conservative estimate of the maximum age of deposition of the sediment can be taken from three grains with a weighted mean $^{206}Pb/^{238}U$ age of 446.0 ± 3.7 Ma (MSWD: 1.0).

A volcaniclastic breccia (sample 09RAYJR165A) was sampled from the more widespread exposures of volcaniclastic rocks in the center of the Reid Lakes complex. Zircons recovered from this sample are generally euhedral, but are usually fragments of either the rectangular prism of the zircon crystal or the pyramidal terminations of the crystal. Most grains have a brown discolouration and appear slightly turbid. A large abundance of inclusions within the zircons contribute to their turbid appearance, few grains are clear and colourless. Zircons range in size between 100 and 300 μm, but may be up to 500 μm in length. CL images reveal faint concentric zoning and occasionally broad irregular zones. Some grains are homogenous and lack internal features. Forty single spots were analysed for this sample; 29 yielded reliable ages ranging between 336 and 360 Ma, with a weighted mean $^{206}Pb/^{238}U$ age of 346.6 ± 2.5 Ma (MSWD: 1.9).

Rocks at the southern margin of the Reid Lakes complex close to the Willow Lake Fault exhibit a weak to pronounced foliation defined by alignment of micas. Zircons recovered from a monzogranite phase (sample 09RAYJR094A) from within this zone are perfectly euhedral and elongate. Grains are clear and colourless with rare brown discolouration. Crystals are generally 100 to 200 μm in length, and as long as 400 μm, with length to width ratio (l/w) between 2-4. Most grains host small inclusions; rarely grains are fractured. The majority of zircons have well-defined but faint oscillatory zoning with highly luminescent (low U) cores (**Fig. 5C)**. Twenty-six spots were analysed on core and rim targets (**Fig. 4**), yielding a single population $^{206}Pb/^{238}U$ age of 345.8 ± 2.0 Ma (n: 24, MSWD: 1.6).

An orthogneiss of probable monzogranite protolith (sample 09RAYJR160A) was collected along the suspected projection of the Willow Lake Fault. Zircon recovery from this sample was relatively poor, and only 66 grains were extracted and mounted for analysis. The majority of crystals are fragmented and fractured, ranging from elongate and euhedral to stubby and anhedral with a l/w ratio of 2-3. In CL most grains display concentric zoning. Some grains have a dark (high U) core which is often obscured by inclusions. Cores and rims were analysed on 24 zircon grains (**Fig. 4**); 10 of these spots were rejected from the final age calculation because of high common lead concentrations. The remaining 14 grains span a broad range of ages between 335 and 360 Ma, yielding a weighted mean $^{206}Pb/^{238}U$ age of 346.1 ± 4.5 Ma (MSWD: 1.7).

Deformed Yukon Tanana Terrane Rocks

Zircon crystals for sample 09RAYMC081A, collected from a metagranodiorite outcrop approximately 3 km south of the projection of the Willow Lake Fault, are euhedral and elongate, 150 to 300 μm in length. Most grains appear to have a rough or pitted outer surface. Inclusions are pervasive throughout the crystals, and may constitute up to approximately 30% of the grain volume. Cracks and microfractures are abundant in back-scatter electron microprobe images, and the prominence of inclusions give the grains a “swiss cheese” appearance (**Fig. 5A)**. Internal oscillatory zoning is remarkably uniform throughout all grains. Nineteen core and rim targets were analysed on individual grains (**Fig. 4**), yielding a weighted mean $^{206}Pb/^{238}U$ age of 362.7 ± 4.4 Ma (n: 15, MSWD: 1.5).

Sample 09RAYMC031A was also collected close to the south side of the Willow

Lake Fault, from a small lens of metafelsite. The zircon population consists of predominantly euhedral and elongate to stubby grains, often with slightly abraded terminations and subangular to subrounded edges. Zircons are colourless or rarely brown, with abundant inclusions. Sector and oscillatory zoning is observed in both transmitted light and CL images. Most grains have cores with either narrow oscillatory zoning or broad and homogenous zones which have been replaced by inclusions. The majority of crystals have mantles up to 20 μm wide, with irregular or poorly-defined concentric zoning (**Fig. 5B)**. The boundary between the core and rim is demarcated by an abrupt truncation of internal zonation, or a ring of inclusions and cavities. Of 40 analysed single spots, 20 reliable spots range in age from 315 to 328 Ma (**Fig. 4**) and yield a weighted mean $^{206}Pb/^{238}U$ age of 322.1 ± 2.7 Ma (MSWD: 1.6). Seventeen spots analysed in the outer rims of the grains yielded ages younger than the main population with a tight clustering of ca. 193 Ma ages. Low Th/U ratios of these spots (0.01 to 0.05) suggest this younger subset are metamorphic overgrowths (Hoskin and Schaltegger, 2003).

Two samples were collected from the Mount Adami pluton, of purported Mid-Permian Sulphur Creek suite affinity in order to test if the compositionally heterogeneous pluton consists of multiple age phases. In transmitted light zircons from a well-foliated metagranodiorite phase (sample 09RAYJR177A) are clear and colourless but obscured by an abundance of inclusions. Some grains have localised brown discolouration. Crystal morphology is generally euhedral and stubby, with l/w of 2. A few grains have poorly developed or dismembered pyramidal terminations or are completely anhedral. In CL images, zircons have well-developed and narrow concentric zoning. Some grains host cores which typically have an irregular core to rim boundary that truncates faint core zonation or a homogeneous domain. Mantles bounding these cores are zoned and appear magmatic in origin (**Fig. 5D)**. Inclusions and fractures are rare; fractures generally radiate outwards from a dark (high U) and inclusion rich core. Thirty-six spots were analysed on 34 different grains, ranging in age from ca. 249 to 359 Ma. The main population of ages yielded a $^{206}Pb/^{238}U$ weighted mean of 262.7 ± 2.0 Ma (n: 27, MSWD: 1.3). Seven grains excluded from the age calculation yielded older ages between 280 and 359 Ma (**Fig. 4**), but predominantly Mississippian, interpreted as xenocryst cores. The younger core ages may reflect binary mixing of core and rim ages. Zircon recovery from a metamonzogranite phase of the Mount Adami pluton (sample 09RAYJR178A) was relatively poor. Grains are colourless or rarely brown, clear to slightly opaque. Inclusions are abundant. Morphology is euhedral and slightly stubby, with l/w of 1-2.5. SEM images show narrow, well-defined zoning and rare irregular or convolute zoning. Many zircons have homogeneous or convoluted cores with radiating fractures; the small core size and presence of inclusions and cavities precludes ion-microprobe analysis. Two single spots analysed in localised irregular homogenous domains at the crystal edge yielded ages of ca. 189 and 190 Ma (**Fig. 5E**). Both spots have Th/U ratios less than 0.02, indicative of metamorphic growth (Hoskin and Schaltegger, 2003). The remaining analyses yielded a $^{206}Pb/^{238}U$ age of 262.6 ± 2.1 Ma (n: 22, MSWD: 1.4).

In the center of the map area, a quartz monzonite sample (09RAYJR179A) was collected from the Coldspring Mountain pluton. Under transmitted light, zircons from this sample are euhedral and acicular. Zircons are typically up to 200 μm in length, but may exceed 400 μm. The l/w ratio of most grains is 3. Grains are colourless to brown, with prominent elongate inclusions in larger grains. Zircons have well-developed oscillatory zoning, some of which have broad, homogenous cores. Twenty analyses (**Fig. 4**) yielded a weighted mean

$^{206}Pb/^{238}U$ age of 262.0 ± 1.9 Ma (MSWD: 0.9).

Aishihik Suite

Sample 09RAYMC123A was collected from a granodioritic body in the south of the study area (**Fig. 2**) thought to belong to the Aishihik suite. Zircons recovered from this sample are generally euhedral, stubby to elongate with l/w between 2-3. Grains are colourless to brown in colour, with abundant inclusions and fractures and well-defined oscillatory zoning (**Fig. 5F)**. Many crystals host cores with internal structures defined as either broad and homogenous or narrowly zoned. Rare anhedral grains have irregular to convolute internal zonation. Six core targets have distinctively older ages than the majority of spot analyses, ranging in age from ca. 331 to 312 Ma and are somewhat discordant; these are interpreted as xenocrystic cores (**Fig. 4**). Thirteen single spots yielded a weighted mean $^{206}Pb/^{238}U$ age of 204.9 ± 3.3 Ma (MSWD: 3.9). When plotted on a probability density diagram, the ages follow a Gaussian distribution, with a peak at ca. 204 Ma. The high MSWD for this sample is likely analytical and not representative of multiple geological populations. However most of these analyses are slightly discordant, and the calculated mean may slightly over-estimate the age of emplacement. Even if we relax our threshold of exclusion for common lead to 2.5%, 17 grains yield an age of 204.4 ± 2.8 Ma (MSWD: 3.4).

$^{40}Ar/^{39}Ar$ THERMOCHRONOLOGY

Methods

Samples for $^{40}Ar/^{39}Ar$ thermochronology were prepared according to standard crushing and processing techniques. Isotopic analysis was conducted at the Geological Survey of Canada, Ottawa, Canada and the New Mexico Institute of Mining and Technology, Socorro, U.S.A. Complete details of sample preparation and laboratory analysis are provided in **Appendix 3**, in addition to results of isotopic analysis and ages in **Table A3** for samples analysed at the Argon Laboratory of the Geological Survey of Canada and **Table A4** for samples analysed at New Mexico Institute of Mining and Technology. Gas release age spectra are presented in **Figure 6.** Ages reported in the text are 2σ. Reported plateau ages are defined as three or more consecutive and overlapping heating steps that comprise greater than 50% of the total ^{39}Ar released. Of 26 minerals analysed, 23 yielded plateaus that fall within this definition, although with degrees of variance. High variance in the plateau age is likely related to subsequent thermal perturbation or poor sample quality, such as varying Ca or Cl content, which would affect Ar diffusion systematics in the crystal lattice and produce erroneous ages. Samples analysed are relatively radiogenic, so on an inverse isochron diagram most increments cluster around the x-axis ($^{39}Ar/^{40}Ar$) and do not precisely define a slope. For the purpose of this project, inverse isochron diagrams are useful to visually assess step data quality and to confirm plateau ages, but are not accurate estimates of cooling ages.

Results

Reid Lakes Complex

Samples collected from the Reid Lakes Complex yielded predominantly Mississippian $^{40}Ar/^{39}Ar$ plateau ages. Hornblende and biotite from a granodiorite phase in the northern extent of the Reid Lakes batholith (sample 09RAYJR122A) yielded plateau ages of 342.8 ± 6.9 Ma and 347.7 ± 2.8 Ma respectively (MSWD: 9.8 and 23.0; **Fig. 6**). Age spectra for both of these minerals step up to a well-defined plateau. In thin-section, biotite is moderately chloritised (**Appendix 1**), which often results in an anomalous cooling age because of differential Ar release patterns between chlorite and biotite during in-vacuo step-heating (Di Vin-

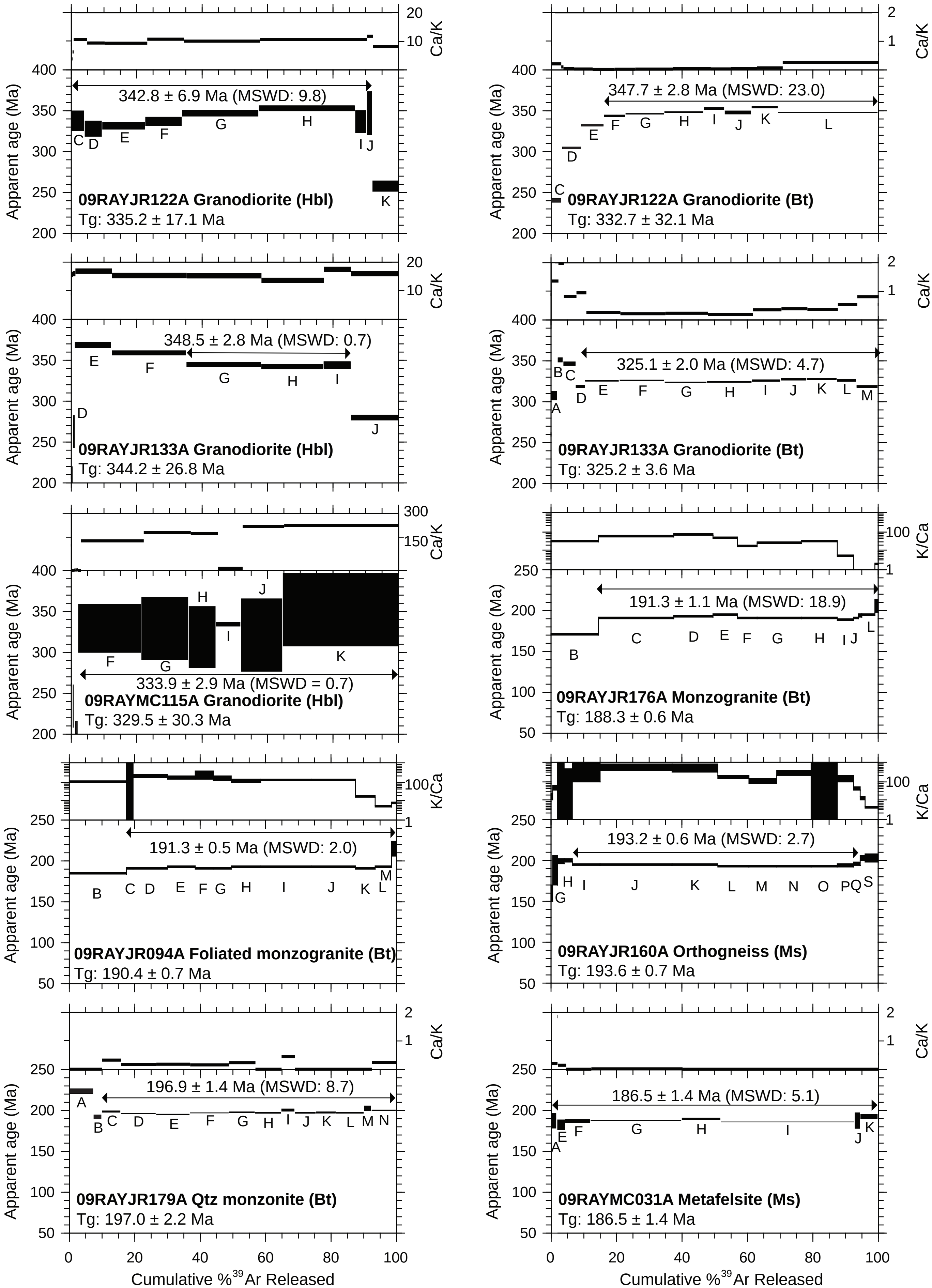
342.8 ± 6.9 Ma (MSWD: 9.8)
09RAYJR122A Granodiorite (Hbl)
Tg: 335.2 ± 17.1 Ma
347.7 ± 2.8 Ma (MSWD: 23.0)
09RAYJR122A Granodiorite (Bt)
Tg: 332.7 ± 32.1 Ma
348.5 ± 2.8 Ma (MSWD: 0.7)
09RAYJR133A Granodiorite (Hbl)
Tg: 344.2 ± 26.8 Ma
325.1 ± 2.0 Ma (MSWD: 4.7)
09RAYJR133A Granodiorite (Bt)
Tg: 325.2 ± 3.6 Ma
333.9 ± 2.9 Ma (MSWD = 0.7)
09RAYMC115A Granodiorite (Hbl)
Tg: 329.5 ± 30.3 Ma
191.3 ± 1.1 Ma (MSWD: 18.9)
09RAYJR176A Monzogranite (Bt)
Tg: 188.3 ± 0.6 Ma
191.3 ± 0.5 Ma (MSWD: 2.0)
09RAYJR094A Foliated monzogranite (Bt)
Tg: 190.4 ± 0.7 Ma
193.2 ± 0.6 Ma (MSWD: 2.7)
09RAYJR160A Orthogneiss (Ms)
Tg: 193.6 ± 0.7 Ma
196.9 ± 1.4 Ma (MSWD: 8.7)
09RAYJR179A Qtz monzonite (Bt)
Tg: 197.0 ± 2.2 Ma
186.5 ± 1.4 Ma (MSWD: 5.1)
09RAYMC031A Metafelsite (Ms)
Tg: 186.5 ± 1.4 Ma
Apparent age (Ma)
Ca/K
K/Ca
Cumulative %39Ar Released

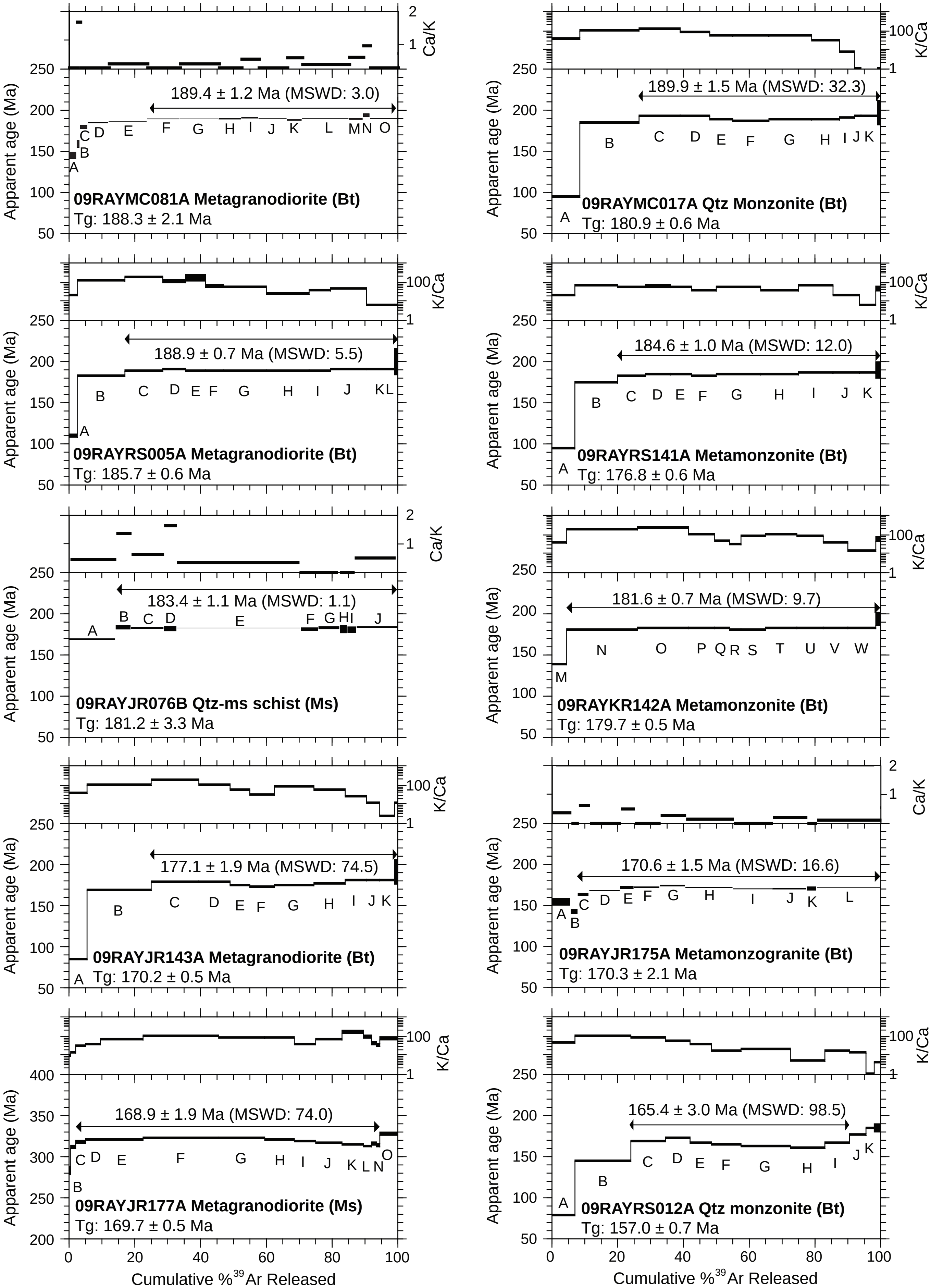
09RAYMC081A Metagranodiorite (Bt)
Tg: 188.3 ± 2.1 Ma
189.4 ± 1.2 Ma (MSWD: 3.0)
09RAYMC017A Qtz Monzonite (Bt)
Tg: 180.9 ± 0.6 Ma
189.9 ± 1.5 Ma (MSWD: 32.3)
09RAYRS005A Metagranodiorite (Bt)
Tg: 185.7 ± 0.6 Ma
188.9 ± 0.7 Ma (MSWD: 5.5)
09RAYRS141A Metamonzonite (Bt)
Tg: 176.8 ± 0.6 Ma
184.6 ± 1.0 Ma (MSWD: 12.0)
09RAYJR076B Qtz-ms schist (Ms)
Tg: 181.2 ± 3.3 Ma
183.4 ± 1.1 Ma (MSWD: 1.1)
09RAYKR142A Metamonzonite (Bt)
Tg: 179.7 ± 0.5 Ma
181.6 ± 0.7 Ma (MSWD: 9.7)
09RAYJR143A Metagranodiorite (Bt)
Tg: 170.2 ± 0.5 Ma
177.1 ± 1.9 Ma (MSWD: 74.5)
09RAYJR175A Metamonzogranite (Bt)
Tg: 170.3 ± 2.1 Ma
170.6 ± 1.5 Ma (MSWD: 16.6)
09RAYJR177A Metagranodiorite (Ms)
Tg: 169.7 ± 0.5 Ma
168.9 ± 1.9 Ma (MSWD: 74.0)
09RAYRS012A Qtz monzonite (Bt)
Tg: 157.0 ± 0.7 Ma
165.4 ± 3.0 Ma (MSWD: 98.5)
Apparent age (Ma)
Ca/K
K/Ca
Cumulative %39Ar Released

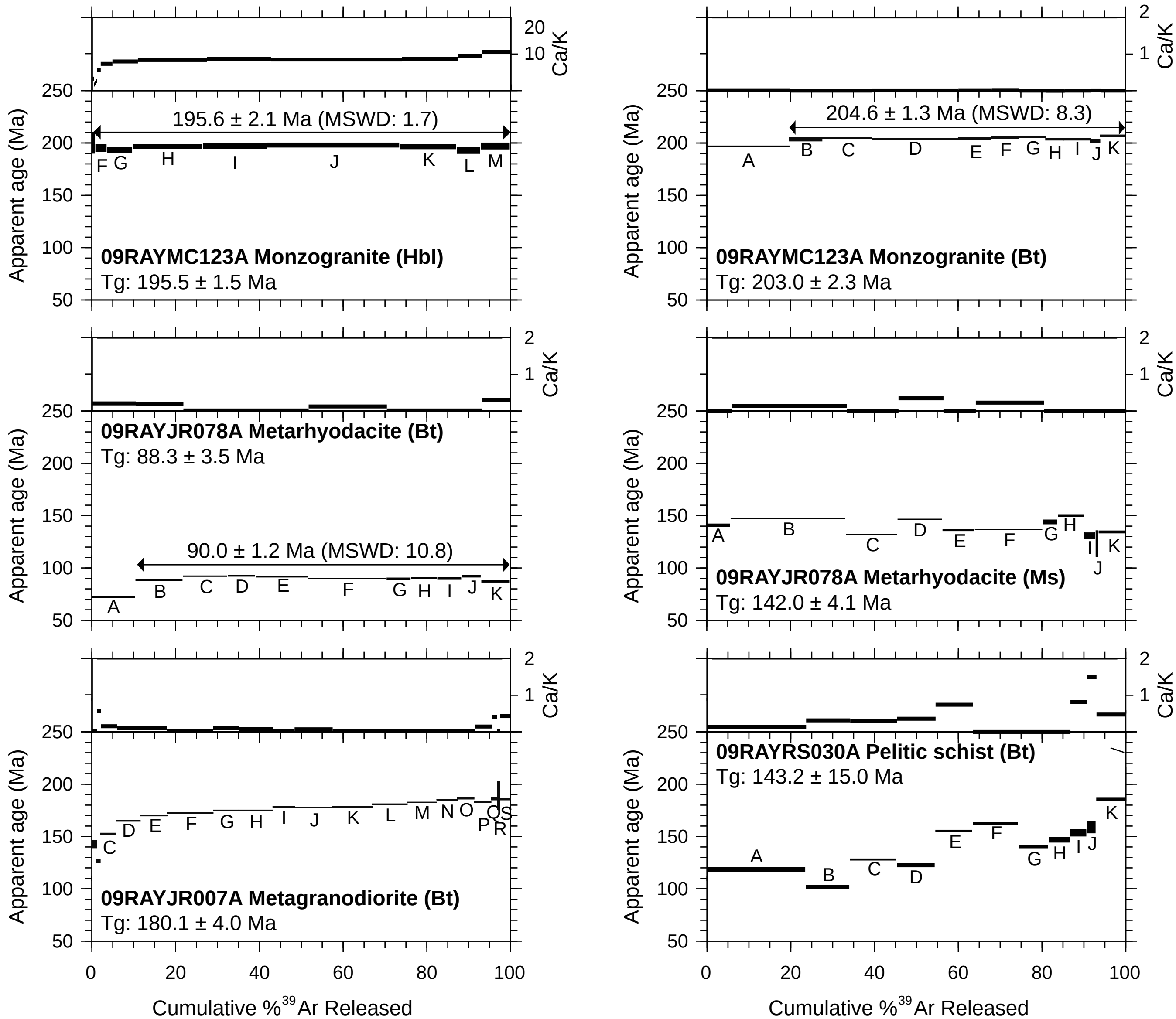

Figure 6. 40Ar/39Ar release spectra for incrementally heated mineral separates from the McQuesten area. Each gas-release spectrum plotted contains step-heating data providing a visual image of replicated heating profiles, evidence for Ar-loss in the low temperature steps, and the error and apparent age of each step. Spectra show the total gas age (Tg), which is the integrated age of each heating step, and the plateau age. Ca/K ratios shown on normal plot, K/Ca ratios shown on logarithmic plot. See Figure 2 for sample locations and Table DR3 and DR4 in Appendix 2 for isotopic data. Abbreviations: Bt-biotite; Hbl-hornblende; Ms-muscovite; Qtz-quartz; Tg-total gas age.

cenzo et al., 2003), contributing to its older-than-hornblende age. Plateau ages for another granodiorite hornblende and biotite pair from the northwestern extent of the Reid Lakes batholith (sample 09RAYJR133A) are in good agreement with 09RAYJR122A, yielding ages of 348.5 ± 2.8 Ma and 325.1 ± 2.0 Ma (MSWD: 0.7 and 4.7), respectively. The hornblende plateau is defined by 3 steps which account for 50% of ^{39}Ar released; the biotite age spectra is defined by a plateau constituting 83% of ^{39}Ar released. Hornblende from sample 09RAYMC115A yielded a plateau age of 333.9 ± 3.4 Ma (MSWD: 0.7), however the age steps that define the plateau have high uncertainty due to high Ca/K ratios, attributed to the low potassium content of the hornblende.

Three samples analysed from the vicinity of the weakly deformed southern margin of the Reid Lakes batholith close to the Willow Lake fault yielded Early Jurassic $^{40}Ar/^{39}Ar$ ages. Biotite from sample 09RAYJR176A yielded a plateau age of 191.3 ± 1.1 Ma (**Fig. 6**; MSWD: 18.9). The higher variance for this sample suggests a complex thermal history. Biotite collected from sample 09RAYJR094A yielded an identical plateau age of 191.3 ± 0.5 Ma (MSWD: 2.0). Both samples have well defined plateaus and are in close agreement with calculated integrated ages. Sample 09RAYJR160A, a high-strain orthogneiss collected from the linear magnetic low thought to demarcate the Willow Lake Fault trace yielded a muscovite plateau age of 193.2 ± 0.6 Ma (MSWD: 2.7).

Deformed Yukon Tanana Terrane Rocks

The majority of $^{40}Ar/^{39}Ar$ ages from the central belt of the study area yielded plateaus consisting of successive heating steps comprising greater than 50% of ^{39}Ar released and are remarkably concordant, ranging in age from ca. 197 to 165 Ma. Three samples (09RAYJR078A-muscovite, 09RAYJR007A-biotite, and 09RAYRS030A-biotite) did not yield plateaus. The total gas age of these samples is also ca. 40 Ma younger than the main grouping of ages. One sample (09RAYJR078A-biotite) yielded an anomalously younger cooling age of 90.0 ± 1.2 Ma.

Biotite from intrusive bodies interpreted as the Simpson Range suite generally occur in a pervasive foliation that wraps around porphyroblasts. A metagranodiorite sampled close to the proposed Willow Lake fault (09RAYMC081A) yielded a biotite plateau age of 189.4 ± 1.2 Ma (**Fig. 6**; MSWD: 3.0). Early gas release steps up consistently to the plateau, which accounts for 76% of the ^{39}Ar released. In the southern extent of the study area, biotite from a metagranodiorite (sample 09RAYRS005A) yielded a flat plateau age of 188.9 ± 0.7 Ma (**Fig. 6**; MSWD: 5.5). Biotite plateau ages of 181.6 ± 0.7 Ma (sample 09RAYKR142A; MSWD: 9.7) and 184.6 ± 1.0 Ma (09RAYRS141A; MSWD: 12.1) were obtained from small metamonzonite bodies in the southeast of the study area. Sample 09RAYJR143A from a small body of metagranodiorite produced a discordant age spectrum with a plateau age of 177.1 ± 1.9 Ma (MSWD: 74.5). The high MSWD does not seem to correspond to changes in K/Ca content, and likely reflects subsequent thermal disturbance.

Three samples were analysed from quartz monzonite of the Coldspring Mountain pluton, in addition to two samples from the Mount Adami pluton: both plutons are interpreted as part of the Sulphur Creek suite based on U/Pb ages. Biotite from sample 09RAYJR179A yielded the oldest cooling age from the central belt of rocks: 196.9 ± 1.4 Ma (**Fig. 6**; MSWD: 8.7). The age spectrum has a slight saddle shape to it suggesting excess argon, and the plateau age is ca. 7 m. y. older than a grouping of the next oldest cooling ages at ca. 190 Ma. This age is therefore interpreted as a maximum cooling age and may overestimate the true cooling age. Biotite from 09RAYMC017A yielded a plateau age of 189.9 ± 1.5 Ma (MSWD: 32.3), comprising 73% of the total ^{39}Ar released. Sample 09RAYRS012A yielded a discordant biotite plateau age of 165.4 ± 3.0 Ma (MSWD: 98.5). Biotite from 09RAYJR175A in the northwestern edge of the Mount Adami pluton yielded a plateau age of 170.6 ± 1.5 Ma (**Fig. 6**; MSWD: 16.6). The slightly high MSWD of this sample can be attributed to young initial heating steps that peak at 40% of ^{39}Ar released, and then decrease slightly. However the plateau age is equivalent to the inverse isochron age of 171.5 ± 1.7 Ma. This is one of the few samples where heating steps define an inverse isochron slope along all points of the line. This slope corresponds to a ^{40}Ar/^{36}Ar intercept of 282.2, in agreement with the composition of atmospheric argon, 295.5. Muscovite from a monzogranite (09RAYJR177A) yielded a plateau age of 168.9 ± 1.9 Ma (MSWD: 74.0); the total gas age of this sample is 169.7 ± 0.5 Ma, suggesting this age is robust despite the high MSWD.

Muscovite from a felsic metavolcanic rock proximal to the proposed fault (09RAYMC031A) yielded a plateau age of 186.5 ± 1.4 Ma (MSWD: 5.1), equivalent to the integrated age. A plateau age of 183.4 ± 1.1 Ma (MSWD: 1.1) was obtained from muscovite in a quartz-muscovite schist interpreted as the Finlayson assemblage (09RAYJR076B).

One sample in the study area yielded an anomalously low cooling age. Biotite from sample 09RAYJR078A, a small lens of strongly foliated metarhyodacite yielded a relatively flat plateau age of 90.0 ± 1.2 Ma (MSWD: 10.8), in close agreement with the integrated age of 88.3 ± 3.4 Ma. Muscovite from this sample yielded a range of alternating old and young steps, ranging in age from ca. 123.2 to 150.0 Ma that do not form a plateau (**Fig. 6**). The integrated age for this sample is 142.0 ± 4.1 Ma, which is considerably older than the anomalously low biotite cooling age of ca. 90.0 Ma.

Two additional samples yielded complex age spectra with no defined plateau. Sample 09RAYJR007A produced an age spectrum with increasing heating steps that never form a contiguous plateau. The integrated age for this sample is 180.1 ± 4.0 Ma, which is in agreement with the range of Jurassic cooling ages for successfully dated samples, and is the preferred age for this sample. Mica from a pelitic schist (09RAYRS030A) was noted to host graphite and other inclusions (**Appendix 1**); contamination from these inclusions likely explains the irregular pattern of heating steps. The integrated age for this sample is 143.2 ± 15.0 Ma, which is younger than the trend of cooling ages in the deformed package of Yukon-Tanana rocks. The oldest step yielded an age of 185.2 ± 1.64 Ma, which is interpreted as the maximum cooling age.

Aishihik Suite

Hornblende and biotite $^{40}Ar/^{39}Ar$ ages from a monzogranite in the southern belt of the study area (09RAYMC123A) are slightly anomalous. Hornblende yielded a plateau age of 195.6 ± 1.5 Ma (**Fig. 6**; MSWD: 1.7), and biotite yielded a plateau age of 204.6 ± 1.3 Ma (MSWD: 8.3). The zircon U-Pb crystallisation age of this sample is 204.9 ± 3.3 Ma (this study), which would indicate extremely rapid cooling between the closure temperature of zircon and biotite. In thin-section, biotite is altered to chlorite (**Fig. 3H**), which may explain the slightly older age (Di Vincenzo et al., 2003).

(U-Th)/He THERMOCHRONOLOGY

Methods

In order to delineate the low-temperature thermotectonic evolution of the McQuesten area, select samples that had zircons previously extracted for U-Pb geochronology were also analysed for zircon (U-Th)/He thermochronology. Eleven samples had zircons of high enough quality to conduct analyses. Details of sample preparation, analysis, and data processing are provided in **Appendix 4**; isotopic data and ages are presented in **Table 2.** Age

TABLE 2. (U-Th)/He DATA FOR SAMPLES FROM THE MCQUESTEN MAP AREA

Grain	U (ppm)	Th (ppm)	He (nmol/g)	Effective FT*	Uncorrected He age (Ma)	Corrected He age (Ma)	± (2σ)
09RAYJR134A; Tuff							
1	441.9	179.2	464.1	0.7366	174	237	19
2	402.0	236.2	440.7	0.6876	175	255	20
3	602.7	325.7	576.3	0.7084	154	218	17
4	580.9	311.4	416.1	0.6803	116	171	14
5	415.6	247.9	342.7	0.6534	132	202	16
					Mean	**216**	**14**
09RAYMC036A; Tuff							
1	627.0	348.9	524.7	0.7229	135	187	15
2	484.9	253.9	403.0	0.7098	135	190	15
3	421.5	225.8	364.9	0.6788	140	206	17
4	601.8	323.3	519.6	0.6622	140	211	17
5	395.7	198.1	429.7	0.6345	177	278	22
					Mean	**214**	**17**
09RAYJR176A; Monzogranite							
1	879.6	238.9	614.0	0.7898	120	152	12
5	547.0	322.1	415.0	0.7228	122	168	13
3	860.9	318.0	695.1	0.7980	135	170	14
4	557.4	191.6	431.2	0.7539	131	173	14
2	755.6	315.4	475.1	0.8375	105	125	10
					Mean	**158**	**9**
09RAYJR122A; Granodiorite							
2	341.8	303.8	227.2	0.7347	101	137	11
3	442.0	182.7	268.1	0.7347	101	171	14
4	650.7	492.4	397.1	0.7307	95	130	10
5†	947.8	1689.0	24.7	0.5911	3	6	1
					Mean	**146**	**13**
09RAYJR094A; Foliated monzogranite							
1	271.8	155.4	160.1	0.7404	95	128	10
2	306.2	169.5	189.5	0.6759	100	148	12
3	328.6	139.6	177.7	0.7633	90	118	9
4	325.0	103.4	278.8	0.7196	145	202	16
5	386.1	133.6	191.1	0.8135	84	103	8
					Mean	**140**	**17**
08RAY003; Granodiorite							
2	353.0	231.8	158.8	0.7396	72	97	8
3	399.8	204.8	210.0	0.7611	86	113	9
4	343.9	202.9	237.4	0.8164	111	136	11
5	287.1	112.7	225.3	0.7571	131	173	14
					Mean	**130**	**17**
09RAYJR178A; Metamonzogranite							
1†	556.4	208.7	545.1	0.6884	164	238	19
2†	527.5	296.7	455.6	0.6294	139	221	18
3	685.4	286.4	585.1	0.7214	142	196	16
4	582.6	322.7	371.0	0.6391	103	161	13
					Mean	**179**	**14**

Grain	U (ppm)	Th (ppm)	He (nmol/g)	Effective FT*	Uncorrected He age (Ma)	Corrected He age (Ma)	± (2σ)
09RAYJR175A; Metamonzogranite							
1	504.7	194.1	294.2	0.7971	98	123	10
2	803.3	345.5	375.9	0.7232	78	108	9
3	632.5	244.7	376.1	0.7133	100	140	11
4	560.9	117.5	277.1	0.7351	86	117	9
5	779.1	279.3	270.0	0.7523	59	78	6
					Mean	**113**	**10**
08RAY004; Metagranodiorite							
1	611.2	93.7	235.6	0.6146	68	111	9
2	675.6	149.8	228.1	0.6244	59	94	8
4	633.6	143.9	281.1	0.5970	77	129	10
5	502.1	68.8	188.6	0.7227	67	92	7
					Mean	**107**	**9**
09RAYJR179A; Quartz monzonite							
1	1180.0	137.0	501.9	0.7344	76	103	8
2	299.6	95.1	170.0	0.7248	97	133	11
3	1149.0	163.6	477.1	0.7796	74	94	8
5	1440.0	179.3	461.0	0.7851	57	73	6
					Mean	**101**	**13**
09RAYJR177A; Metagranodiorite							
1	415.7	136.1	128.0	0.7223	53	73	6
3	772.0	272.0	283.5	0.5934	62	105	8
4	407.0	123.3	145.0	0.6381	61	96	8
5	344.3	116.5	116.0	0.6712	57	85	7
					Mean	**90**	**7**

*FT is alpha-stopping correction factor calculated by HeFTy (Ketcham, 2005).

†Data point excluded from mean age calculation.

errors are reported at the 2σ level. Estimated 2σ uncertainty for mean zircon He ages is 8% (Reiners et al., 2004), based on accuracy and reproducibility of U and Th concentrations measured on Durango apatite, combined with the error of He analyses. Helium extraction was conducted at the Dalhousie University Argon Geochronology Laboratory, Halifax, Canada. Uranium and thorium concentrations were measured using laser-ablation inductively-coupled plasma mass spectrometry (LA-ICP-MS) at the Geological Survey of Canada, Ottawa, Canada. Applying LA-ICP-MS methods is a relatively new technique for modeling the bulk concentration of U and Th for (U-Th)/He dating and is actively being developed (Hourigan et al., 2005; Boyce et al., 2006; Farley et al., 2011; Vermeesch et al., 2012). The pronounced benefit of this method is the ability to image the grains using a SEM in order to assess individual grain quality and visually estimate the severity of intra-grain U and Th zonation, a source of considerable error for this dating method. Alpha correction and bulk U and Th concentrations were calculated with the HeFTy computer program (Ketcham, 2005). All ages discussed in the text have been corrected for alpha ejection and redistribution.

Results

Reid Lakes Complex

Two zircon samples from the volcanogenic suite of the Reid Lakes complex were analysed for (U-Th)/He dating. Zircons from sample 09RAYJR134A host rare to minor inclusions, and are generally free of cracks. Zoning of U and Th is asymmetrical, with low concentrations in the cores and elevated concentrations approaching the rims. Variation in intensity from core to rim is subdued. Five grains yielded individual (U-Th)/He ages ranging from 171 ± 14 to 255 ± 20 Ma, with a mean age of 216 ± 14 Ma. Sample 09RAYMC036A hosts a moderate amount of inclusions and cracks in individual grains. U and Th concentrations are generally highest in the core of the grain, but relatively homogenous across the grain. Five zircons yielded ages from 187 ± 15 to 278 ± 22 Ma; the mean of these ages is 214 ± 17 Ma.

Four samples taken from the structurally lower intrusive suite of the Reid Lakes complex have younger (U-Th)/He ages than the volcanogenic package. Five zircons from sample 09RAYJR176A yielded a mean age of 158 ± 9 Ma; individual ages range between 125 ± 10 Ma and 173 ± 14 Ma. Grains from this sample host a moderate amount of inclusions, and some cracks are visible in SEM images. Concentrations of U and Th are relatively constant for the majority of grain traverses, although two grains (1 and 5) have asymmetric and heterogeneous concentration profiles. Four grains from sample 09RAYJR122A yielded clear grains with very few inclusions and relatively homogenous U and Th concentration transects with only minor core to rim gradients. The exception is grain 4 which is strongly and symmetrically zoned in U and Th, with a wide, high concentration core and depleted rims. The He concentration (24.7 nmol/g) of 09RAYJR122A-5 is an order of magnitude lower than the rest of the study population, and yielded an anomalously young age of 6 ± 1 Ma. It is assumed there was an issue with He degassing of this grain, and it is excluded from the mean age calculation. Three other grains range in age from 130 ± 10 to 171 ± 14 Ma; the mean of this group is 146 ± 13 Ma. Five zircons from sample 09RAYJR094A appear to host abundant and large inclusions in SEM images (**Fig. 5C**). U and Th concentration profiles across the grains are highly variable, except 09RAYJR094A-4 which is homogenous. The mean age of this sample is 140 ± 17 Ma; individual ages span 103 ± 8 to 202 ± 16 Ma. Four stubby grains from sample 08RAY003 ranging from 97 ± 8 to 173 ± 14 Ma yielded a mean age of 130 ± 17 Ma. These grains host moderate inclusions and generally have variable U and Th concentration transects.

Deformed Yukon Tanana Terrane Rocks

Five samples were analysed for (U-Th)/He from the polydeformed rocks in the southwest of the study area. Sample 09RAYJR178A revealed moderate inclusions and faint cracks in SEM images (**Fig. 5E**). U and Th profiles vary in accordance with inclusion locations, and are generally heterogeneous. Four grains from this sample yielded individual ages between 161 ± 13 Ma and 238 ± 19 Ma, which combine to a mean age of 204 ± 17 Ma. The age of this sample is anomalously old relative to the other (U-Th)/He ages from the deformed block of Yukon-Tanana terrane rocks and is older than the U-Pb age of metamorphic zircon rims analysed on the same sample. The final He extract of the oldest two grains yielded a high concentration of the total He degassed from the sample, 8.2 and 13.4%, respectively, suggesting irregular degassing, potentially related to intra-grain deformities or heterogeneities. These ages, therefore, are interpreted as erroneously old, and a more conservative mean age estimate of the remaining two grains is 179 ± 14 Ma.

Sample 09RAYJR175A yielded five prismatic grains with abundant inclusions and fractures apparent in SEM images. Concentrations of U and Th are heterogeneous in most grains, and significant anomalies correspond to inclusions. Individual ages range from 78 ± 6 to 140 ± 11 Ma. The mean age of this sample is 113 ± 10 Ma. Zircons from sample 08RAY004 host moderate inclusions, yet have relatively flat U and Th concentration profiles with slightly enriched rims. Four grains from this sample range in age from 92 ± 7 to 129 ± 10 Ma; the mean age of this group is 107 ± 9 Ma. Four zircons recovered from sample 09RAYJR179A host significant inclusions and have relatively homogenous U and Th profiles; minor concentration anomalies correspond to the location of inclusions. The range of individual ages for this sample is 73 ± 6 to 133 ± 11 Ma, with a mean age of 101 ± 13 Ma. Sample 09RAYJR177A yielded four zircons with minor to moderate inclusions, and relatively variable and heterogeneous U and Th concentration profiles. These grains yielded a mean age of 90 ± 7 Ma, ranging in age from 73 ± 6 to 105 ± 8 Ma.

DISCUSSION

Arc Magmatism

Our new U-Pb ages improve the resolution of Middle to Late Paleozoic magmatic activity of the Yukon-Tanana arc system. A compilation of ages obtained in this study for each dating technique are presented in **Figure 7** in map view; **Figure 8** shows the age distribution of samples relative to their distance from the Willow Lake fault. Lithostratigraphic relationships are schematically illustrated in a generalised cross-section through the McQuesten area (**Fig. 9**). In the north of the study area, zircon U-Pb crystallisation ages of 346.3 ± 2.8 Ma and 346.1 ± 4.5 Ma were obtained from a weakly foliated and highly strained, respectively, component of the Reid Lakes batholith (**Fig. 7A**). These ages are in agreement with unpublished Mississippian U-Pb ages between ca. 360 and 342 Ma (N. Joyce, 2010, personal commun.). These ages delineate the timing of emplacement of the batholith, and are coeval and equivalent to zircon U-Pb crystallisation ages of extrusively related Reid Lakes volcanogenic rocks.

Previous dates of ca. 360 and 357 Ma (N. Joyce, 2010, personal commun.) from tuffaceous rocks of the Reid Lakes complex are slightly older than the 346.4 ± 3.7 Ma date obtained from a coarse volcaniclastic breccia (this study). The single population of zircon ages for this polymictic rock suggests a single, proximal synvolcanic source. The dominant clast

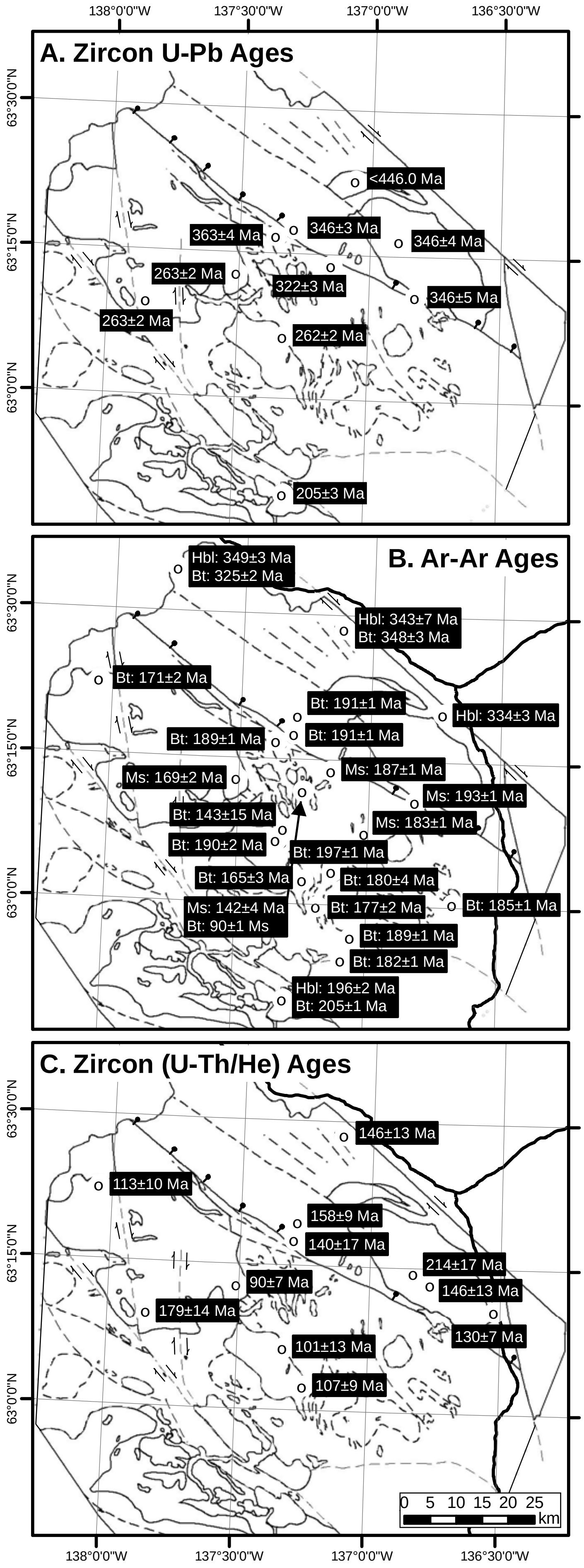

Figure 7. Distribution of ages investigated in this study from the McQuesten map area. See Figure 2 for map details and legend. (A) Zircon U-Pb ages. (B) 40Ar/39Ar ages. (C) Zircon (U-Th)/He ages.

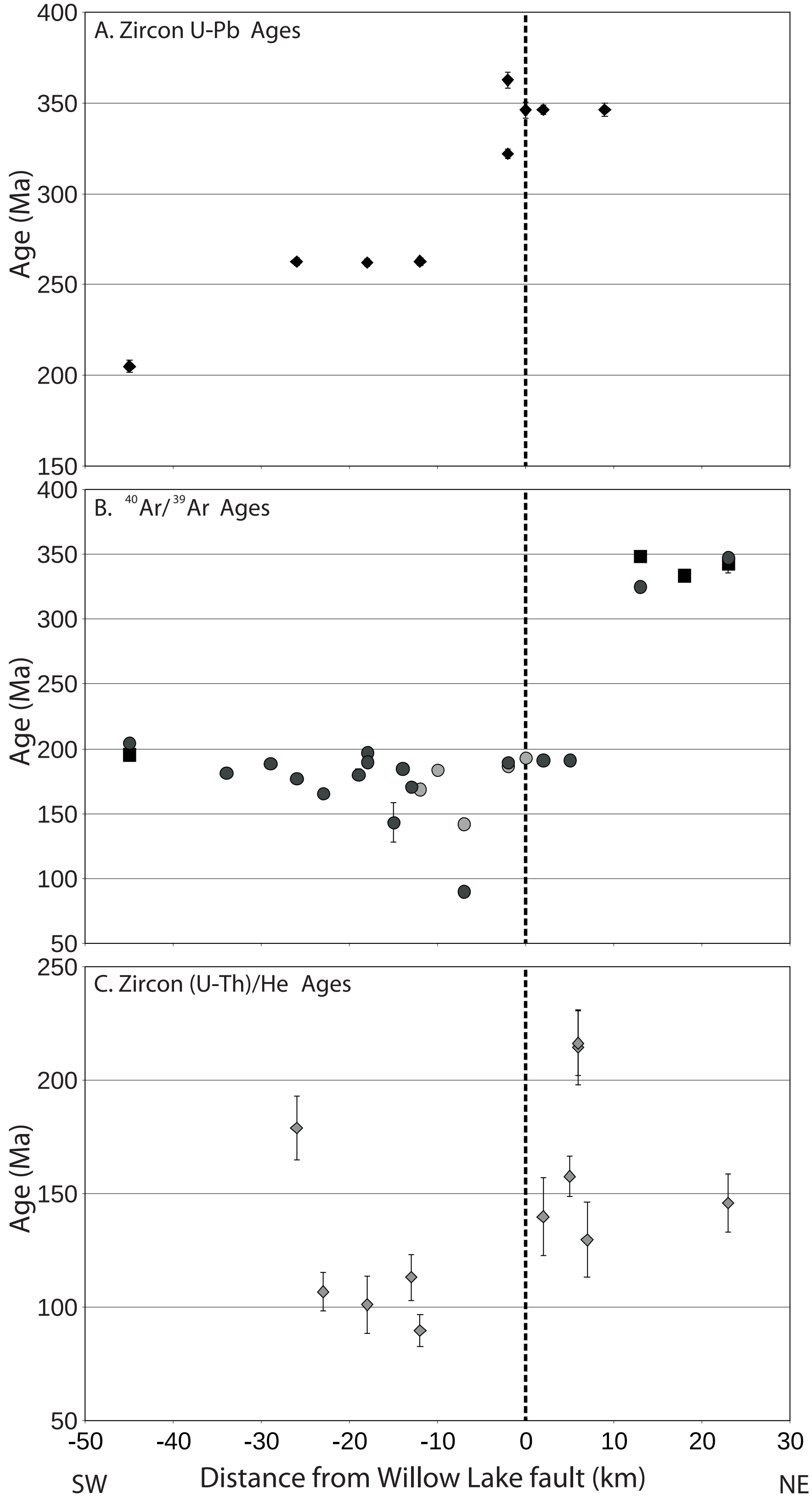

Figure 8: Age of samples dated relative to their position from the Willow Lake Fault, which is represented by the vertical dashed line. Positive distance is to the northwest in the Reid Lakes complex; negative distance is southwest of the fault. Age error bars shown are 2σ, and are less than the size of the symbol when not visible. (A) Zircon U-Pb ages. (B) $^{40}Ar/^{39}Ar$ ages. Squares-hornblende; grey circles-muscovite; black circles-biotite. (C) Zircon (U-Th)/He ages.

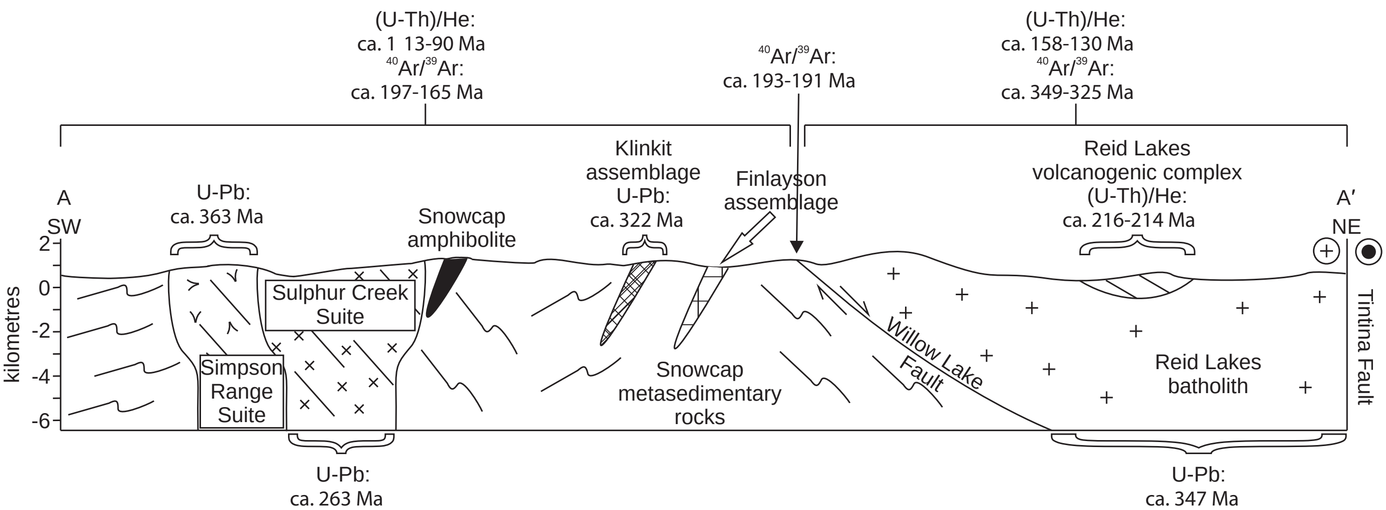

Figure 9. Generalised cross-section of the McQuesten area, showing the Willow Lake fault, key lithological relationships, and summarised age determinations. Orientation of squiggly lines shows generalised fabric trends. See Figure 2 for transect location.

lithologies of this sample, such as limestone and chert, do not typically generate zircon which would also explain the unexpected single population of zircon ages in this sample. The quartz sandstone horizon sampled from the northern part of the Reid Lakes volcanic rocks yielded detrital zircon population probability peaks at ca. 1510, 1870, and 2700 Ma. These ages are identical to detrital zircon populations derived from metasedimentary units elsewhere in the Yukon-Tanana terrane and are indicative of primary detrital derivation from cratonic north-central North American provinces and the Cordilleran miogeocline (Gehrels et al., 1995; Colpron et al., 2006*b*; Devine et al., 2006; Murphy et al., 2006; Nelson et al., 2006; Nelson and Gehrels, 2007; Dusel-Bacon and Williams, 2009; Piercey and Colpron, 2009; Beranek and Mortensen, 2011). Due to poor exposure in the area, it is not possible to conclude if this sandstone is at the base of the Reid Lakes volcanics, or within the volcanic pile. If the sandstone is at the base of the Reid Lakes complex, it may provide an erosional window through them to underlying siliciclastic rocks of the Snowcap assemblage. The maximum age of deposition of this unit is constrained by three grain ages ca. 446 Ma. Zircons of Silurian age in the Yukon-Tanana terrane are rare, but have been reported from Snowcap assemblage rocks in the Stewart River area (M. Villeneuve, 2003, personal commun.), and Klinkit assemblage correlative rocks in the Glenlyon area (Colpron et al., 2006*b*) and northern British Columbia (Gleeson et al., 2000). Gehrels et al. (1999) reported six ca. 434-424 Ma detrital zircons from autochthonous North American rocks in the vicinity of the Yukon-Tanana upland (**Fig. 1**) north of the Tintina Fault. These grains are posited to have been derived from: Cordilleran arcs, particularly the Alexander terrane; the Caledonian orogen; or exotic crustal fragments in northern Asia with depositional ties to the Innutian orogen (Gehrels et al., 1999). Silurian-age detrital grains from miogeoclinal strata of the Spray Lakes Group of southeastern British Columbia are thought to be derived from the Canadian-

Alaskan Arctic margin (Gehrels and Ross, 1998). Silurian-age grains are also reported from: miogeoclinal strata in the northern Cordillera (Gehrels et al., 1995); and a metaconglomerate belonging to the Bob Lake assemblage in south-central British Columbia (Erdmer et al., 2002).

The Reid Lakes pluton is inferred as the feeder system that is intruding its own volcanic carapace (**Fig. 9**), and is coeval with the more regionally known Simpson Range plutonic suite, plutonic and volcanic rocks of the Little Kalzas arc in the Glenlyon area to the southeast (**Fig. 1**), and formation of the Wolverine Lake back-arc group in the Finlayson region (Colpron et al., 2006*b*; Murphy et al., 2006). The relatively undeformed nature of the Reid Lakes complex suggests it occupied a higher crustal level than polydeformed rocks southwest of the Willow Lake fault.

In the deformed package of rocks to the southwest of the Reid Lakes complex, a zircon U-Pb age of 362.7 ± 4.4 Ma from a metagranite body truncated by the Willow Lake Fault confirms it is part of the Simpson Range plutonic suite (**Fig. 7A**). Lithological and textural characteristics distinguish this pluton from the weakly foliated component of the Reid Lakes complex, notably the high degree of strain, multiple foliations, and absence of porphyritic smoky-quartz. The Simpson Range suite is inferred as the deep-seated plutonic component of the Finlayson Assemblage (Colpron et al., 2006*a*).

Sample 09RAYMC031 from a metafelsite yielded a U-Pb age of 322.1 ± 2.7 Ma. This small lens was originally mapped as Klondike schist due to its composition and textural appearance (Colpron and Ryan, 2010). The U-Pb age, however, demonstrates this to be incorrect, and is more likely correlative with rocks of the Klinkit assemblage, which is interpreted as the remnants of a primitive short-lived Pennsylvanian to Early Permian arc.

Klinkit-type rocks in the Yukon are thought to be correlative with the Lay Range and Harper Ranch arc and back-arc assemblages of Quesnellia in British Columbia (Mihalynuk et al., 2000; Roots et al., 2002; Simard et al., 2003; Nelson and Friedman, 2004; Colpron et al., 2006*a*; Roots et al., 2006, Colpron et al., 2007). The full ramifications of Klinkit assemblage rocks lying on the Snowcap assemblage this far to the north has not been fully reconciled, however it is safe to conclude that the Klinkit arc was of a grander scale than previously known.

Permian magmatism is represented by two identical U-Pb crystallisation ages from the Mount Adami pluton of 262.7 ± 2.0 and 262.2 ± 2.1 Ma (**Fig. 7A**). These ages are typical of the Sulphur Creek plutonic suite (Colpron et al., 2006*a*), and are in agreement with unpublished dates of ca. 263 and 261 Ma (N. Joyce, 2010, personal commun.). A weakly foliated granitoid body northwest of the Coldspring Mountain pluton was originally mapped as a separate Cretaceous body (Colpron and Ryan, 2010), due to its anomalously low-strain character and apparently fresh-looking phenocrysts of quartz, potassium feldspar and hornblende that was coincidentally similar in composition to the Coldspring Mountain pluton. However the U-Pb age of 262.0 ± 1.9 Ma confirms it is also Permian, demonstrating significant strain variation across the Coldspring Mountain pluton, with increasing strain gradient from northwest to southeast. Mississippian-age zircon cores are consistent with the Sulphur Creek suite having intruded through Simpson Range plutons.

In the south of the study area, a U-Pb age of 204.9 ± 3.3 Ma (**Fig. 7A**) places a temporal constraint on Late Triassic magmatism associated with the Stikinia/Quesnellia arc. The age of the sample and the presence of magmatic epidote are characteristic of the Aishihik suite, which is predominantly Early Jurassic in age, but older latest Triassic phases are also reported (Johnston et al., 1996; Mortensen et al., 2000). Pennsylvanian-age cores from this sample suggest it may have intruded Klinkit assemblage rocks of the Yukon-Tanana terrane, hinting at a spatial association of these unrelated arc systems, and further expanding the known extent of the Klinkit assemblage.

Early Terrane Cooling

$^{40}Ar/^{39}Ar$ and (U-Th)/He thermochronology delineate the cooling and deformation history of the Yukon-Tanana terrane, and allude to its subsequent interaction with other arc systems and orogenic events related to its accretion to North America. **Figure 10** presents the temperature-time evolution of the Yukon-Tanana terrane in the McQuesten area, from arc magmatism and crystallisation of key units to cooling and exhumation through the upper-most crust.

$^{40}Ar/^{39}Ar$ ages from the Reid Lakes batholith are predominantly Mississippian, ca. 349 to 325 Ma (**Fig. 7B** and **Fig. 10**), and are interpreted as primary ages related to post-emplacement cooling. The youngest $^{40}Ar/^{39}Ar$ age of 325.1 ± 2.0 Ma on biotite demonstrates that the pluton underwent moderate cooling from the Pb closure temperature of zircon, >900 ^{o}C (Lee et al., 1997; Cherniak and Watson, 2000), to 300 ^{o}C in 25 m.y., at a rate of 25 ^{o}C $m.y.^{-1}$. The preservation of Mississippian cooling ages indicates the Reid Lakes complex was not subjected to subsequent metamorphism or heating in excess of 300 ^{o}C after emplacement. Mississippian $^{40}Ar/^{39}Ar$ ages are also preserved in eclogites associated with the Yukon-Tanana terrane in the Finlayson Lake area of southeast Yukon (**Fig. 1**; Erdmer et al., 1998; Devine et al., 2006), which would be proximal to the McQuesten area if the ca. 430 km of Eocene displacement on the Tintina fault were restored.

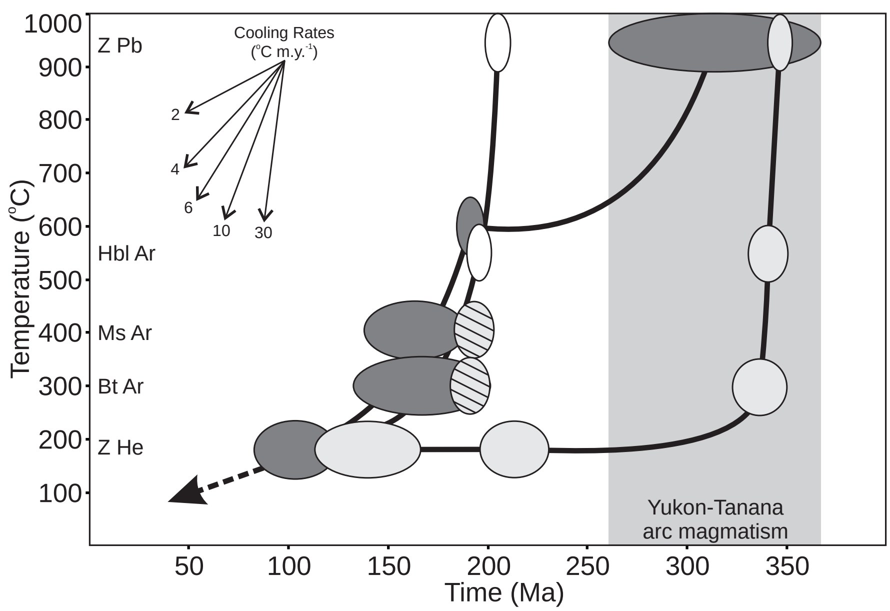

Figure 10. Temperature-time diagram showing the cooling paths for the three main belts of the McQuesten area. Note locus of activity in the Early Jurassic. Ellipses shown are: dark grey - typical deformed Yukon-Tanana terrane; light grey - Reid Lakes complex; cross-hatched - foliated Reid Lakes complex; white - Aishihik suite. Abbreviations on the left-hand side refer to nominal closure temperature: Z - zircon; Hbl - hornblende; Ms - muscovite; Bt - biotite.

Willow Lake Fault

The juxtaposition of unmetamorphosed and predominantly undeformed rocks of the Reid Lakes complex with polydeformed and metamorphosed rocks of typical Yukon-Tanana terrane is indicative of a significant structural discontinuity between the two domains. The Willow Lake fault, an apparently >100 km long northwest to southeast trending linear feature (Ryan et al., 2010), is defined mainly on the basis of a low intensity aeromagnetic anomaly that coincides with a topographic lineament (Colpron and Ryan, 2010). Ground-truth evidence of the fault is an isolated outcrop of highly-strained granitic rock with similar lithological attributes to the Reid Lakes complex. The rock exhibits up to protomylonite characteristics defined by dynamically recrystallised quartz ribbons with sutured grain boundaries (**Fig. 3I**; **Appendix 1**). Schistosity of this rock dips moderately to the northeast (Colpron and Ryan, 2010). Pervasive schistosity in deformed rocks immediately to the southwest of the Willow Lake Fault and the modest foliation observed in rocks on the south side of the Reid Lakes complex adjacent to the fault are generally synthetic to the protomylonite foliation, suggesting a diffuse zone of shear approximately 5 km wide that intensifies inward, and may have culminated with a narrow, brittle overprint.

Three biotite samples from the foliated zone of the Reid Lakes complex yielded $^{40}Ar/^{39}Ar$ ages ca. 193-191 Ma (**Fig. 8B**), interpreted as the age of foliation development associated with deformation along the Willow Lake fault. One of these samples (09RAYJR176A) lacks a foliation, but the sample location lies within the zone defined by other foliated outcrops. In the central and southern domains of the study area, $^{40}Ar/^{39}Ar$ ages are also predominantly Early Jurassic in age (**Fig. 10**). Omitting a slightly older age of ca. 197 Ma, the three oldest biotite cooling ages of ca. 190, 189, and 189 Ma are in excellent agreement with the U-Pb ages of metamorphic zircon overgrowths of ca. 193 Ma (**Fig. 10**).

This is interpreted as the maximum cooling age through biotite closure temperature for the package of deformed Yukon-Tanana rocks southwest of the Willow Lake Fault. Temporal variations in cooling ages for the deformed Yukon Tanana terrane rocks between ca. 197 and 165 Ma lack a spatial trend and do not seem to bear a relation to fault proximity (**Fig. 8B**), and may be attributed to intra-grain ^{40}Ar anomalies or subsequent localised thermal disturbances, such as reheating due to later nearby igneous activity or a localised hydrothermal event. For example, a sample in the central belt yielded a biotite ^{40}Ar/^{39}Ar age of ca. 90 Ma, which is considerably younger than the main population of Early Jurassic ages. Muscovite from the same sample yielded a discontiguous age spectrum with a total gas age of ca. 142 Ma, suggesting thermal disruption of the grains. It is interpreted that these ages were completely to partially reset by the extrusion of one of the numerous Cretaceous Carmacks volcanic plugs that dot the study area (Grond et al., 1984; Lowey et al., 1986; Hart, 1995; Colpron and Ryan, 2010). Alternatively, samples with younger ^{40}Ar/^{39}Ar ages may have occupied a lower structural position in the crust and subsequently took a longer period of time to cool and be exhumed through the respective cooling temperature. In the southwest of the study area, the plutonic Aishihik suite has ^{40}Ar/^{39}Ar ages that suggest rapid cooling at a rate of 65 ^{o}C m.y.$^{-1}$ from crystallisation at ca. 205 Ma through hornblende and biotite cooling at 196 Ma (**Fig. 10**). Fast cooling rates due to Jurassic exhumation are also reported for the Aishihik batholith to the south of the study area (Johnston et al., 1996). Rapid cooling may be expected for plutons that intruded at a high level in the crust, however the presence of epidote in this sample that may be magmatic in origin would suggest crystallisation at mid-crustal depths (Zen and Hammarstrom, 1984), such that rapid cooling and exhumation is likely driven by tectonic processes (Johnston et al., 1996; Mortensen et al., 2000). Irrespective of minor age variations, the ^{40}Ar/^{39}Ar ages prominently delineate two discrete domains:

Mississippian cooling ages preserved in the Reid Lakes complex in the northern part of the study area, and Early Jurassic cooling ages proximal to the fault and in the deformed Yukon Tanana terrane rocks and Aishihik suite.

In the McQuesten area, both the pattern of young against old cooling ages and juxta-position of rocks with contrasting metamorphic and deformation histories are observed, indicative of tectonic exhumation by normal faulting. The bimodal age distribution of $^{40}Ar/^{39}Ar$ ages on either side of the fault (**Fig. 8B**) and zircon recrystallisation ca. 193 Ma suggest cooling and probably exhumation of the entire block southwest of the fault in the Early Jurassic, at ca. 193 to 165 Ma. The northeast dipping foliation observed in Reid Lakes rocks close to the fault suggests a northeast dipping normal fault. In this configuration, the Reid Lakes complex forms the hanging-wall of the fault, and the polydeformed Yukon-Tanana belt is the footwall (**Fig. 9**).

As exhumation ensues, heat is advected upwards, compressing isotherms and increasing the geothermal gradient. Cooling rates increase sharply because rock is exhumed through the compressed isotherms, representing a greater temperature change, over a shorter distance (Foster and John, 1999). This is evident in the Willow Lake fault: footwall rocks cooled at a rate of 4 ^{o}C $m.y.^{-1}$ between 950-400 ^{o}C, increasing to 10 ^{o}C $m.y.^{-1}$ between 400-300 ^{o}C (**Fig. 10**).

In collisional settings, syn- or post-tectonic extension and crustal thinning may occur in response to vertical thickening, crustal loading, and tectonic burial at the orogenic welt. Slab retreat may also cause extension in the overriding plate (Royden, 1993; Waschbusch and Beaumont, 1996; Ring et al., 1999). Considering a scenario where the Slide Mountain Ocean crust was still subducting beneath the Yukon-Tanana terrane in the Late Triassic or Early Jurassic (Berman et al., 2007), distal orogenesis as the Yukon-Tanana arc converged with North America and rollback and eventual foundering of the remaining Slide Mountain slab likely contributed to extension and tectonic exhumation of the Klondike plateau and Yukon-Tanana upland. Alternatively, if the Yukon-Tanana terrane was accreted to North America in the Permo-Triassic (Beranek and Mortensen, 2011), retreat of an eastward-dipping subducting slab beneath the western North American margin may also have been responsible for extension and exhumation in the Klondike plateau and Yukon-Tanana upland in the Jurassic.

Low-Temperature Cooling

In the footwall of the Willow Lake fault, zircon helium cooling ages range from ca. 179 to 90 Ma (**Fig. 7C** and **Fig. 8C**). The ca. 179 Ma cooling age is anomalously old relative to other samples from the deformed Yukon-Tanana domain, which are Early to Late Cretaceous in age. The sample locale of the older age is bounded by two subparallel north-south trending dextral strike-slip faults that propagate to the south into a northwest-southeast trending dextral fault (**Fig. 2**; sample 09RAYJR178A), thought to be a northern extension of the Teslin fault system (Colpron and Ryan, 2010). The sliver of rocks bounded by the fault splays may have been exhumed earlier to 180 ^{o}C if there was a transtensional component of fault displacement. The Teslin fault is presumed to have been active during the Jurassic (Snyder et al., 2005), which coincides with the age of this sample. Ignoring the anomalously old age, the remaining (U-Th)/He ages southwest of the Willow Lake fault (i.e. the footwall) delineate exhumation through 180 ^{o}C from ca. 113 to 90 Ma (**Fig. 10**). In the hanging-wall of the Willow Lake fault, the volcanogenic component of the Reid Lakes complex yielded ca. 216-214 Ma (U-Th)/He cooling ages, suggesting Late Triassic cooling through the uppermost crust to 180 ^{o}C. This is followed by Late Jurassic to Early Cretaceous (ca. 158 to 130 Ma) cooling of the structurally lower plutonic phase of the Reid Lakes complex.

The low-temperature thermal evolution constrained by zircon (U-Th)/He ages also delineates two distinct domains of cooling ages that mirrors the distribution of $^{40}Ar/^{39}Ar$ ages (**Fig. 8C**). Cooling of footwall rocks through the He closure temperature may have been accommodated by the termination of heat advection in the footwall subsequent to fault activity, and stabilisation of isotherms which were compressed during tectonic exhumation along the Willow Lake fault (Stockli, 2005). Alternatively, the asymmetric distribution of zircon He ages and the time lag between Reid Lakes complex and Yukon-Tanana rocks reaching the uppermost crust may be suggestive of renewed Mid-Cretaceous fault activity or prolonged fault displacement. Cessation of displacement on the Willow Lake Fault is constrained by a body of Late Cretaceous Carmacks Group volcanic rocks that straddles both sides of the fault (Colpron and Ryan, 2010), which is in excellent agreement with the youngest (U-Th)/He age of ca. 90 Ma. However the slow rate of cooling 1.5 ^{o}C m.y.$^{-1}$ observed in both the footwall and hanging-wall rocks between 300 and 180 ^{o}C is more typical of erosion rates or post-tectonic relaxation of an overly steepened geothermal gradient, as opposed to tectonic uplift (Ring et al., 1999). In the Stewart River area (**Fig. 2**), Ryan et al. (2003) noted that the base of the Carmacks Group coincides with Eocene and younger erosional surfaces, postulating that the paleotopography of the region had been maintained since the Eocene. This observation is in agreement with our assertion that the McQuesten area had undergone exhumation through the uppermost crust by the Late Cretaceous.

In the Freegold Mountain area of the Dawson Range in west-central Yukon, Late Cretaceous zircon (U-Th)/He ages spanning ca. 89 to 66 Ma are reported (Betsi et al., 2012). These ages are interpreted as the result of slow cooling due to uplift and erosion following mineralisation and hydrothermal activity. Some ages from this study were also rejected due to the effects of proximal Late Cretaceous intrusions. In the west of the Dawson Range, Late Cretaceous gold-bearing quartz veins are reported to have been emplaced ca. 93 to 92 Ma into ca. 100 to 96 Ma felsic to intermediate intrusions in the Moosehorn Range (Joyce, 2002, and references therein). The asymmetric distribution of zircon (U-Th)/He cooling ages across the Willow Lake fault is more likely indicative of differential cooling and erosion related to tectonism as opposed to hydrothermal activity, which presumably would reset cooling ages both in the hanging-wall and the footwall of the fault. However the potential still exists for resetting of the zircon (U-Th)/He ages in the McQuesten area by hydrothermal activity, and may indicate areas prospective for mineralisation.

Following on the work of Dodson (1973), Reiners and Farley (2001) found a correlation between age and apatite grain size based on the ability of larger crystals to retain a larger proportion of radiogenic He, particularly in an environment where the rocks have resided in the partial He retention zone for long periods of time. This yields anomalously younger ages for smaller crystals; data collected in this study do not reflect this positive correlation as the maximum and minimum grain sizes show no relation to the calculated age of the grain.

Using the LA-ICP-MS technique to measure the bulk U and Th concentrations lacks the precision of the conventional isotope dilution method. The advantages are the ability to obtain SEM images of analysed grains to assess homogeneity and overall quality, and to direct LA-ICP-MS transects or spot analyses to avoid inclusions or other grain imperfections. Although the (U-Th)/He ages lack the precision of conventional U-Pb and $^{40}Ar/^{39}Ar$ dating methods, for the purpose of this study they clearly delineate an asymmetry of cooling that mimics the same trend as the $^{40}Ar/^{39}Ar$ ages. In conjunction with U-Pb and $^{40}Ar/^{39}Ar$ ages, anomalous ages of both individual zircons and combined (U-Th)/He ages can be assessed and identified, allowing for greater accuracy and confidence in the low temperature thermochronological dates. When integrated with more conventional dating methods, the results of this study demonstrate the power of (U-Th)/He dating methods to constrain the low temperature thermochronological evolution of tectonic domains.

TECTONIC SYNTHESIS

These new data place the McQuesten area in a regional framework consistent with published P-T-t evolutions in the Stewart River area (Berman et al., 2007). The current model for the active phase of the Yukon-Tanana terrane details Mid-Paleozoic arc construction and opening of the Slide Mountain back-arc basin under an east-dipping subduction zone outboard of the western margin of North America. In the Middle Permian, the polarity of subduction flipped to westward dipping, initiating consumption of the Slide Mountain Ocean. Previous studies suggest complete subduction of the Slide Mountain Ocean by the Late Triassic, followed by accretion of the Yukon-Tanana terrane to western North America. Subduction subsequently flipped again, leading to eastward dipping subduction of the paleo-Pacific Ocean (Mortensen, 1992; Dusel-Bacon et al., 1995; Dusel-Bacon et al., 2002; Dusel-Bacon et al., 2004; Devine et al., 2006; Murphy et al., 2006; Nelson et al., 2006; Piercey et al., 2006; Berman et al., 2007). A recent study, however, suggests that the Slide Mountain Ocean was consumed by the Late Permian, and accretion of the Yukon-Tanana terrane occurred during the Latest Permian to Early Triassic Klondike orogeny (Beranek and Mortensen, 2011). Reconciliation of the timing of accretion is beyond the scope of this study, although it has ramifications for the mechanism and driving force of Early Jurassic exhumation of the Klondike plateau.

During the Devono-Mississippian, the initiation of east-dipping subduction of oceanic lithosphere offshore of the western North America margin caused ca. 365-360 Ma incipient arc magmatism that intruded the thinned siliciclastic western margin of North America (Dusel-Bacon et al., 2002; Dusel-Bacon et al., 2004; Colpron et al., 2006*b*; Dusel-Bacon et al., 2006; Ruks et al., 2006; Berman et al., 2007). Incipient subduction-related magmatism is evident in the McQuesten area by ca. 363 Ma intrusion of the Simpson Range suite into the Snowcap assemblage during the Ecstall cycle (Colpron et al., 2006*a*). A west-facing arc and back-arc pair were the locus for igneous activity and sediment deposition at this time (Piercey et al., 2006). During the Late Devonian back-arc rifting widened the basin that became the Slide Mountain Ocean (Nelson et al., 2006; Berman et al., 2007).

Rifting and expansion of the Slide Mountain Ocean is concurrent with Finlayson arc magmatism (Colpron et al., 2006*a*), represented by emplacement of the Reid Lakes batholith ca. 360 to 342 Ma, and coeval extrusion of its volcanic carapace. The Reid Lakes complex spans both the Finlayson and Wolverine magmatic cycles (Colpron et al., 2006*a*; Nelson et al., 2006; Piercey et al., 2006). The batholith underwent moderate cooling at mid-crustal conditions ca. 325 Ma. The Reid Lakes complex was not affected by Late Permian metamorphism and deformation (Berman et al., 2007; Beranek and Mortensen, 2011) suggesting it occupied a high structural level in the crust at this time.

Renewed arc magmatism of the Little Salmon magmatic cycle is represented by deposition of volcanic and volcaniclastic rocks of the Klinkit assemblage ca. 322 Ma in the Klondike plateau, although magmatism of this age is more prolific in the southerly extent of the Yukon-Tanana terrane (**Fig. 1**; Mihalynuk et al., 2000; Roots et al., 2002; Simard et al., 2003; Piercey et al., 2006). This may reflect only localised arc activity or a spatial migration of peak magmatic activity. At this time, the Yukon-Tanana terrane was part of an intra-oceanic island arc system, separated from the North American margin by the expanding Slide Mountain Ocean (Colpron et al., 2006*a*; Nelson et al., 2006). Cessation of magmatism and a prolonged period of non-deposition and/or erosion followed the demise of the Klinkit arc at the end of the Early Permian, until widespread arc magmatism resumed ca. 265-253 Ma

(Nelson et al., 2006; Berman et al., 2007).

The Klondike cycle represents the final pulse of active arc magmatism associated with the Yukon-Tanana terrane, which is evident in the McQuesten area by multiple monzogranite intrusions of the Sulphur Creek suite ca. 262 Ma. Magmatism is marked by a change to westward dipping subduction of the Slide Mountain Ocean beneath the Yukon-Tanana arc, concurrent with metamorphism and deformation resulting from arc shortening (Nelson et al., 2006; Berman et al., 2007; Beranek and Mortensen, 2011).

Late Triassic to Early Jurassic magmatism was widespread along the northern Cordillera (Mortensen, 1992; Tafti and Mortensen, 2004), reflected in the study area by extrusion of Triassic volcanic rocks of the Semenof formation (Colpron and Ryan, 2010) and emplacement of the Aishihik suite at ca. 205 Ma. Mortensen (1992) and Tafti and Mortensen (2004) suggest that burial, low-pressure metamorphism and deformation ca. 198-195 Ma were immediately followed by rapid exhumation. In the McQuesten area, pre-exhumation burial and metamorphism is also suggested by ca. 209-186 Ma zircon overgrowths and metamorphic rims, subsequent exhumation is indicated by the large population of ca. 193-165 Ma mica $^{40}Ar/^{39}Ar$ ages, and cooling and exhumation of the Aishihik suite from >900 ^{o}C at ca. 205 Ma to 300 ^{o}C by ca. 196 Ma. Our ages are in agreement with regional Early Jurassic cooling ages in the Yukon-Tanana upland of eastern Alaska (Dusel-Bacon et al., 1995; Dusel-Bacon et al., 2002) and the Stewart River area to the east (Villeneuve et al., 2003) suggesting widespread exhumation at that time.

In the Stewart River area (**Fig. 1**) Berman et al. (2007) invoked a metamorphic event ca. 195-187 Ma which is interpreted as the result of tectonic imbrication and crustal thickening due to collision of the Yukon-Tanana terrane with North America. Following accretion of the Yukon-Tanana terrane via the Inconnu thrust (**Fig. 1**), an east-dipping subduction zone developed under the western margin of North America. $^{40}Ar/^{39}Ar$ ages ca. 185-175 Ma (Villeneuve et al., 2003) are attributed to rollback of the downgoing slab in a sinistral transtensional regime, leading to displacement and exhumation of the outboard regions of the terrane (Berman et al., 2007). Although ground-truth evidence of such a structure was not found in the Stewart River area to explain the data, it seems highly probable that the Willow Lake fault is a segment of such a transtensional structure. Extension and exhumation along the fault may have been caused by: collapse of the orogen subsequent to accretion of the Yukon-Tanana terrane along the Inconnu thrust fault (Murphy et al., 2006; Berman et al., 2007), oblique convergence during terrane accretion (Johnston et al., 1996), rollback and retreat of the subducting slab (Royden, 1993; Waschbusch and Beaumont, 1996; Berman et al., 2007), or a combination of these processes. In the event that the Yukon-Tanana terrane was accreted to North America during the Late Permian to Early Triassic, another mechanism independent of Yukon-Tanana accretion must be sought to resolve regional Early Jurassic exhumation of the Klondike plateau. One such mechanism may be retreat of an east-dipping slab beneath the western margin of North America.

CONCLUSIONS

The extensive dataset of geochronological and thermochronological ages presented here elucidate the Mid-Paleozoic to Late Cretaceous tectonothermal history of the Yukon-Tanana terrane in the northern Cordillera. These ages conform remarkably well to ages of previous studies in the terrane, and their interpreted tectonic events. This data chronicles the birth and death of arc magmatism in the Yukon-Tanana terrane, its interaction with the Stikinia/Quesnellia arcs, and subsequent accretion to western North America. Early Jurassic cooling ages across the Klondike plateau and the Yukon Tanana upland to the west suggest regional exhumation of an extensive fault block from mid-crustal levels.

1. Middle to Late Paleozoic U-Pb ages constrain arc magmatism of the composite Yukon-Tanana terrane. In the McQuesten area, the earliest phase of magmatism occurred ca. 363 Ma during the Ecstall cycle. Rocks of the Klinkit assemblage yielded a ca. 322 Ma U-Pb age. Permian magmatism associated with the Sulphur Creek suite yielded three identical ca. 262 Ma ages. The Reid Lakes complex, a product of Finlayson and Wolverine cycle magmatism, is unmetamorphosed and predominantly undeformed. The Reid Lakes batholith was emplaced from ca. 360 to 342 Ma, coeval with extrusion of the overlying volcanic package. A subvolcanic to intervolcanic sandstone yielded a detrital zircon profile indicative of a North American source. The youngest grains in the sample are ca. 446 Ma, suggesting the sandstone is devoid of any syn-volcanic Yukon-Tanana arc detritus.

2. Mississippian $^{40}Ar/^{39}Ar$ cooling ages ca. 349 to 325 Ma from biotite and hornblende of the Reid Lakes complex suggest a moderate rate of cooling for the batholith. Three biotite samples exhibiting mild to high strain yielded younger ca. 193 to 191 Ma $^{40}Ar/^{39}Ar$ ages. A belt of polydeformed and up to amphibolite facies rocks of the Yukon-Tanana terrane yielded ca. 197 to 165 Ma $^{40}Ar/^{39}Ar$ ages.

3. The Willow Lake fault is interpreted as a normal fault that juxtaposes primarily undeformed and unmetamorphosed rocks of the Reid Lakes complex in the hanging-wall with polydeformed and greenschist to amphibolite facies rocks of the Yukon-Tanana terrane in the footwall. Early Jurassic fault displacement is constrained by the extensive dataset of $^{40}Ar/^{39}Ar$ ages in the footwall and three ages in the hanging-wall proximal to the fault, in addition to ca. 193 Ma zircon overgrowths and patches of recrystallised zircon with low Th/U ratios. We suggest extension along the Willow Lake fault is due to orogenic collapse during or subsequent to contraction and thrusting associated with the collision and accretion of the

Yukon-Tanana terrane to North America.

4. Zircon (U-Th)/He ages from the Reid Lakes complex reflect ca. 216 to 214 Ma cooling through the uppermost crust (180 ^{o}C) of structurally higher volcanogenic rocks, followed by ca. 159 to 130 Ma cooling of the deeper-seated plutonic phase. Yukon-Tanana rocks that yielded Early Jurassic $^{40}Ar/^{39}Ar$ ages yielded ca. 113 to 90 Ma zircon (U-Th)/He ages.

5. Magmatism of the Aishihik suite of the Stikinia/Quesnellia arc is dated at ca. 205 Ma in the study area. Predominantly Pennsylvanian-age xenocrystic cores in this sample suggest it may have intruded through the Klinkit assemblage. $^{40}Ar/^{39}Ar$ cooling ages of the Aishihik suite ca. 205 – 196 Ma in conjunction with the presence of epidote that appears to be magmatic suggest rapid cooling and exhumation from mid-crustal levels, further illustrating the pervasiveness of the Jurassic event that exhumed the central belt of Yukon-Tanana rocks.

REFERENCES

Beranek, L. P., and Mortensen, J. L., 2011, The timing and provenance of the Late Permian Klondike orogeny in northwestern Canada and arc-continent collision along western North America: Tectonics, v. 30, TC5017, doi:10.1029/2010TC002849.

Berman, R. G., Ryan, J. J., Gordey, S. P., and Villeneuve, M., 2007, Permian to Cretaceous polymetamorphic evolution of the Stewart River region, Yukon-Tanana terrane, Yukon, Canada: P-T evolution linked with in situ SHRIMP monazite geochronology: Journal of Metamorphic Geology, v. 25, p. 803-287.

Betsi, T. B., Lentz, D., McInnes, B., and Evans, N. J., 2012, Emplacementages and exhumation rates for intrusion-hosted Cu-Mo-Sb-Au mineral systems at Freegold Mountain (Yukon, Canada): assessment from U-Pb, Ar-Ar, and (U-Th)/He geochronometers: Canadian Journal of Earth Sciences, v. 49, p. 653-670.

Bostock, H. S., 1964, Geology, McQuesten, Yukon Territory: Geological Survey of Canada Map 1143A, scale 1:253 400, 1 sheet.

Boyce, J. W., Hodges, K. V., Olszewski, W. J., Jercinovic, M. J., Carpenter, B. D., and Reiners, P. W., 2006, Laser microbe (U-Th)/He geochronology: Geochimica et Cosmochimica Acta, v. 70, p. 3031-3039.

Cherniak, D. J., and Watson, E. B., 2000, Pb diffusion in zircon: Chemical Geology, v. 172, p. 5-24.

Ciolkiewicz, W., in preparation, Late Cretaceous tectonics and metallogeny in west-central Yukon and east-central Alaska, [Ph. D. Thesis]: Vancouver, University of British Columbia.

Colpron, M., and Ryan, J. J., 2010, Bedrock geology of southwest McQuesten (NTS 115P) and part of northern Carmacks (NTS 115I) map area, *in* MacFarlane, K. E., Weston, L. H., and Blackburn, L. R., eds., Yukon Exploration and Geology 2009, Yukon Geological Survey, p. 159-184.

Colpron, M., Gladwin, K., Johnston, S. T., Mortensen, J. K., and Gehrels, G. E., 2005, Geology and juxtaposition history of the Yukon-Tanana, Slide Mountain, and Cassiar terranes in the Glenlyon area of central Yukon: Canadian Journal of Earth Sciences, v. 42, p. 1431-1448.

Colpron, M., Nelson, J. L., and Murphy, D. C., 2006a, A tectonostratigraphic framework for the pericratonic terranes of the northern Canadian Cordillera, *in* Colpron, M., and Nelson, J. L., eds., Paleozoic Evolution and Metallogeny of Pericratonic Terranes at the Ancient Pacific Margin of North America, Canadian and Alaskan Cordillera: Geological Association of Canada, Special Paper No. 45, p. 1-23.

Colpron, M., Mortensen, J. K., Gehrels, G. E., and Villeneuve, M., 2006b, Basement complex, Carboniferous magmatism and Paleozoic deformation in Yukon-Tanana terrane of central Yukon: Field, geochemical and geochronological constraints from Glenlyon map area, *in* Colpron, M., and Nelson, J. L., eds., Paleozoic Evolution and Metallogeny of Pericratonic Terranes at the Ancient Pacific Margin of North America, Canadian and Alaskan Cordillera: Geological Association of Canada, Special Paper No. 45, p. 131-151.

Colpron, M., Nelson, J. L., and Murphy, D. L., 2007, Northern Cordilleran terranes and their interactions through time: Geological Society of America Today, v. 17, p. 4-10.

Coney, P. J., Jones, D. L., and Monger, J. W. H., 1980, Cordilleran suspect terranes: Nature, v. 288, p. 329-333.

Davis, G. H., and Coney, P. J., 1979, Geologic development of the Cordilleran metamorphic core complexes: Geology, v. 7, p. 120-124.

Devine, F., Carr, S. D., Murphy, D. C., Davis, W. J., Smith, S., and Villeneuve, M., 2006, Geochronological and geochemical constraints on the origin of the Klatsa metamorphic complex: Implications for Early Mississippian high-pressure metamorphism within Yukon-Tanana terrane, *in* Colpron, M., and Nelson, J. L., eds., Paleozoic Evolution and Metallogeny of Pericratonic Terranes at the Ancient Pacific Margin of North America, Canadian and Alaskan Cordillera: Geological Association of Canada, Special Paper No. 45, p. 107-130.

Di Vincenzo, G., Viti, C., and Rocchi, S., 2003, The effect of chlorite interlayering on 40Ar-39Ar biotite dating: an 40Ar-39Ar laser probe and TEM investigations of variably chloritised biotites: Contributions to Mineralogy and Petrology, v. 145, p. 643-568.

Dodson, M. H., 1973, Closure temperature in cooling geochronological and petrological systems: Contributions to Mineralogy and Petrology, v. 40, p. 259-274.

Dusel-Bacon, C., and Williams, I. S., 2009, Evidence for prolonged mid-Paleozoic plutonism and ages of crustal sources in east-central Alaska from SHRIMP U-Pb dating of syn-magmatic, inherited, and detrital zircon: Canadian Journal of Earth Sciences, v. 46, p. 21-39.

Dusel-Bacon, C., Hansen, V. L., and Scala, J. A., 1995, High-pressure amphibolite facies dynamic metamorphism and the Mesozoic tectonic evolution of an ancient continental margin, east-central Alaska: Journal of Metamorphic Geology, v. 13, p. 9-24.

Dusel-Bacon, C., Lanphere, M. A., Sharp, W. D., Layer, P. W., and Hansen, V. L., 2002, Mesozoic thermal history and timing of structural events for the Yukon-Tanana Upland, east-central Alaska: 40Ar/39Ar data from metamorphic and plutonic rocks: Canadian Journal of Earth Sciences, v. 39, p. 1013-1051.

Dusel-Bacon, C., Wooden, J. L., and Hopkins, M. J., 2004, U-Pb zircon and geochemical evidence for bimodal mid-Paleozoic magmatism and syngenetic base-metal mineralization in the Yukon-Tanana terrane, Alaska: Geological Society of America Bulletin, v. 116, p. 989-1015.

Dusel-Bacon, C., Hopkins, M. J., Mortensen, J. K., Dashevsky, S. S., Bressler, J. R., and Day, W. C., 2006, Paleozoic tectonic and metallogenic evolution of the pericratonic rocks of east-central Alaska and adjacent Yukon, *in* Colpron, M., and Nelson, J. L., eds., Paleozoic Evolution and Metallogeny of Pericratonic Terranes at the Ancient Pacific Margin of North America, Canadian and Alaskan Cordillera: Geological Association of Canada, Special Paper No. 45, p. 25-74.

Erdmer, P., 1982, Nature and significance of the metamorphic minerals and structures of the cataclastic allochthonous rocks in the White Mountains, Last Peak, and Fire Lake areas, Yukon Territory [Ph.D. Thesis]: Kingston, Queen's University, 254 p.

Erdmer, P., Ghent, E. D., Archibald, D. A., and Stout, M. Z., 1998, Paleozoic and Mesozoic high-pressure metamorphism at the margin of ancestral North America in central Yukon: Geological Society of America Bulletin, v. 110, p. 615-629.

Erdmer, P., Moore, J. M., Heaman, L., Thompson, R. I., Daughtry, K. L., and Creaser, R. A., 2002, Extending the ancient margin outboard in the Canadian Cordillera: record of Proterozoic crust and Paleocene regional metamorphism in the Nicola horst, southern British Columbia: Canadian Journal of Earth Sciences, v. 39, p. 1605-1623.

Farley, K. A., Shuster, D. L., and Ketcham, R. A., 2011, U and Th zonation in apatite observed by laser ablation ICPMS and implications for the (U-Th)/He system: Geochimica et Cosmochimica Acta, v. 75, p. 4515-4530.

Foster, D. A., and John, B. E., 1999, Quantifying tectonic exhumation in an extensional orogen with thermochronology: examples from the southern Basin and Range province, *in* Ring, U., Brandon, M. T., Lister, G. S., and Willett, S. D., eds., Exhumation Processes: Normal Faulting, Ductile Flow, and Erosion: Geological Society of London, Special Publications, v. 154, p. 343-364.

Foster, H. L., Keith, T. E. C., and Menzie, W. D., 1994, Geology of the Yukon-Tanana area of east-central Alaska (Chapter 6), *in* Plafker, G., and Berg, H. C., eds., The Geology of Alaska: Geological Society of America, The Geology of North America, v. G-1, p. 205-240.

Gabrielse, H., Murphy, D. C., and Mortensen, J. K., 2006, Cretaceous and Cenozoic dextral orogen-parallel displacements, magmatism, and paleogeography, north-central Canadian Cordillera, *in* Haggart, J. W., Enkin, R. J., and Monger, J. W. H., eds., Paleogeography of the North American Cordillera: Evidence for and against large-scale displacements: Geological Association of Canada, Special Paper No. 46, p. 255-276.

Gehrels, G. E., and Ross, G. M., 1998, Detrital zircon geochronology of Neoproterozoic to Permian miogeoclinal strata in British Columbia and Alberta: Canadian Journal of Earth Sciences, v. 35, p. 1380-1401.

Gehrels, G. E., Dickinson, W. R., Ross, G. M., Stewart, J. H., and Howell, D. G., 1995, Detrital zircon reference for Cambrian to Triassic miogeoclinal strata of western North America: Geology, v. 23, p. 831-834.

Gehrels, G. E., Johnsson, M. J., and Howell, D. G., 1999, Detrital zircon geochronology of the Adams Argillite and Nation River Formation, east-central Alaska, U. S. A.: Journal of Sedimentary Research, v. 69, p. 135-144.

Gleeson, T. P., Friedman, R. M., and Wahl, K., 2000, Stratigraphy, structure, geochronology and provenance of the Logjam Area, northwestern British Columbia (NTS 104O/14W): British Columbia Geological Survey, Geological Fieldwork 1999, Paper 2000-1, p. 297-306.

Grond, H. C,. Churchill, S. J., Armstrong, R. L., Harakal, J. E,. and Nixon, G. T., 1984, Late Cretaceous age of the Hutshi, Mount Nansen, and Carmacks groups, southwestern Yukon Territory and northwestern British Columbia: Canadian Journal of Earth Sciences, v. 21, p. 554-558.

Hansen, V. L., and Dusel-Bacon, C., 1998, Structural and kinematic evolution of the Yukon-Tanana upland tectonites, east-central Alaska: A record of late Paleozoic to Mesozoic crustal assembly: Geological Society of America Bulletin, v. 110, p. 211-230.

Hansen, V. L., Heizler, M. T., and Harrison, T. M., 1991, Mesozoic thermal evolution of the Yukon-Tanana composite terrane: New evidence from 40Ar/39Ar data: Tectonics, v. 10, p. 51-76.

Harrison, T. M., 1981, Diffusion of 40Ar in hornblende: Contributions to Mineralogy and Petrology, v. 78, p. 324-331.

Harrison, T. M., Duncan, I., and McDougall, I., 1985, Diffusion of 40Ar in biotite: Temperature, pressure, and compositional effects: Geochimica et Cosmochimica Acta, v. 49, p. 2461-2468.

Harrison, T. M., Célérier, J., Aikman, A. B., Hermann, J., and Heizler, M. T., 2009, Diffusion of 40Ar in muscovite: Geochimica et Cosmochimica Acta, v. 73, p. 1039-1051.

Hart, C. J. R., 1995, Magmatic and tectonic evolution of the Intermontane Superterrane and Coast Plutonic Complex in southern Yukon Territory [M. Sc. Thesis]: Vancouver, University of British Columbia, 198 p.

Hood, S., Hickey, K., Colpron, M. and Mercer, B., 2009. High-grade hydrothermal copper-gold mineralization in foliated granitoids at the Minto mine, central Yukon, *in* Weston, L. H., Blackburn, L. R., and Lewis, L. L., eds., Yukon Exploration and Geology 2008, Yukon Geological Survey, p. 137-146.

Hoskin, P. W. O., and Schaltegger, U., 2003, The composition of zircon and igneous and metamorphic petrogenesis, *in* Hanchar, J., and Hoskin, P. W. O., eds., Zircon: Reviews in Mineralogy and Geochemistry, v. 53, p. 27-62.

Hourigan, J. K., Reiners, P. W., and Brandon, T. M., 2005, U-Th zonation-dependent alpha-ejection in (U-Th)/He chronometry: Geochimica et Cosmochimica Acta, v. 69, p. 3349-3365.

Johnston, S. T., Mortensen, J. K., and Erdmer, P., 1996, Igneous and metaigneous age constraints for the Aishihik metamorphic suite, southwest Yukon: Canadian Journal of Earth Sciences, v. 33, p. 1543-1555.

Joyce, N. L. J., 2002, Geologic setting, nature, and structural evolution of intrusion-hosted Au-bearing quartz veins at the Longline occurrence, Moosehorn Range area, west-central Yukon Territory, [M. Sc. Thesis]: Vancouver, University of British Columbia, 199 p.

Ketcham, R. A., 2005, Forward and inverse modeling of low-temperature thermochronometry data, *in* Reiners, P. W., and Ehlers, T. A., eds., Low Temperature Thermochronology: Techniques, Interpretations, and Applications: Reviews in Mineralogy and Geochemistry, v. 58, p. 275-314.

Lee, J. K. W., Williams, I. S., and Ellis, D. J., 1997, Pb, U and Th diffusion in natural zircon: Nature, v. 390, p. 159-162.

Lister, G. S., and Davis, G. A., 1989, The origin of metamorphic core complexes and detachment faults formed during Tertiary continental extension in the northern Colorado River region, U. S. A.: Journal of Structural Geology, v. 11, p. 65-94.

Ludwig, K.R., 2003, User's manual for Isoplot/Ex rev. 3.00, A geochronological toolkit for Microsoft Excel: Berkeley Geochronology Center, Special Publication No. 4, 74 p.

Lowey, G. W., Sinclair, W. D., and Hills, L. V., 1986, Additional K-Ar isotopic dates for the Carmacks Group (Upper Cretaceous), west central Yukon: Canadian Journal of Earth Sciences, v. 23, p. 1857-1859.

Mihalynuk, M. G., Nelson, J. A., Roots, C. F., Friedman, R. M., and de Keijzer, M., 2000, Ancient Pacific Margin Part III: Regional geology and mineralization of the Big Salmon Complex (NTS 104N/9E,16 & 104O/12,13,14W): British Columbia Geological Survey, Geological Fieldwork 1999, Paper 2000-1, p. 27-46.

Monger, J. W. H., Souther, J. G., and Gabrielse, H., 1972, Evolution of the Canadian Cordillera: A plate-tectonic model: American Journal of Science, v. 272, p. 577-602.

Mortensen, J. K., 1992, Pre-mid Mesozoic tectonic evolution of the Yukon-Tanana terrane, Yukon and Alaska: Tectonics, v. 11, p. 836-853.

Mortensen, J. K., 2009, U-Pb age and geochemical studies of Mississippian and Cretaceous plutonic rocks in south-central McQuesten map area, Yukon, *in* Weston, L. H., Blackburn, L. R., and Lewis, L. L., eds., Yukon Exploration and Geology 2008: Yukon Geological Survey, p. 187-194.

Mortensen, J. K., Emon, K., Johnston, S. T., and Hart, C. J. R., 2000, Age, geochemistry, paleotectonic setting and metallogeny of late Triassic-early Jurassic intrusions in the Yukon and eastern Alaska: A preliminary report, *in* Esmond, D. S., and Weston, L. H., eds., Yukon Exploration and Geology 1999: Exploration and Geological Services Division, Yukon, Indian and Northern Affairs Canada, p. 139- 144.

Murphy, D. C., Colpron, M., Roots, C. F., Gordey, S. P., and Abbott, J. G.., 2002, Finlayson Lake Targeted Geoscience Initiative (southeastern Yukon), Part 1: Bedrock geology, *in* Esmond, D. S., Weston, L. H., and Lewis, L. L., eds., Yukon Exploration and Geology 2001: Exploration and Geological Services Division, Yukon, Indian and Northern Affairs Canada, p. 189-207.

Murphy, D. C., Mortensen, J. K., Piercey, S. J., Orchard, M. J., and Gehrels, G. E., 2006, Mid-Paleozoic to early Mesozoic tectonostratigraphic evolution of Yukon-Tanana and Slide Mountain terranes and affiliated overlap assemblages, Finlayson Lake massive sulphide district, southeastern Yukon, *in* Colpron, M., and Nelson, J. L., eds., Paleozoic Evolution and Metallogeny of Pericratonic Terranes at the Ancient Pacific Margin of North America, Canadian and Alaskan Cordillera: Geological Association of Canada, Special Paper No. 45, p. 75-105.

Nelson, J. L., and Friedman, R., 2004, Superimposed Quesnel (Late Paleozoic-Jurassic) and Yukon-Tanana (Devonian-Mississippian) arc assemblages, Cassiar Mountains, northern British Columbia: field, U-Pb, and igneous petrochemical evidence: Canadian Journal of Earth Sciences, v. 41, p. 1201-1235.

Nelson, J., and Gehrels, G., 2007, Detrital zircon geochronology and provenance of the southeastern Yukon-Tanana terrane: Canadian Journal of Earth Sciences, v. 44, p. 297-316.

Nelson, J. L., Colpron, M., Piercey, S. J., Dusel-Bacon, C., Murphy, D. C., and Roots, C. F., 2006, Paleozoic tectonic and metallogenic evolution of pericratonic terranes in Yukon, northern British Columbia and eastern Alaska, *in* Colpron, M., and Nelson, J. L., eds., Paleozoic Evolution and Metallogeny of Pericratonic Terranes at the Ancient Pacific Margin of North America, Canadian and Alaskan Cordillera: Geological Association of Canada, Special Paper No. 45, p. 323-360.

Oliver, D. H., 1996, Structural, kinematic, and thermochronologic studies of the Teslin suture zone, south-central Yukon Territory [Ph.D. Thesis]: Dallas, Southern Methodist University, 231 p.

Piercey, S. J., and Colpron, M., 2009, Composition and provenance of the Snowcap assemblage, basement to the Yukon-Tanana terrane, northern Cordillera: Implications for Cordilleran crustal growth: Geosphere, v. 5, p. 439-464.

Piercey, S. J., Nelson, J. A., Colpron, M., Dusel-Bacon, C., Simard, R. –L., and Roots, C. F., 2006, Paleozoic magmatism and crustal recycling along the ancient Pacific margin of North America, northern Cordillera, *in* Colpron, M., and Nelson, J. L., eds., Paleozoic Evolution and Metallogeny of Pericratonic Terranes at the Ancient Pacific Margin of North America, Canadian and Alaskan Cordillera: Geological Association of Canada, Special Paper No. 45, p. 281-322.

Reiners, P. W., 2005, Zircon (U-Th)/He Thermochronometry, *in* Reiners, P.W., and Ehlers, T.A., eds., Low Temperature Thermochronology: Techniques, Interpretations, and Applications: Reviews in Mineralogy and Geochemistry, v. 58, p. 151-179.

Reiners, P.W., and Farley, K.A., 2001, Influence of crystal size on apatite (U-Th)/He thermochronology: an example from the Bighorn Mountains, Wyoming: Earth and Planetary Science Letters, v. 188, p. 413-420.

Reiners, P. W., Spell, T. L., Nicolescu, S., and Zanetti, K. A., 2004, Zircon (U-Th)/He thermochronometry: He diffusion and comparisons with 40Ar/39Ar dating: Geochimica et Cosmochimica Acta, v. 68, p. 1857-1887.

Ring, U., Brandon, M. T., Willett, S. D., and Lister, G. S., 1999, Exhumation processes, *in* Ring, U., Brandon, M. T., Lister, G. S., and Willett, S. D., eds., Exhumation Processes: Normal Faulting, Ductile Flow, and Erosion: Geological Society of London, Special Publications, v. 154, p. 1-27.

Roots, C. F., Harms, T. A., Simard, R. -L., Orchard, M. J., and Heaman, L., 2002, Constraints on the age of the Klinkit assemblage east of Teslin Lake, northern British Columbia: Geological Survey of Canada, Current Research 2002-A7, p. 11.

Roots, C. F., Nelson, J. L., Simard, R. -L., and Harms, T. A., 2006, Continental fragments, mid-Paleozoic arcs and overlapping late Paleozoic arc and Triassic sedimentation in the Yukon-Tanana terrane of northern British Columbia and southern Yukon, *in* Colpron, M., and Nelson, J. L., eds., Paleozoic Evolution and Metallogeny of Pericratonic Terranes at the Ancient Pacific Margin of North America, Canadian and Alaskan Cordillera: Geological Association of Canada, Special Paper No. 45, p. 153-177.

Rosenbaum, G., Regenauer-Lieb, K., and Weinberg, R., 2005, Continental extension: From core complexes to rigid block faulting: Geology, v. 33, p. 609-612.

Royden, L., 1993, The tectonic expression slab pull at continental convergent boundaries: Tectonics, v. 12, p. 303-325.

Ruks, T. W., Piercey, S. J., Ryan, J. J., Villeneuve, M. E., and Creaser, R. A., 2006, Mid- to late Paleozoic K-feldspar granitoids of the Yukon-Tanana terrane, Yukon, Canada: Implications for crustal growth and tectonic evolution of the northern Cordillera: Geological Society of America Bulletin, v. 118, p. 1212-1231.

Ryan, J. J., Gordey, S. P., Glombick, P., Piercey, S. J., and Villeneuve, M. E., 2003, Update on bedrock geological mapping of the Yukon-Tanana terrane, southern Stewart River map area, Yukon Territory: Geological Survey of Canada, Current Research 2003-A9, 7 p.

Ryan, J. J., Colpron, M., and Hayward, N., 2010, Geology, southwestern McQuesten and parts of northern Carmacks, Yukon, Geological Survey of Canada, Canadian Geoscience Map 7 (preliminary edition), 1:125 000, 1 sheet.

Silberling, N. J., Jones, D. L., Monger, J. W. H., and Coney, P. J., 1992, Lithotectonic terrane map of the North American Cordillera: U.S. Geological Survey Miscellaneous Investigation Map I-2176, 1:5 000 000, 2 sheets.

Simard, R. -L., Dostal, J., and Roots, C. F., 2003, Development of late Paleozoic volcanic arcs in the Canadian Cordillera: an example from the Klinkit Group, northern British Columbia and southern Yukon: Canadian Journal of Earth Sciences, v. 40, p. 907-924.

Snyder, D. B., Roberts, B. J., and Gordey, S. P., 2005, Contrasting seismic characteristics of three major faults in northwestern Canada: Canadian Journal of Earth Sciences, v. 42, p. 1223-1237.

Staples, R. D., Gibson, H. D., Colpron, M., Ryan, J. J., and Berman, R. G., 2012, Mid-Cretaceous amphibolite-facies metamorphism and decompression recorded in multi-stage garnet within a tectonic window of the Yukon-Tanana terrane, west-central Yukon, Canada: Journal of Metamorphic Geology [in preparation].

Stockli, D. F., 2005, Application of low-temperature thermochronometry to extensional tectonic settings, *in* Reiners, P.W., and Ehlers, T.A., eds., Low Temperature Thermochronology: Techniques, Interpretations, and Applications: Reviews in Mineralogy and Geochemistry, v. 58, p. 411-448.

Tafti, R., 2005, Nature, Age and Origin of Cu-Au mineralization at the Minto and Williams Creek Deposits, Yukon, Canada [M. Sc. Thesis]: Vancouver, University of British Columbia, 213 p.

Tafti, R., and Mortensen, J. K., 2004, Early Jurassic porphyry (?) copper (-gold) deposits at Minto and Williams Creek, Carmacks Copper belt, western Yukon, *in* Esmond, D. S., and Lewis, L. L., eds., Yukon Exploration and Geology 2003, Yukon Geological Survey, p. 289-303.

Vermeesch, P., Sherlock, S. C., Roberts, N. M. W., and Carter, A., 2012, A simple method for in-situ U-Th-He dating: Geochimica et Cosmochimica Acta, v. 79, p. 140-147.

Villeneuve, M. E., Ryan, J. J., Gordey, S. P., and Piercey, S. J., 2003, Detailed thermal and provenance history of the Stewart River area (Yukon-Tanana terrane, western Yukon) through application of SHRIMP, Ar-Ar, and TIMS, *in* Geological Association of Canada – Mineralogical Association of Canada Annual Meeting: Vancouver, British Columbia, Geological Association of Canada, Abstract #344.

Waschbusch, P., and Beaumont, C., 1996, Effect of a retreating subduction zone on deformation in simple regions of plate convergence: Journal of Geophysical Research, v. 101, p. 28133-28148.

Wheeler, J.O., and McFeely, P., 1991, Tectonic assemblage map of the Canadian Cordillera and adjacent parts of the United States of America: Geological Survey of Canada Map 1712A, 1:2 000 000, 2 sheets.

Wheeler, J., and Butler, R. W. H., 1994, Criteria for identifying structures related to true crustal extension in orogens: Journal of Structural Geology, v. 16, p. 1023-1027.

Zen, E., and Hammarstron, J. M., 1984, Magmatic epidote and its petrologic significance: Geology, v. 12, p. 515-518.

APPENDIX 1

Thin-Section Descriptions

SAMPLE PETROGRAPHY

Through the following petrographic description section, deformation foliations are described as S_m (main foliation), subsequent foliations are S_{m+1}, S_{m+2} etc, and earlier foliations are S_{m-1}. The S_m refers to that thin section, and does not attempt to correlate generations of structures across the map area because this study does not have the required level of field information. For example, S_m in the Reid Lake complex may be Jurassic, whereas S_m in the YTT may be Permian. Similarly, F_m refers to the dominant fold axis in the sample.

Mineral name abbreviations used in the text and diagrams are: Bt-biotite; Chl-chlorite; Ep-epidote; Hbl-hornblende; K-spar-potassium feldspar; Ms-muscovite; Qtz-quartz.

Reid Lakes plutonic suite

09RAYJR122A

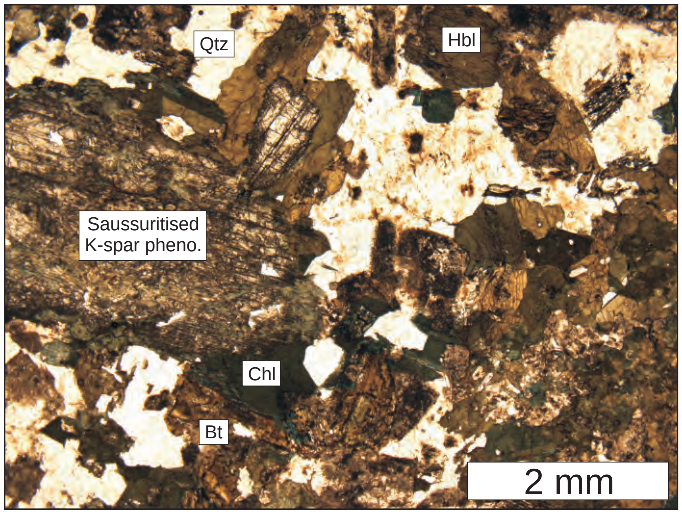

Sample 09RAYJR122A consists of a hornblende-rich K-spar-phyric granite with prolific saussuritisation of feldspar. Biotite and hornblende are euhedral. Chlorite is common throughout the sample, generally pseudomorphing hornblende, and locally biotite.

08RAY003

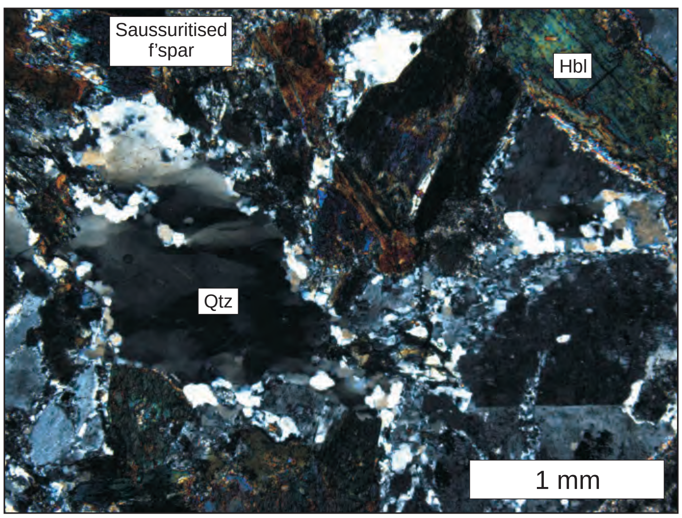

Sample 08RAY003 consists of a granodiorite with K-feldspar and hornblende phenocrysts. Saussuritisation of feldspar is ubiquitous throughout the sample. Euhedral hornblende phenocrysts are moderately altered to chlorite.

09RAYJR176A

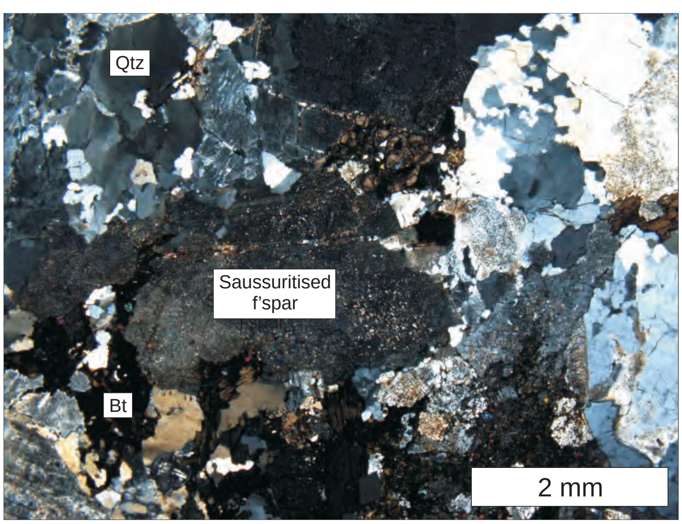

Sample 09RAYJR176 is a coarse, unfoliated K-feldspar and quartz bearing monzogranite from the northern extent of the foliated zone of Reid Lakes complex rocks. Saussuritisation and lesser seritisation is prolific throughout the sample, although primary twins are still visible in the grains. Biotite is euhedral, with little to no alteration.

09RAYJR133A

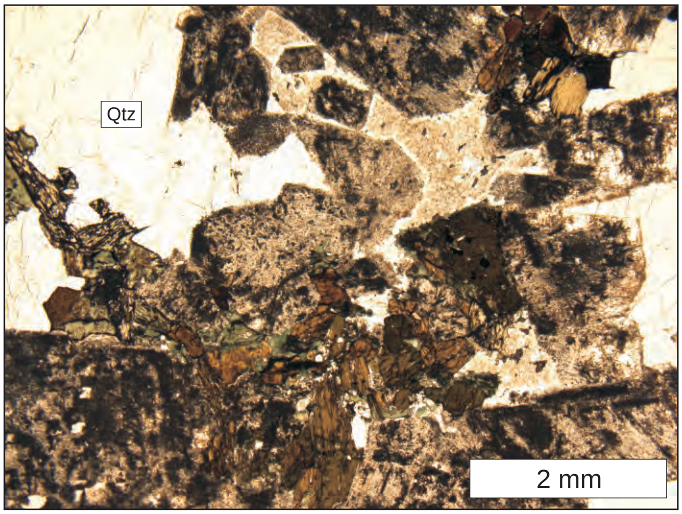

This sample of the Reid Lakes batholith is a coarse-grained quartz-phyric granodiorite. Feldspar grains have been saussuritised and seritised to such a strong extent that their primary features are obliterated. Biotite is coarse-grained, euhedral, with little alteration or inclusions. Hornblende is also coarse-grained, euhedral, and is commonly altered to chlorite or rarely biotite.

09RAYMC115A

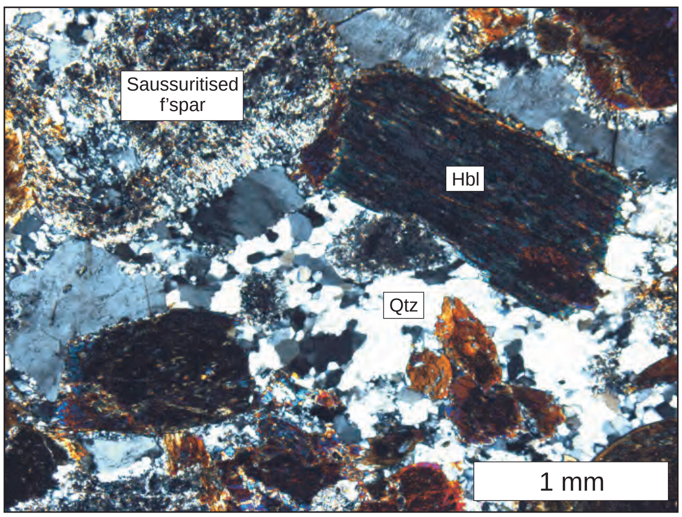

Sample 09RAYMC115A is from the northern margin of the Reid Lakes batholith, collected from within 500 m of the Tintina fault. The rock consists of a granodiorite with large (up to 0.5 cm) K-feldspar phenocrysts. Hornblende is generally euhedral, locally showing minor alteration to chlorite. The majority of feldspar grains have been saussuritised and sericitized (?) to such a strong extent that their primary features are obliterated.

09RAYJR094A

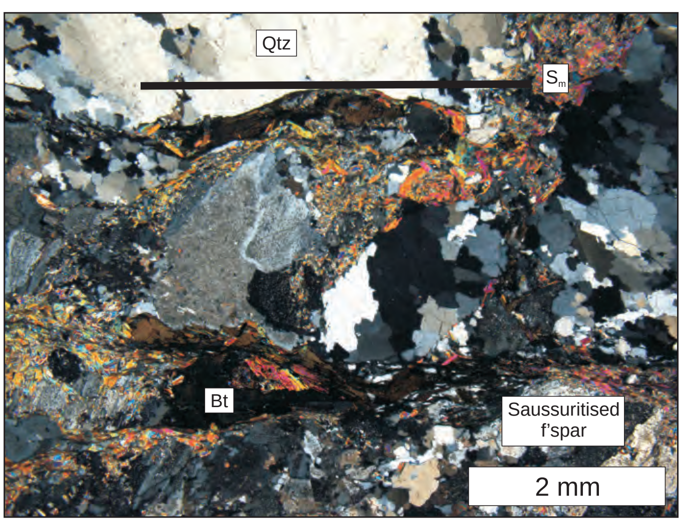

Sample 09RAYJR094A is from the zone of foliated rocks in the Reid Lakes complex proximal to the Willow Lake fault. The sample consists of monzogranite with quartz phenocrysts. Quartz grains have a seriate grain-size distribution, with prevalent undulose extinction and interlobate grain boundaries. A weak to moderate continuous cleavage is defined by alignment of muscovite and lesser biotite grains and quartz-rich bands. Biotite occurs as medium-grained aggregates discordant to the foliation, and may be recrystallised from larger primary grains of biotite or possibly hornblende. Seritisation of plagioclase is prevalent throughout the sample.

09RAYJR160A

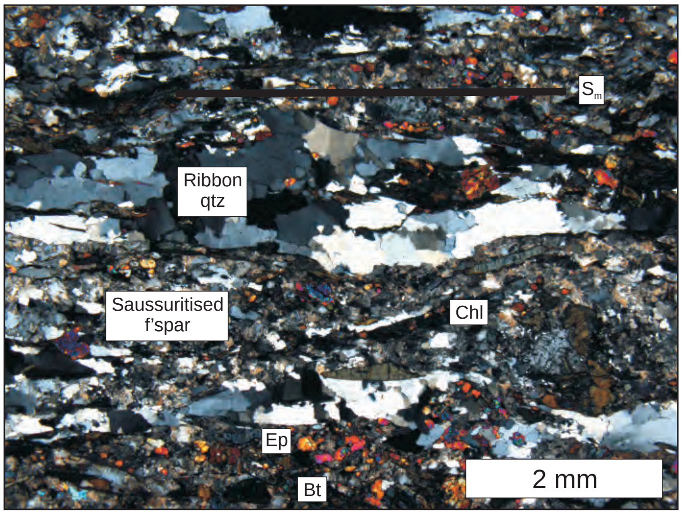

Sample 09RAYJR160A is from the projected trace of the Willow Lake fault. The sample is a high-strain, protomylonitic orthogneiss. The foliation in this sample is defined by a spaced cleavage consisting of quartz ribbons alternating with bands of aligned mica and heavily saussuritised relict feldspar. Quartz grains and subgrains exhibit strong undulose extinction, and evidence of dynamic recrystallisation (grain boundary migration, bulging, amoeboid and sutured grain boundaries, and bimodal grain size distribution). White-mica in this sample is fine-grained and sparce in thin-section. Biotite is heavily altered to chlorite. Epidote minerals (clinozoisite?) are abundant throughout the sample. Late-stage microfaults of unknown significance overprint the ductile foliation.

Reid Lakes volcanic suite

09RAYMC092A

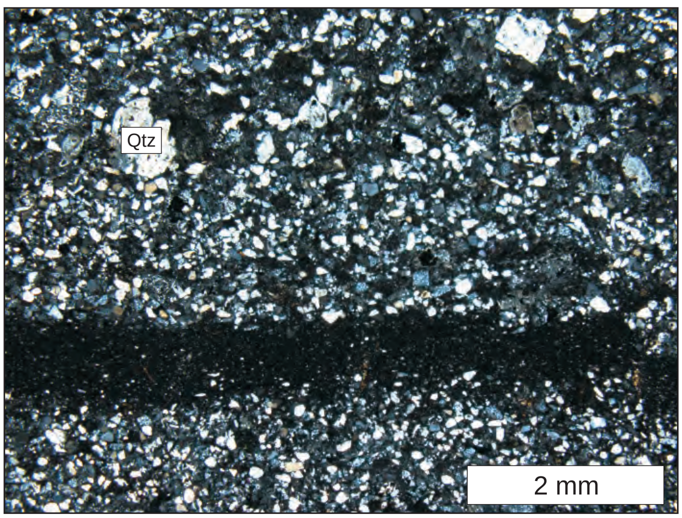

Sample 09RAYMC092A consists of a volcanogenic quartz sandstone horizon from within an outcrop dominated by volcanic conglomerate. The sandstone shows graded bedding and is predominantly comprised of quartz granules, wherein subangular grains are as large as 0.1 mm, and rare subrounded grains are as large as 0.5mm. Rare euhedral to subhedral plagioclase granules are present. The rock has a fine-grained siliceous matrix and minor opaque minerals.

09RAYJR134A

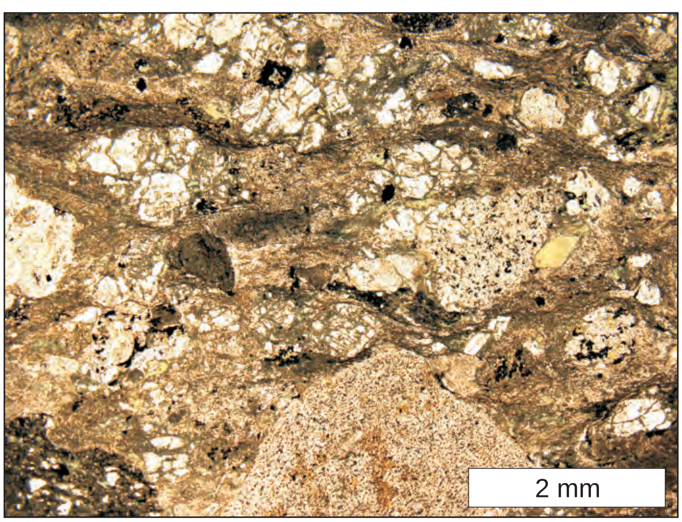

Sample 09RAYJR134A is a polymict tuffaceous rock or volcaniclastic breccia that is interbedded with sandstone at the outcrop scale. The groundmass is fine-grained, siliceous and mixed with prolific secondary chlorite. Phenocrysts are up to 4mm in size, and comprise quartz, heavily saussuritised feldspar, autoclasts and lesser calcite. There seems to be a weak alignment of elongate clasts, exhibiting a faint foliaiton.

09RAYMC036A

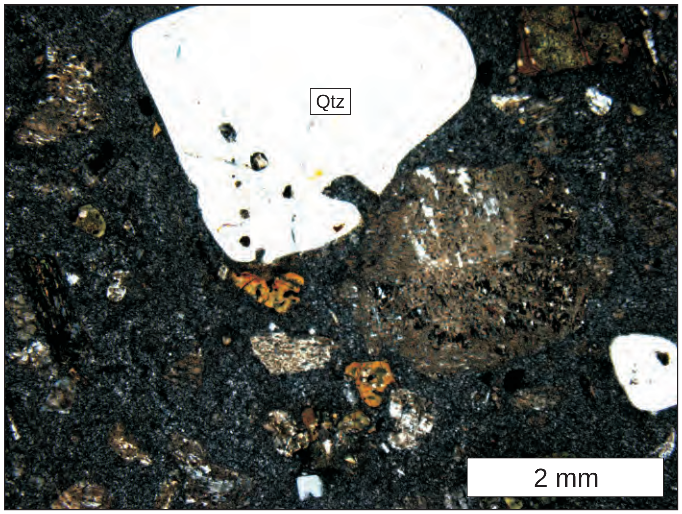

This sample is a polymictic tuffaceous rock with clasts of intermediate composition. The groundmass is fine-grained, siliceous, and mixed. Phenocrysts of quartz and saussuritised K-feldspar are angular to subangular, and less than 1 cm in size.

09RAYJR165A

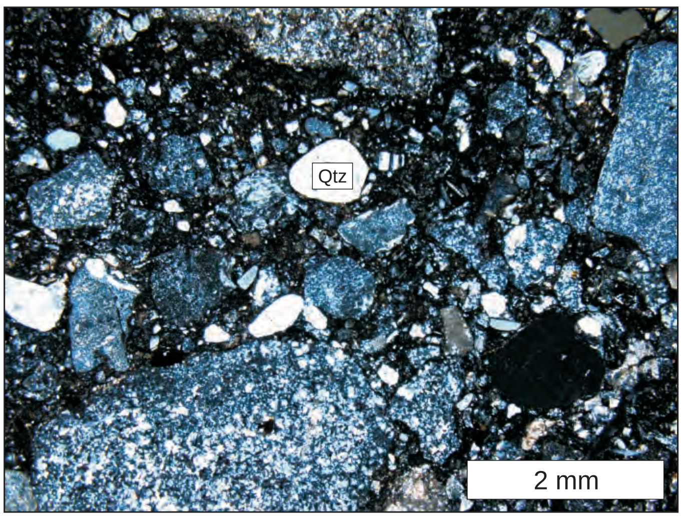

Sample 09RAYJR165A is a massive, polymictic volcaniclastic breccia. Clasts are predominantly angular and embayed and composed of rhyolite to dacite, rhyolite, pumice, minor limestone and rare black chert. Clasts are generally up to 2 cm in horizons of lithic tuff, and commonly 10-15 cm in size in breccia horizons with mixed silty-sand matrix.

Snowcap Assemblage

09RAYRS030A

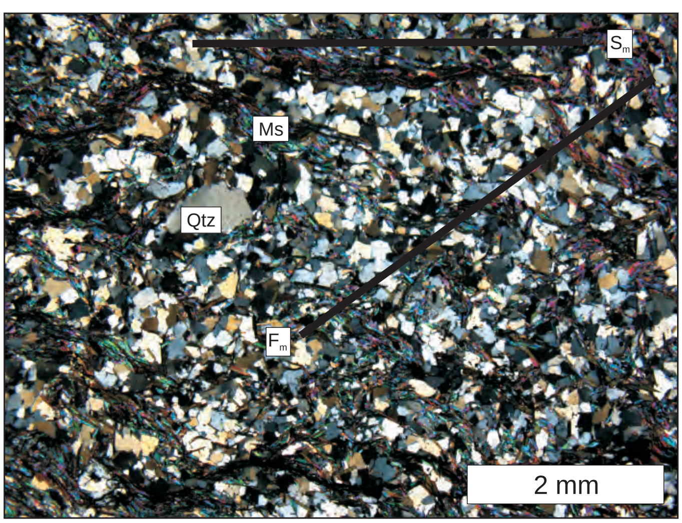

This sample is a quartz-muscovite-biotite schist. The rock exhibits at least one foliation that is defined by the alignment of muscovite. This foliation is deformed by one or more phase of close to tight folding. Quartz grains exhibit polygonal grain boundaries, suggestive of post-kinematic static recrystallisation. Relict garnet porphyroclasts are heavily chloritised, suggesting retrograde greenschist facies metamorphism. Muscovite is fine-grained and commonly occurs in association with opaque (graphite?) minerals. Chlorite blades grow discordant to the main fabric, indicating they are post-kinematic in nature.

Simpson Range Suite

09RAYMC081A

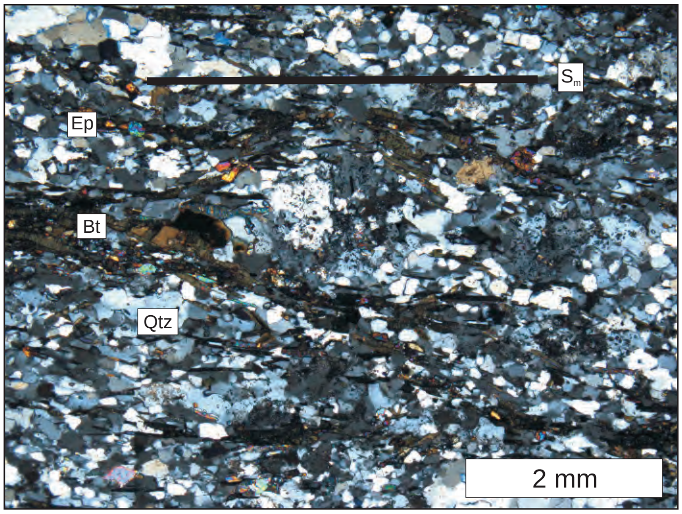

Sample 09RAYMC081A constitutes a strongly foliated granodiorite. In thin section, the rock exhibits one strong foliation (S_m), defined by recrystallised quartz-rich layers and strongly aligned biotite grains. The foliation wraps around rigid cores of quartz and plagioclase. The coarse recrystallised quartz grains record subsequent weak deformation recorded by undulose extinction and minor subgrain development. Biotite is generally euhedral with some irregular orientations. It shows minor chloritisation and has inclusions of epidote group minerals (clinozoisite?). This rock is one of the more highly strained examples of the Simpson Range rocks, but it is unclear if this is due to the relative proximity to the Willow Lake fault.

09RAYRS005A

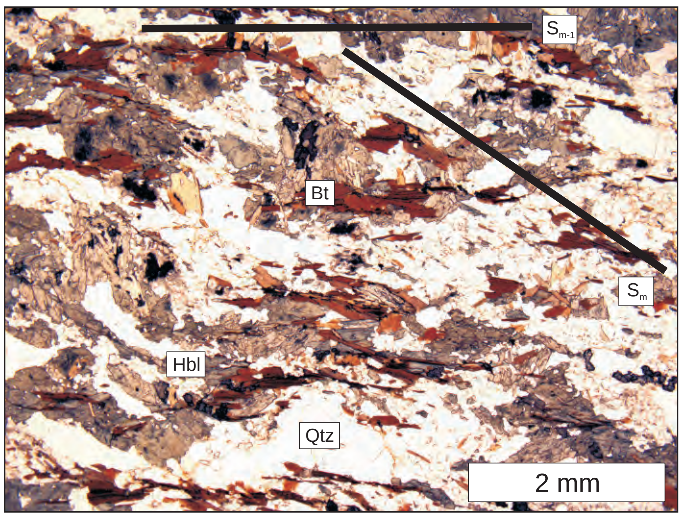

Sample 09RAYRS005A is composed of a granite to granodiorite protolith. A faint foliation (S_{m-1}) is defined by alignment of biotite and anhedral hornblende with recrystallised quartz microlithons. The S_t foliation is deformed by a moderate to strongly developed crenulation cleavage (S_m) that is defined by alignment of biotite and hornblende and bands of recrystallised and subgrain quartz. Minor to moderate undulose extinction in coarse quartz and subgrains are indicative of subsequent weak deformation. Relict feldspar is heavily saussuritised. Biotite grains are generally unaltered and euhedral, and locally pseudomorphs hornblende.

09RAYRS141A

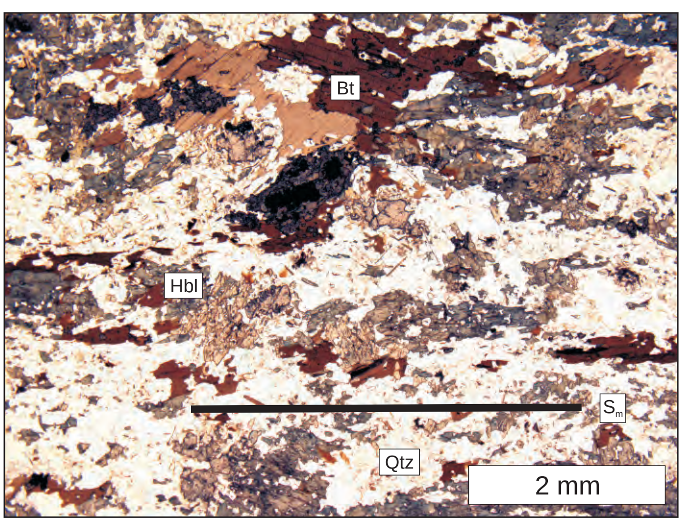

This sample is comprised of a quartz monzonite protolith. A weak continuous foliation (S_m) is defined by alignment of biotite grains, although coarse pre-kinematic biotite grains also occur in random orientations outside of this cleavage. Biotite is euhedral to subhedral and generally unaltered, but locally may be chloritised. Irregular and anhedral hornblende in this sample is moderately chloritised, and rarely pseudomorphed by biotite. Weak undulose extinction and prevalent subgrain quartz are indicative of a weak late-stage deformation.

09RAYKR142A

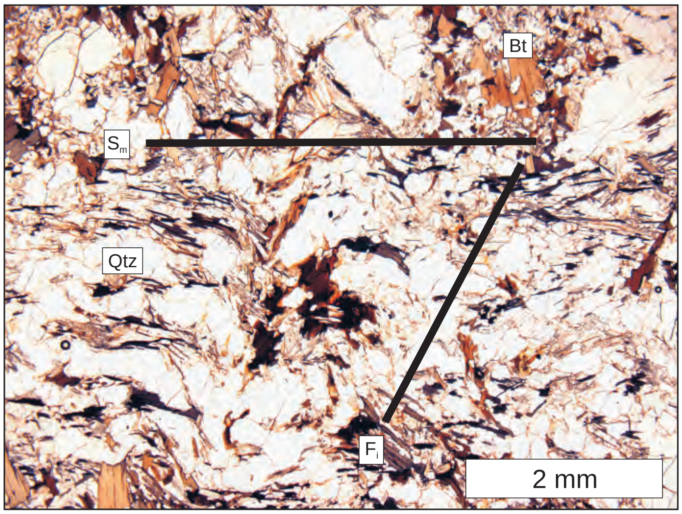

Sample 09RAYKR142A is a quartz monzonite with a weak continuous foliation defined by a preferred orientation of subparallel biotite grains. This foliation may be deformed by weak open folding. Pre-kinematic biotite and rare white-mica commonly occur at random orientations to the weak foliation. Biotite is unaltered and predominantly euhedral. Quartz exhibits moderate undulose extinction and generally coarse subgrain growth. Plagioclase is preserved, and shows rare saussuritisation.

09RAYJR143A

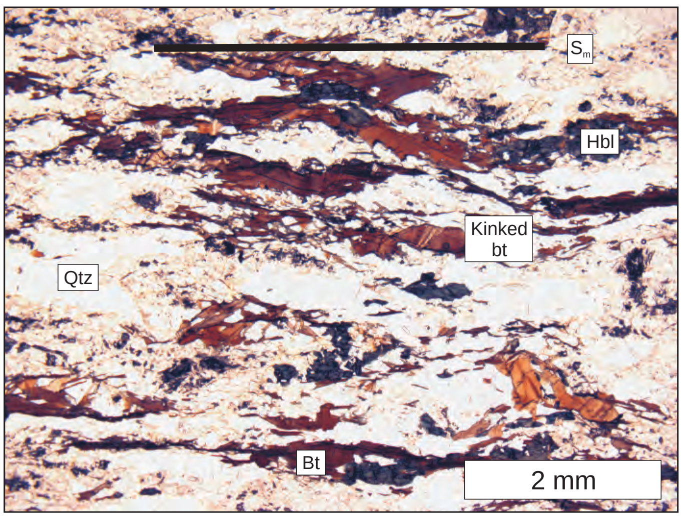

This sample is comprised of a highly strained granodiorite protolith with a strongly developed spaced foliation (S_m). The S_m foliation is defined by quartz-rich layers and alignment of biotite grains parallel to the quartz layers. Biotite-rich layers wrap around coarse quartz grains with prominent subgrains and undulose extinction. Biotite is coarse-grained, and generally euhedral; some grains are prominently kinked, indicative of pre-kinematic growth. Hornblende may occur discordant to the main foliation, suggestive of post-kinematic amphibolite facies metamorphism. Relict feldspar is strongly saussuritised and locally seritised.

Finlayson Assemblage

09RAYJR076B

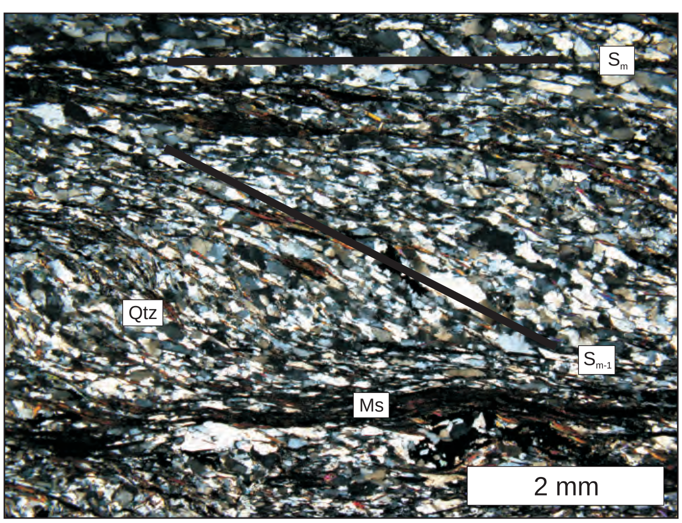

Sample 09RAYJR076B is a quartz-muscovite schist. A moderately developed and narrowly spaced foliation (S_{m-1}) is defined by alignment of muscovite grains. This foliation is deformed about a strong crenulation cleavage (S_m). The crenulation cleavage is unevenly-spaced, and is defined by mats of muscovite alternating with bands of recrystallised quartz. Quartz bands consist of either fine or coarse grains and subgrains. Muscovite within the S_{t+1} foliation wraps around relict garnet porphyroclasts, suggesting garnet growth is pre or syn-kinematic.

Klinkit Assemblage

09RAYJR078A

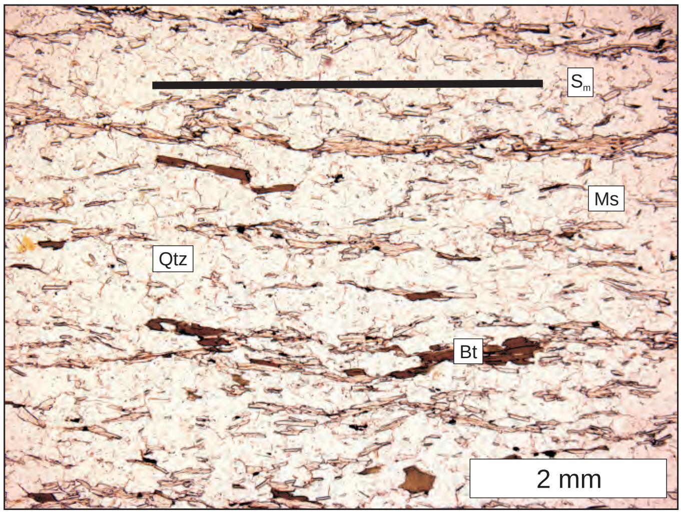

Sample 09RAYJR078A consists of a highly strained quartz-muscovite-biotite schist. The protolith was a quartz-rich rock, likely a rhyodacite or tuff. A strongly developed foliation is characterised by alignment of micas and bands of subgrain quartz with interlobate grain boundaries. Muscovite in this sample is fine-grained, euhedral, free of inclusions and unaltered. Biotite occurs in lesser concentrations and is slightly coarser-grained than muscovite. It is euhedral and grows in the same direction as the continuous foliation, although larger and presumably post-kinematic crystals may grow within and across the quartz-rich domains. At the macroscopic level, a moderate stretching lineation is present.

Sulphur Creek Suite

09RAYJR175A

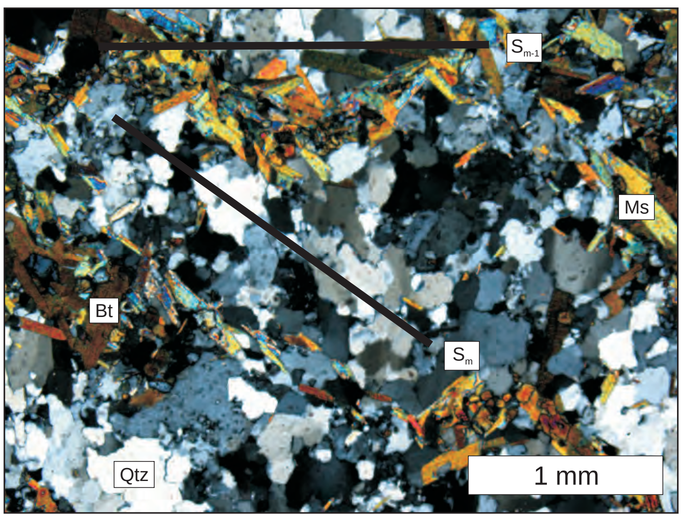

Sample 09RAYJR175A consists of a granite to monzogranite protolith, comprised of predominantly quartz, coarse-grained biotite, fine-grained muscovite, and lesser plagioclase. Feldspars have undergone minor saussuritisation. A weak foliation is defined by alignment of micas (S_{m-1}), and is overprinted by a shallow crenulation cleavage (S_m). Undulatory extinction of quartz and subgrain quartz is prevalent. The locally irregular direction of mica growth along the S_{m-1} plane suggests there may have been an intermediate phase of deformation prior to development of the S_m foliation. Mica crystals are euhedral and unaltered.

09RAYJR177A

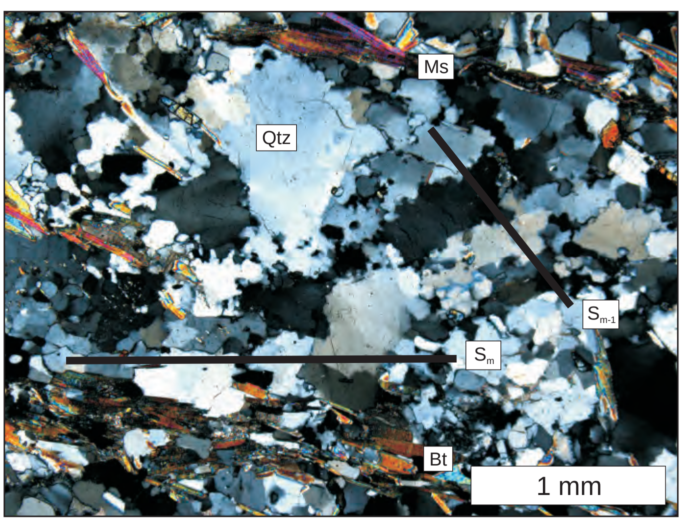

Sample 09RAYJR177A is a metagranodiorite. The rock hosts an S_{m-1} and S_m crenulation cleavage, both of which are defined by preferred alignment of micas. Quartz grains in this sample are distinctively seriate, with interlobate to amoeboid grain boundaries. The micaceous foliation wraps around quartz phenocrysts (porphyroblasts?). Feldspars are preserved, but have undergone moderate saussuritisation. Micas are generally euhedral and unaltered. Rare chlorite is found throughout the sample.

09RAYJR178A

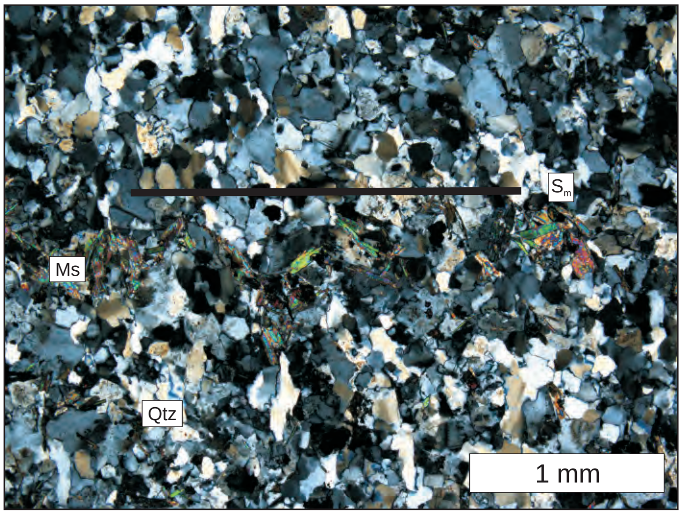

This sample consists of a fine-grained metamonzogranite, composed primarily of recrystallised quartz, with lesser feldspar, muscovite and rare biotite, chlorite and opaque minerals. A weak continuous foliation is defined by locally subparallel mica grains. The quartz matrix is fine-grained, with prolific undulose extinction of the grains. Feldspar grains are relatively unaltered, with only minor saussuritisation visible.

09RAYJR179A

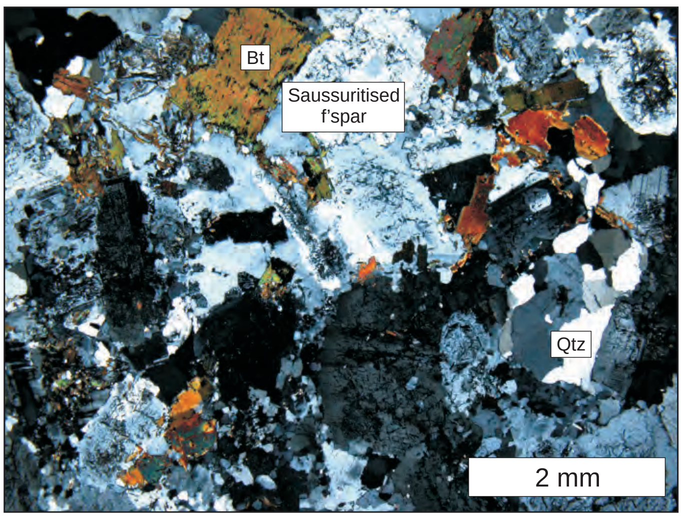

Sample 09RAYJR179A is an unfoliated medium to coarse-grained quartz monzonite. Saussuritisation of feldspar crystals is ubiquitous. Hornblende is locally replaced by biotite and chlorite. Biotite is generally unaltered.

08RAY004

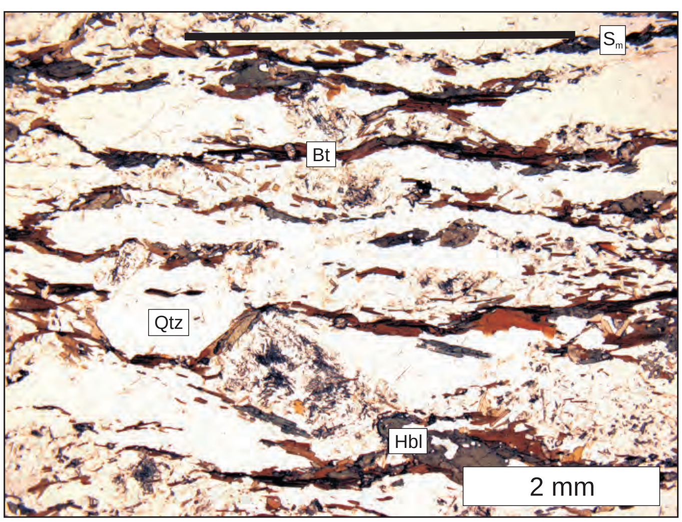

Sample 08RAY004 is a moderately strained quartz monzodiorite to granodiorite. A strong continuous schistosity is characterised by alignment of biotite and biotite-after-hornblende crystals that wraps around relict feldspar and quartz cores. This foliation may overprint a shallow weak earlier foliation that appears to be defined by alignment of biotite. Quartz locally exhibits a polygonal fabric, indicative of static recrystallisation. The dominant texture of quartz, however, consists of fine to medium-grained aggregates of subgrains with irregular grain boundaries and prevalent undulose extinction. Biotite tends to be more randomly oriented, discordant to the dominant foliation, suggestive of post-kinematic growth. Feldspar is preserved, and commonly hosts an abundance of inclusions or is moderately to mildly saussuritised.

09RAYMC017A

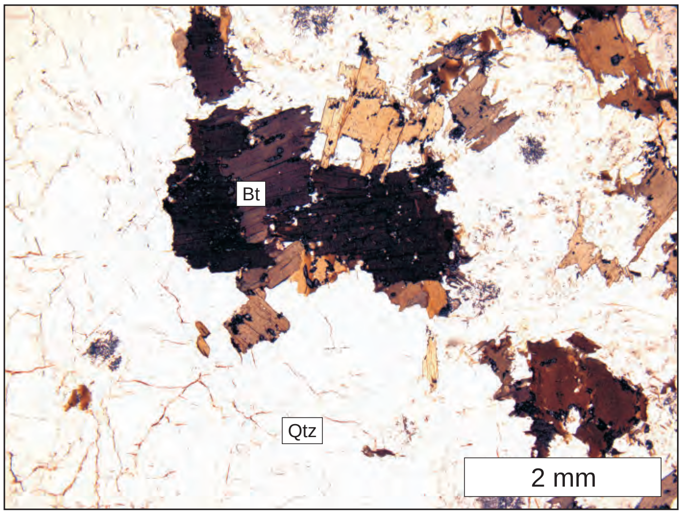

Sample 09RAYMC017A is a medium-grained quartz-monzonite, lacking a foliation. Coarse euhedral biotite grains host minor inclusions, but are unaltered and relatively pristine.

09RAYRS012A

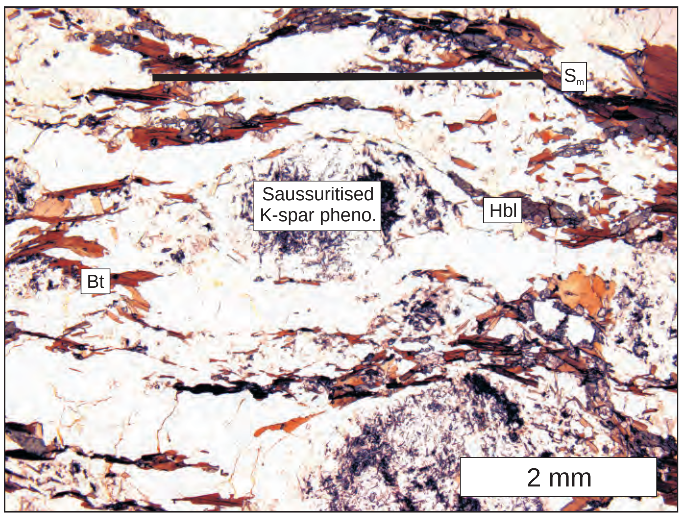

This sample is composed of a quartz monzonite to granite protolith. A strong foliation is defined by alignment of biotite and hornblende crystals. The foliation wraps around K-feldspar porphyroblasts and coarse quartz cores. Quartz occurs in a variety of grain sizes, ranging from coarse to fine, and with interlobate and irregular grain boundaries. Biotite grains are euhedral and pristine, with only rare inclusions. Saussuritisation and local seritisation of feldspar is prevalent. Hornblende is locally chloritised and replaced by biotite.

Aishihik Suite

09RAYMC123A

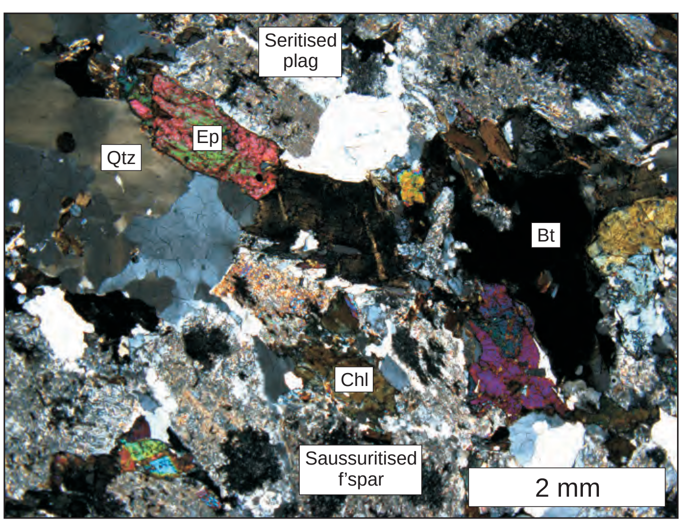

This sample is medium-grained and monzogranitic in composition. The sample is composed primarily of quartz and feldspar, with lesser biotite, hornblende, epidote, and titanite. Epidote is euhedral and appears to be igneous; however it may be secondary in origin, replacing hornblende. Saussuritisation of K-feldspar and seritisation of plagioclase is prevalent throughout the sample. Hornblende weakly moderately chloritised or replaced by biotite. Biotite is mildly to moderately chloritised, and occurs predominantly as coarse euhedral crystals. The sample is generally undeformed, although rare biotite grains exhibit kinking.

APPENDIX 2

U-Pb Methodology

METHODS

Samples were crushed at the University of Ottawa, then processed and analyzed at the Geological Survey of Canada geochronology laboratory in Ottawa, Ontario using standard techniques. Rocks were crushed with a jaw crusher, run through a disc mill, and sieved to between 500 and 105 µm. The intermediate size fraction was passed over a Wilfley table, and the heavy mineral separate extracted from methylene iodide. Foreign and magnetic minerals were separated from zircons with a Frantz magnetic separator. Approximately 100 zircons were picked from each sample of varying size, colour, and morphology to prevent an age bias due to grain selection. Grains were mounted on 25 mm diameter double-sided tape within a Teflon mold, in addition to zircon standards BR6266 ($^{206}Pb/^{238}U$ ID-TIMS age of 559.0 ± 0.2 Ma; Stern and Amelin, 2003) and TEMORA 1 ($^{206}Pb/^{238}U$ ID-TIMS age of 416.8 ± 0.2 Ma; Black et al., 2003). Epoxy was poured into the mold and allowed to cure overnight. The mount was polished to 9, 6, and 1 µm with diamond compound to expose the center of the zircon, washed with soap and rinsed with deionised water. Photographs of the mount were taken in plane and polarized light. Finally a gold coat was applied to the mount for back-scatter electron and cathodoluminescence imaging using a Zeiss EVO scanning electron microscope at the GSC in Ottawa. Isotopic analysis was conducted using the SHRIMP II, which is configured with an electron multiplier and ion counting system. Zircons were probed with a spot size of either 13 x 16 µm or 17 x 23 µm, depending on the average size of the grain targets. Prior to analysis, the ion beam was rastered over the analysis spot at a slightly larger size for 2 to 3 minutes to eliminate surface common lead. Measurements were made over six data cycles, with a deadtime of 11 seconds. Counting times were optimized for each target mass based on signal intensity and purpose. SHRIMP U-Pb data for igneous samples are reported in Table 1, and data for a detrital sample is in

Table 2. All uncertainties for individual analyses listed in the table are reported at the 1σ level. Uncertainties in the U-Pb calibration were 1.0, 1.1, and 1.27% for three analytical sessions. Age calculations are based on decay constants from Steiger and Jäger (1977). Isoplot v. 3.66 (Ludwig, 2003) was used to calculate weighted mean ages and generate Tera-Wasserburg plots.

In order to compare data collected from multiple analytical sessions and from different mounts, the reported uncertainty of the weighted mean age combines the uncertainty of the calculated mean age, the 2σ external spot-to-spot error of the Temora standard, and the 2σ error of the mean of the BR6266 zircon calibration standard. Single-spot analyses are excluded from the weighted mean age calculation based on the following criteria: common Pb concentrations greater than 2.0%; suspected Pb-loss; inherited age; overgrowth age; age of mixed inherited and/or overgrowth components; concentrations of U greater than 1800 ppm; and UO^+/U^+ (254/238 amu) values far outside the range of the BR6266 zircon standard analyses for that calibration. Analyses with high U concentrations or anomalous UO^+/U^+ values are problematic because of matrix effects and issues arising from non-linear calibration with the standard at extreme values (Claoué-Long et al., 1995; Williams, 1998).

REFERENCES

Black, L. P., Kamo, S. L., Allen, C. M., Aleinikoff, J., N., Davis, D. W., Korsch, R. J., and Foudoulis, C., 2003, TEMORA 1: a new zircon standard for Phanerozoic U-Pb geochronology: Chemical Geology, v. 200, p. 155-170.

Claoué-Long, J. C., Compston, W., Roberts, J. and Fanning, C. M., 1995, Two Carboniferous ages: a comparison of SHRIMP zircon dating with conventional zircon ages and $^{40}Ar/^{39}Ar$ analysis, *in* Berggren, W. A., Kent, D. V., Aubry, M.-P., and Hardenbol, J., eds., Geochronology, Time Scales and Global Stratigraphic correlation: SEPM (Society for Sedimentary Geology) Special Publication No. 4, p. 3-21.

Ludwig, K.R., 2003, User's manual for Isoplot/Ex rev. 3.00, A geochronological toolkit for Microsoft Excel: Berkeley Geochronology Center, Special Publication No. 4, 74 p.

Steiger, R., and Jäger, E., 1977, Subcommission on geochronology: Convention on the use of decay constants in geo- and cosmochronology: Earth and Planetary Science Letters, v. 36, p. 359-362.

Stern, R. A., and Amelin, Y., 2003, Assessment of errors in SIMS zircon U-Pb geochronology using a natural zircon standard and NIST SRM 610 glass: Chemical Geology, v. 197, p. 111-142.

Williams, I. S., 1998, U-Th-Pb geochronology by ion microprobe, *in* McKibben, M. A., Shanks III, W. C., and Ridley, W. I., eds., Applications of microanalytical techniques to understanding mineralizing processes: Reviews in Economic Geology, v. 7, p. 1-35.

TABLE A1. SHRIMP U-Pb DATA FOR SAMPLES FROM THE MCQUESTEN MAP AREA

Spot name	U (ppm)	Th (ppm)	Th/U	^{206}Pb* (ppm)	^{204}Pb/^{206}Pb	% ±	f(206)^{204} %	^{208*}Pb/^{206*}Pb	% ±	^{238}U/^{206}Pb	% ±	^{207}Pb/^{206}Pb	% ±	^{207*}Pb/^{235}U	% ±	^{206*}Pb/^{238}U	% ±	Corr Coeff	^{207*}Pb/^{206*}Pb	% ±	Apparent Ages (Ma) 204 corrected ^{206}Pb/^{238}U	204 corrected ±^{206}Pb/^{238}U	207 corrected ^{206}Pb/^{238}U	207 corrected ±^{206}Pb/^{238}U
09RAYJR165A; Lab#10229; Volcaniclastic breccia; NAD 83 Zone 8 7017865 N 405222 E																								
10229-93.2[f]	6221	4218	0.700	243.5	1.1E-4	18	0.19	0.207	1.5	21.91	1.3	0.0546	0.8	0.333	1.6	0.0456	1.3	0.8	0.0530	1.0	287	4	287	4
10229-16.1	435	206	0.488	20.0	5.1E-4	38	0.88	0.159	6.1	18.55	1.3	0.0590	2.4	0.380	6.4	0.0534	1.4	0.2	0.0516	6.2	336	4	**336**	**4**
10229-75.2	88	26	0.305	4.1	3.3E-4	81	0.57	0.109	17.2	18.28	1.5	0.0711	4.8	0.498	7.9	0.0544	1.5	0.2	0.0664	7.7	341	5	**336**	**5**
10229-64.1	404	158	0.403	18.6	6.1E-4	29	1.05	0.129	6.8	18.44	1.7	0.0599	3.6	0.377	6.9	0.0537	1.8	0.3	0.0510	6.7	337	6	**338**	**6**
10229-89.1	248	82	0.341	11.4	1.0E-3	28	1.80	0.115	8.7	18.35	1.3	0.0638	3.0	0.359	9.9	0.0535	1.4	0.1	0.0486	9.8	336	5	**338**	**5**
10229-54.3	227	72	0.329	10.6	8.6E-4	38	1.49	0.118	9.0	18.18	1.4	0.0667	3.1	0.405	9.7	0.0542	1.5	0.2	0.0542	9.6	340	5	**340**	**5**
10229-67.1[a]	779	421	0.558	35.6	1.2E-2	7	21.63	0.142	2.2	14.72	1.8	0.2243	4.4	0.290	53.2	0.0533	2.6	0.0	0.0394	53.2	334	9	340	8
10229-90.2	236	72	0.314	11.1	4.3E-4	24	0.75	0.098	10.2	18.18	1.6	0.0647	3.1	0.440	4.6	0.0546	1.6	0.3	0.0585	4.3	343	5	**341**	**5**
10229-110.1	553	221	0.413	25.6	3.8E-4	35	0.66	0.124	6.1	18.41	1.4	0.0534	2.2	0.356	5.0	0.0540	1.4	0.3	0.0478	4.8	339	5	**341**	**5**
10229-108.2	585	303	0.535	27.3	1.7E-4	57	0.29	0.158	5.3	18.34	1.3	0.0557	2.1	0.399	3.7	0.0544	1.3	0.4	0.0533	3.4	341	4	**341**	**4**
10229-82.2	401	147	0.378	18.9	2.5E-4	19	0.44	0.104	8.1	18.15	1.3	0.0592	2.5	0.419	3.3	0.0548	1.3	0.4	0.0555	3.0	344	4	**343**	**5**
10229-55.1	469	183	0.402	22.1	2.8E-4	21	0.49	0.130	6.7	18.1	1.5	0.061	2.3	0.43	3.3	0.0549	1.5	0.46	0.0566	2.9	345	5	**343**	**5**
10229-114.1	1639	796	0.501	77.3	-1.1E-5	149	-0.02	0.163	3.3	18.21	1.4	0.0546	1.3	0.415	2.0	0.0549	1.4	0.7	0.0548	1.3	345	5	**344**	**5**
10229-83.1	642	300	0.484	30.3	1.5E-4	24	0.26	0.130	5.6	18.16	1.3	0.0566	2.0	0.412	2.6	0.0549	1.3	0.5	0.0544	2.3	345	4	**344**	**4**
10229-85.1	341	167	0.505	16.2	-1.8E-4	1	-0.32	0.138	7.9	18.14	1.3	0.0530	2.8	0.425	3.0	0.0553	1.3	0.4	0.0557	2.7	347	4	**346**	**5**
10229-9.1	632	243	0.397	30.0	2.8E-4	35	0.48	0.126	5.7	18.0	1.0	0.059	1.9	0.42	3.5	0.0552	1.1	0.30	0.0548	3.3	347	4	**346**	**4**
10229-77.1	769	380	0.511	36.4	2.2E-4	35	0.38	0.136	5.0	18.07	1.3	0.0554	2.2	0.397	3.5	0.0551	1.3	0.4	0.0523	3.2	346	4	**346**	**4**
10229-55.3	919	478	0.538	43.4	2.7E-4	31	0.47	0.166	4.3	18.08	1.5	0.0545	1.8	0.383	3.5	0.0551	1.5	0.4	0.0505	3.1	346	5	**347**	**5**
10229-99.1	520	232	0.461	24.7	2.7E-4	45	0.46	0.144	5.8	18.03	1.3	0.0548	2.2	0.388	4.4	0.0552	1.3	0.3	0.0510	4.2	346	4	**347**	**4**
10229-66.2	1774	795	0.463	84.3	6.8E-5	18	0.12	0.143	3.2	18.05	1.3	0.0537	1.2	0.402	1.8	0.0553	1.3	0.7	0.0527	1.3	347	4	**347**	**4**
10229-27.2	1596	799	0.517	75.9	2.8E-4	21	0.48	0.163	3.0	17.99	1.3	0.0562	1.2	0.398	2.4	0.0553	1.3	0.5	0.0522	2.1	347	4	**348**	**4**
10229-102.1	963	584	0.627	45.8	3.4E-4	31	0.60	0.193	3.7	17.97	1.3	0.0554	1.6	0.384	3.9	0.0553	1.3	0.3	0.0504	3.6	347	4	**348**	**4**
10229-95.2	98	77	0.810	4.7	9.4E-4	33	1.63	0.283	9.8	17.69	2.4	0.0648	4.8	0.392	11.1	0.0556	2.4	0.2	0.0511	10.8	349	8	**350**	**8**
10229-51.2	567	179	0.325	27.0	4.6E-4	29	0.79	0.095	6.6	17.89	1.7	0.0543	2.7	0.364	5.4	0.0554	1.7	0.3	0.0476	5.2	348	6	**350**	**6**
10229-42.1	1502	562	0.387	72.1	2.8E-4	26	0.48	0.119	3.6	17.80	1.3	0.0577	1.2	0.414	2.7	0.0559	1.3	0.5	0.0537	2.4	351	5	**351**	**5**
10229-36.1	466	250	0.553	22.3	6.0E-4	37	1.04	0.175	5.7	17.7	1.1	0.060	2.3	0.39	7.2	0.0558	1.1	0.16	0.0509	7.1	350	4	**351**	**4**
10229-74.1[f]	1953	1132	0.599	94.0	2.2E-4	21	0.38	0.187	2.7	17.77	1.3	0.0566	1.1	0.413	2.2	0.0561	1.3	0.6	0.0534	1.7	352	4	352	4
10229-70.2[a]	204	85	0.432	9.9	4.0E-3	15	6.94	0.182	6.2	16.49	1.4	0.1138	2.4	0.433	18.1	0.0564	1.8	0.1	0.0557	18.0	354	6	353	5
10229-80.1	539	248	0.474	26.1	2.3E-4	27	0.39	0.174	5.5	17.6	1.4	0.057	2.2	0.42	3.2	0.0564	1.4	0.45	0.0534	2.9	354	5	**354**	**5**
10229-24.2	1363	870	0.659	66.1	3.6E-4	25	0.62	0.202	3.6	17.60	1.3	0.0573	1.6	0.405	3.4	0.0565	1.3	0.4	0.0521	3.1	354	4	**355**	**5**
10229-46.1	333	97	0.300	16.2	6.6E-4	21	1.14	0.087	9.1	17.4	1.2	0.064	2.6	0.43	5.0	0.0567	1.3	0.25	0.0544	4.8	356	4	**355**	**4**
10229-75.1[a]	100	33	0.336	4.9	2.6E-3	19	4.48	0.076	13.2	16.8	1.3	0.089	4.1	0.40	16.7	0.0568	1.6	0.09	0.0508	16.6	356	5	357	5
10229-48.1	265	80	0.311	13.3	-3.7E-5	90	-0.06	0.125	9.1	17.1	1.5	0.070	2.7	0.57	3.2	0.0585	1.5	0.47	0.0702	2.8	366	5	**359**	**5**
10229-100.1	439	202	0.474	21.6	2.7E-4	37	0.48	0.146	6.9	17.36	1.4	0.0573	2.6	0.422	4.1	0.0573	1.4	0.3	0.0533	3.9	359	5	**360**	**5**

Spot name	U (ppm)	Th (ppm)	Th/U	$^{206}Pb^*$ (ppm)	$^{204}Pb/^{206}Pb$	% ±	$f(206)^{204}$ %	$^{208*}Pb/^{206*}Pb$	% ±	$^{238}U/^{206}Pb$	% ±	$^{207}Pb/^{206}Pb$	% ±	$^{207*}Pb/^{235}U$	% ±	$^{206*}Pb/^{238}U$	% ±	Corr Coeff	$^{207*}Pb/^{206*}Pb$	% ±	Apparent Ages (Ma) 204 corrected $^{206}Pb/^{238}U$	204 corrected $\pm^{206}Pb/^{238}U$	207 corrected $^{206}Pb/^{238}U$	207 corrected $\pm^{206}Pb/^{238}U$
10229-34.2[a]	405	136	0.347	20.4	1.8E-3	22	3.07	0.132	6.5	16.54	1.4	0.0763	2.4	0.407	12.5	0.0586	1.5	0.1	0.0504	12.4	367	5	369	5
10229-62.2[a]	477	187	0.405	24.2	1.2E-3	25	2.07	0.094	8.6	16.57	1.4	0.0580	2.9	0.329	11.9	0.0591	1.5	0.1	0.0404	11.8	370	5	376	5
10229-37.1[g]	487	151	0.320	26.0	6.2E-4	18	1.07	0.084	11.8	15.9	1.1	0.059	3.5	0.43	5.5	0.0621	1.1	0.20	0.0497	5.4	388	4	391	4
10229-32.2[a]	486	240	0.510	25.4	1.3E-2	20	21.82	0.053	9.7	12.88	4.1	0.2072	3.7	0.130	314.8	0.0607	6.8	0.0	0.0155	314.8	380	25	397	17
10229-58.2[a]	498	217	0.449	26.7	2.8E-3	16	4.79	0.079	7.2	15.26	1.6	0.0779	2.5	0.317	20.1	0.0624	1.8	0.1	0.0368	20.1	390	7	398	6
10229-40.1[a]	627	194	0.320	36.2	2.3E-3	23	3.90	0.060	9.0	14.29	1.5	0.0741	2.8	0.378	20.3	0.0673	1.8	0.1	0.0408	20.2	420	7	427	7
Analytical details: Mount IP 566, K100 spot size, primary beam intensity 12 nA, 6 scans.																								
Error in $^{206}Pb/^{238}U$ calibration 1.0% for calibration 1 and 1.27% for calibration 4 (included).																								
Standard Error in Standard calibration was 0.31% for calibration 1 and 0.41% for calibration 4 (not included in above errors but required when comparing data from different mounts).																								
09RAYJR094A; Lab#10184; Foliated granite; NAD 83 Zone 8 7020377 N 385113 E																								
10184-47.1[b]	611	169	0.286	22.7	2.5E-4	24	0.43	0.091	4.4	23.0	1.1	0.0522	1.9	0.290	3.0	0.0433	1.1	0.37	0.0485	2.8	273	3	274	3
10184-86.1	486	178	0.378	22.5	6.7E-5	68	0.12	0.117	4.3	18.5	1.1	0.0515	2.1	0.375	2.7	0.0538	1.1	0.41	0.0506	2.5	338	4	**339**	**4**
10184-72.1	511	176	0.356	23.8	1.1E-4	47	0.19	0.111	3.8	18.4	1.1	0.0540	1.7	0.392	2.6	0.0542	1.1	0.44	0.0524	2.3	340	4	**340**	**4**
10184-64.1	433	161	0.385	20.2	4.6E-5	143	0.08	0.122	4.8	18.4	1.1	0.0560	2.2	0.415	3.1	0.0544	1.1	0.37	0.0553	2.9	342	4	**341**	**4**
10184-47.2	665	261	0.41	31.0	2.9E-5	41	0.05	0.135	3.4	18.4	1.0	0.0502	1.8	0.372	2.1	0.0543	1.0	0.49	0.0497	1.8	341	3	**342**	**3**
10184-79.1	447	162	0.375	20.9	3.6E-5	66	0.06	0.113	4.3	18.3	1.1	0.0532	2.0	0.396	2.4	0.0546	1.1	0.47	0.0526	2.1	343	4	**343**	**4**
10184-81.1	583	215	0.381	27.4	5.2E-6	456	0.01	0.123	3.8	18.3	1.1	0.0531	1.8	0.399	2.2	0.0546	1.1	0.50	0.0531	1.9	343	4	**343**	**4**
10184-5.1	379	148	0.403	17.8	-2.9E-5	27	-0.05	0.130	4.3	18.3	1.2	0.0513	2.2	0.389	2.5	0.0546	1.2	0.48	0.0517	2.1	342	4	**343**	**4**
10184-4.1	402	129	0.332	18.9	8.3E-5	74	0.14	0.103	4.6	18.2	1.1	0.0555	2.0	0.411	2.9	0.0548	1.1	0.39	0.0543	2.6	344	4	**344**	**4**
10184-91.1	451	222	0.508	21.1	5.4E-5	23	0.09	0.162	3.4	18.3	1.1	0.0498	1.9	0.369	2.3	0.0546	1.1	0.49	0.0491	2.0	342	4	**344**	**4**
10184-75.1	528	151	0.295	24.9	1.4E-4	34	0.25	0.084	4.6	18.1	1.1	0.0541	1.9	0.394	2.6	0.0550	1.1	0.43	0.0520	2.4	345	4	**346**	**4**
10184-67.1	580	160	0.285	27.4	1.1E-4	35	0.20	0.084	4.6	18.1	1.1	0.0536	1.8	0.394	2.5	0.0550	1.1	0.45	0.0520	2.2	345	4	**346**	**4**
10184-12.1	447	140	0.323	21.1	2.2E-4	28	0.39	0.088	4.7	18.1	1.1	0.0532	2.0	0.378	3.0	0.0549	1.1	0.37	0.0499	2.8	345	4	**346**	**4**
10184-51.1	519	217	0.432	24.6	1.2E-4	32	0.20	0.136	3.7	18.1	1.1	0.0543	1.9	0.400	2.5	0.0551	1.1	0.45	0.0526	2.2	346	4	**346**	**4**
10184-34.1	448	168	0.387	21.2	2.9E-5	85	0.05	0.125	4.1	18.1	1.1	0.0527	2.0	0.398	2.4	0.0552	1.1	0.47	0.0523	2.1	347	4	**347**	**4**
10184-16.1	399	152	0.393	19.0	5.6E-5	125	0.10	0.128	3.9	18.0	1.1	0.0559	1.9	0.421	2.9	0.0554	1.1	0.39	0.0551	2.7	348	4	**347**	**4**
10184-3.1	170	89	0.540	8.0	5.4E-4	39	0.94	0.161	4.8	18.0	1.1	0.0578	4.0	0.379	8.0	0.0551	1.2	0.15	0.0499	7.9	346	4	**347**	**4**
10184-59.1	431	135	0.323	20.5	2.6E-4	27	0.44	0.101	4.5	18.0	1.1	0.0549	2.0	0.390	3.2	0.0553	1.1	0.36	0.0512	3.0	347	4	**348**	**4**
10184-43.1	746	542	0.750	35.5	7.1E-5	19	0.12	0.241	2.3	18.0	1.1	0.0528	1.5	0.395	2.0	0.0554	1.1	0.57	0.0518	1.6	347	4	**348**	**4**
10184-17.1	421	161	0.394	20.1	9.2E-5	136	0.16	0.126	3.8	18.0	1.1	0.0540	1.9	0.403	4.2	0.0556	1.1	0.27	0.0526	4.0	349	4	**349**	**4**
10184-83.1	656	298	0.469	31.5	3.1E-5	213	0.05	0.150	3.1	17.9	1.1	0.0541	1.6	0.414	2.7	0.0559	1.1	0.42	0.0537	2.4	351	4	**351**	**4**
10184-30.1	407	221	0.560	19.5	3.0E-4	31	0.52	0.165	4.6	17.8	1.2	0.0537	2.6	0.379	4.1	0.0557	1.2	0.28	0.0493	4.0	350	4	**351**	**4**
10184-27.1	376	196	0.539	18.1	6.6E-5	46	0.11	0.169	3.8	17.9	1.1	0.0532	2.1	0.403	2.6	0.0559	1.1	0.43	0.0523	2.3	351	4	**351**	**4**
10184-39.1	398	153	0.398	19.2	4.6E-5	69	0.08	0.125	4.5	17.7	1.2	0.0547	2.1	0.420	2.6	0.0563	1.2	0.46	0.0541	2.3	353	4	**353**	**4**
10184-23.1	553	167	0.313	27.4	-1.1E-5	166	-0.02	0.103	3.8	17.4	1.1	0.0533	1.6	0.424	2.1	0.0576	1.1	0.54	0.0535	1.7	361	4	**361**	**4**
Analytical details: Mount IP 574, K120 spot size, primary beam intensity 7 nA, 6 scans.																								
Error in $^{206}Pb/^{238}U$ calibration 1.1% for calibration 1 and 1.0% for calibration 2 (included).																								
Standard error in standard calibration was 0.28% for calibration 1 and 0.21% for calibration 2 (not included in above errors but required when comparing data from different mounts).																								

Spot name	U (ppm)	Th (ppm)	Th/U	^{206}Pb* (ppm)	^{204}Pb/^{206}Pb	% ±	f(206)^{204} %	^{208*}Pb/^{206*}Pb	% ±	^{238}U/^{206}Pb	% ±	^{207}Pb/^{206}Pb	% ±	^{207*}Pb/^{235}U	% ±	^{206*}Pb/^{238}U	% ±	Corr Coeff	^{207*}Pb/^{206*}Pb	% ±	Apparent Ages (Ma) 204 corrected ^{206}Pb/^{238}U	204 corrected ±^{206}Pb/^{238}U	207 corrected ^{206}Pb/^{238}U	207 corrected ±^{206}Pb/^{238}U
09RAYJR160A; Lab#10032; Metagranodiorite; NAD 83 Zone 8 7007091 N 408367 E																								
10032-62.1[a]	254	97	0.395	11.9	2.0E-3	94	3.55	0.229	15	17.74	3.8	0.119	9.6	0.68	34	0.0544	5.2	0.15	0.090	33	341	17	326	13
10032-59.1[a]	129	39	0.314	5.9	5.5E-3	32	9.48	-0.040	36	17.13	1.6	0.130	14.9	0.36	71	0.0528	3.8	0.05	0.050	71	332	12	333	10
10032-38.1[a]	334	147	0.454	14.8	3.9E-3	19	6.73	0.062	12	18.14	1.3	0.083	11.6	0.17	64	0.0514	1.9	0.03	0.024	64	323	6	334	6
10032-66.1	145	61	0.431	6.6	6.3E-4	43	1.10	0.206	9.6	18.55	2.5	0.0618	4.1	0.386	9.5	0.0533	2.5	0.3	0.0525	9.1	335	8	**335**	**8**
10032-55.1[a]	168	63	0.384	7.7	1.9E-3	25	3.37	0.067	11.0	18.21	1.5	0.0669	5.9	0.279	22.5	0.0531	1.8	0.1	0.0381	22.5	333	6	339	5
10032-27.1	271	83	0.315	12.6	7.5E-4	32	1.30	0.080	10.2	18.33	1.4	0.0616	2.9	0.376	8.0	0.0539	1.4	0.2	0.0506	7.8	338	5	**339**	**5**
10032-46.1	392	155	0.408	18.1	8.6E-4	26	1.49	0.123	6.7	18.34	1.4	0.0610	2.4	0.358	7.7	0.0537	1.5	0.2	0.0484	7.5	337	5	**339**	**5**
10032-43.1	387	246	0.656	18.5	1.1E-3	38	1.96	0.230	11	17.63	1.2	0.091	4.1	0.57	10	0.0556	1.5	0.15	0.075	10	349	5	**340**	**4**
10032-51.1[a]	290	127	0.451	13.5	2.5E-3	25	4.39	0.265	13	17.69	2.2	0.088	5.5	0.38	21	0.0541	2.4	0.11	0.051	21	339	8	340	7
10032-30.1[a]	395	89	0.233	18.0	2.4E-3	28	4.24	-0.009	14	18.06	1.3	0.070	3.4	0.24	33	0.0530	1.8	0.06	0.033	33	333	6	341	5
10032-16.1	426	210	0.509	20.0	1.0E-3	49	1.79	0.150	15	17.95	1.1	0.072	3.2	0.43	14	0.0547	1.4	0.10	0.057	14	343	5	**342**	**4**
10032-21.1[a]	767	410	0.553	35.3	2.3E-3	20	4.07	0.138	6	17.91	1.1	0.072	2.4	0.28	20	0.0536	1.4	0.07	0.037	20	336	5	343	4
10032-18.1	486	210	0.446	22.8	3.5E-4	35	0.61	0.133	6.3	18.16	1.4	0.0572	2.3	0.393	4.5	0.0547	1.4	0.3	0.0520	4.3	344	5	**344**	**5**
10032-56.1[a]	659	402	0.631	30.4	2.6E-3	32	4.57	0.152	10	17.77	1.3	0.073	4.2	0.25	40	0.0537	2.0	0.05	0.034	40	337	7	345	5
10032-9.1	470	237	0.521	22.2	4.3E-4	32	0.74	0.158	5.6	18.06	1.3	0.0571	2.2	0.386	4.9	0.0550	1.4	0.3	0.0509	4.7	345	5	**346**	**5**
10032-24.1	333	144	0.448	15.8	5.6E-4	31	0.96	0.154	7.1	17.94	1.3	0.0616	2.7	0.407	5.8	0.0552	1.4	0.2	0.0535	5.6	346	5	**346**	**5**
10032-1.1[a]	441	220	0.515	20.4	2.0E-3	21	3.44	0.141	8	17.88	1.9	0.064	4.3	0.26	20	0.0540	2.0	0.10	0.035	20	339	7	346	7
10032-53.1	348	130	0.386	16.4	7.3E-4	12	1.26	0.100	7.9	17.96	2.0	0.0600	2.6	0.374	4.6	0.0550	2.0	0.4	0.0493	4.2	345	7	**347**	**7**
10032-33.1	499	241	0.500	24.1	---	100	0.00	0.192	10	17.78	1.1	0.067	3.8	0.52	4	0.0562	1.1	0.29	0.067	4	353	4	**347**	**4**
10032-26.1	344	127	0.381	16.4	2.8E-4	25	0.48	0.123	7.7	17.91	1.5	0.0576	3.3	0.410	4.3	0.0556	1.5	0.3	0.0535	4.0	349	5	**349**	**5**
10032-10.1	606	297	0.507	29.0	7.8E-4	20	1.35	0.160	8	17.68	1.1	0.063	2.9	0.40	6	0.0558	1.2	0.20	0.052	6	350	4	**351**	**4**
10032-64.1	222	105	0.489	11.3	1.6E-3	375	2.69	0.243	19	16.44	1.5	0.117	4.6	0.78	87	0.0592	10.5	0.12	0.096	87	371	38	353	6
10032-48.1	543	294	0.560	26.6	6.2E-4	111	1.07	0.175	10	17.32	1.2	0.070	3.8	0.48	17	0.0571	1.7	0.10	0.062	17	358	6	**355**	**4**
10032-32.1	675	203	0.310	33.1	5.1E-4	26	0.88	0.084	6.4	17.38	1.4	0.0564	1.9	0.386	4.8	0.0570	1.4	0.3	0.0490	4.5	358	5	**360**	**5**

Analytical details: Mount IP 566, K100 spot size, primary beam intensity 2 nA, 6 scans.

Error in ^{206}Pb/^{238}U calibration is 1.0% for calibration 3 and 1.3% for calibration 4 (included).

Standard error in standard calibration was 0.31% for calibration 3 and 0.41% for calibration 4 (not included in above errors but required when comparing data from different mounts).

Spot name	U (ppm)	Th (ppm)	Th/U	^{206}Pb* (ppm)	^{204}Pb/^{206}Pb	% ±	f(206)^{204} %	^{208*}Pb/^{206*}Pb	% ±	^{238}U/^{206}Pb	% ±	^{207}Pb/^{206}Pb	% ±	^{207*}Pb/^{235}U	% ±	^{206*}Pb/^{238}U	% ±	Corr Coeff	^{207*}Pb/^{206*}Pb	% ±	204 corrected ^{206}Pb/^{238}U	204 corrected ±^{206}Pb/^{238}U	207 corrected ^{206}Pb/^{238}U	207 corrected ±^{206}Pb/^{238}U
09RAYMC081A; Lab#10077; Metagranodiorite; NAD 83 Zone 8 7019050 N 381613 E																								
10077-36.1[a]	251	91	0.375	11.9	2.0E-3	34	3.51	0.101	11.2	17.5	2.4	0.085	7.5	0.42	22.3	0.0551	2.7	0.12	0.0551	22.1	346	9	345	9
10077-58.1	598	296	0.510	28.6	3.2E-4	28	0.56	0.143	7.2	17.9	2.0	0.061	2.5	0.43	4.1	0.0555	2.0	0.48	0.0566	3.6	349	7	**347**	**7**
10077-27.1[a]	164	39	0.244	7.6	3.1E-3	29	5.42	0.077	11.4	17.5	1.7	0.074	3.9	0.20	55.0	0.0540	2.4	0.04	0.0273	54.9	339	8	350	6
10077-61.1	138	74	0.554	6.7	8.3E-4	17	1.44	0.172	9.9	17.31	1.6	0.0772	3.7	0.512	5.7	0.0569	1.6	0.3	0.0652	5.4	357	6	**352**	**6**
10077-7.1[a]	285	83	0.302	13.6	1.2E-3	24	2.09	0.069	9.2	17.55	1.5	0.0650	2.8	0.364	10.0	0.0558	1.6	0.2	0.0473	9.9	350	5	352	5
10077-1.1	293	210	0.740	14.3	4.4E-4	162	0.76	0.252	6.1	17.40	1.3	0.0613	3.5	0.432	19.5	0.0570	1.8	0.1	0.0549	19.4	358	6	**357**	**5**
10077-52.1	506	211	0.431	24.9	3.1E-4	42	0.54	0.123	8.4	17.38	2.6	0.0575	2.9	0.418	5.4	0.0572	2.6	0.5	0.0529	4.8	359	9	**359**	**9**
10077-35.1	353	115	0.336	17.1	1.1E-3	27	1.83	0.090	8.5	17.34	1.3	0.0590	3.4	0.339	10.9	0.0566	1.4	0.1	0.0435	10.8	355	5	**359**	**5**
10077-76.1	532	284	0.552	26.1	4.7E-4	37	0.81	0.169	5.4	17.33	1.3	0.0563	2.2	0.390	5.9	0.0572	1.3	0.2	0.0494	5.7	359	5	**361**	**5**
10077-28.1	379	131	0.356	18.7	1.7E-4	39	0.30	0.121	7.2	17.33	1.7	0.0548	2.5	0.414	3.7	0.0575	1.7	0.5	0.0522	3.2	360	6	**361**	**6**
10077-67.1	274	93	0.350	13.6	2.4E-4	292	0.42	0.155	7.5	17.26	1.4	0.0579	2.9	0.432	19.6	0.0577	1.9	0.1	0.0543	19.5	362	7	**361**	**5**

Spot name	U (ppm)	Th (ppm)	Th/U	^{206}Pb* (ppm)	^{204}Pb/^{206}Pb	% ±	f(206)^{204} %	^{208*}Pb/^{206*}Pb	% ±	^{238}U/^{206}Pb	% ±	^{207}Pb/^{206}Pb	% ±	^{207*}Pb/^{235}U	% ±	^{206*}Pb/^{238}U	% ±	Corr Coeff	^{207*}Pb/^{206*}Pb	% ±	Apparent Ages (Ma) 204 corrected ^{206}Pb/^{238}U	±^{206}Pb/^{238}U	Apparent Ages (Ma) 207 corrected ^{206}Pb/^{238}U	±^{206}Pb/^{238}U
10077-14.1	389	177	0.470	19.3	3.4E-4	32	0.59	0.168	6.0	17.17	1.4	0.0592	2.4	0.433	4.2	0.0579	1.4	0.3	0.0543	3.9	363	5	**363**	**5**
10077-23.1	1736	721	0.429	85.9	9.8E-4	17	1.70	0.120	4.0	17.1	1.0	0.063	2.5	0.39	6.1	0.0576	1.1	0.18	0.0491	6.0	361	4	**363**	**4**
10077-24.1	330	141	0.442	16.4	5.5E-4	31	0.95	0.127	7.3	17.13	1.3	0.0602	2.6	0.416	5.8	0.0578	1.4	0.2	0.0522	5.7	362	5	**363**	**5**
10077-89.1	2505	1517	0.626	125.5	5.9E-5	30	0.10	0.210	2.7	17.1	1.1	0.057	1.2	0.45	1.6	0.0583	1.1	0.64	0.0558	1.3	365	4	**364**	**4**
10077-68.1	332	149	0.463	16.7	3.9E-4	46	0.68	0.149	11.1	16.94	1.6	0.0575	2.7	0.419	6.1	0.0586	1.6	0.3	0.0518	5.9	367	6	**368**	**6**
10077-22.1	812	266	0.338	41.2	1.6E-4	30	0.28	0.106	5.9	16.9	1.0	0.059	1.8	0.46	2.5	0.0591	1.0	0.41	0.0571	2.3	370	4	**369**	**4**
10077-92.1	321	121	0.389	16.5	8.3E-4	38	1.43	0.097	8.0	16.48	1.3	0.0636	3.9	0.425	10.4	0.0598	1.4	0.1	0.0516	10.3	375	5	**376**	**5**
10077-42.1[c]	798	218	0.282	58.3	1.9E-4	19	0.34	0.129	5.5	11.7	1.1	0.082	1.6	0.92	2.1	0.0850	1.1	0.55	0.0788	1.8	526	6	513	6

Analytical details: Mount IP 566, K100 spot size, primary beam intensity 2 nA, 6 scans.

Error in ^{206}Pb/^{238}U calibration 1.0% for calibration 1 and 1.27% for calibration 4 (included).

Standard error in standard calibration was 0.31% for calibration 3 and 0.41% for calibration 4 (not included in above errors but required when comparing data from different mounts).

09RAYMC031A; Lab#10189; Felsic schist; NAD 83 Zone 8 7013219 N 392247 E

Spot name	U (ppm)	Th (ppm)	Th/U	^{206}Pb* (ppm)	^{204}Pb/^{206}Pb	% ±	f(206)^{204} %	^{208*}Pb/^{206*}Pb	% ±	^{238}U/^{206}Pb	% ±	^{207}Pb/^{206}Pb	% ±	^{207*}Pb/^{235}U	% ±	^{206*}Pb/^{238}U	% ±	Corr Coeff	^{207*}Pb/^{206*}Pb	% ±	Apparent Ages (Ma) 204 corrected ^{206}Pb/^{238}U	±^{206}Pb/^{238}U	Apparent Ages (Ma) 207 corrected ^{206}Pb/^{238}U	±^{206}Pb/^{238}U
10189-31.2[d]	233	11	0.05	5.6	1.0E-3	35	1.82	-0.018	26.3	34.9	1.1	0.0536	5.0	0.148	16.5	0.0282	1.3	0.08	0.0380	16.4	179	2	181	2
10189-3.1[a, d]	93	0	0.01	2.3	1.5E-3	45	2.62	-0.005	18.8	33.5	1.1	0.0677	5.1	0.183	24.1	0.0291	1.7	0.07	0.0455	24.0	185	3	186	2
10189-7.2[d]	167	2	0.01	4.2	7.5E-4	26	1.30	0.011	21.4	33.8	1.2	0.0593	5.1	0.195	8.8	0.0292	1.3	0.15	0.0483	8.7	186	2	186	2
10189-17.1[d]	265	2	0.006	6.7	1.7E-4	35	0.30	0.003	25.7	33.7	1.1	0.0511	4.2	0.198	4.9	0.0296	1.1	0.23	0.0485	4.8	188	2	188	2
10189-85.1[a, d]	77	1	0.02	2.0	2.1E-3	54	3.56	-0.021	26.2	32.6	1.9	0.0734	7.0	0.176	41.6	0.0295	2.8	0.07	0.0431	41.5	188	5	189	4
10189-20.2[d]	1445	8	0.01	37.2	1.7E-5	99	0.03	0.005	14.1	33.4	1.0	0.0518	1.5	0.213	1.9	0.0299	1.0	0.55	0.0515	1.6	190	2	190	2
10189-19.1[d]	617	9	0.01	16.3	1.9E-4	51	0.34	0.003	19.0	32.4	1.0	0.0526	2.5	0.211	4.1	0.0307	1.0	0.25	0.0497	4.0	195	2	195	2
10189-56.1[a, d]	188	2	0.01	5.0	2.4E-3	20	4.10	0.013	10.0	31.2	1.0	0.0787	3.6	0.186	17.8	0.0308	1.3	0.08	0.0439	17.7	195	3	197	2
10189-70.1[d]	630	9	0.01	16.7	5.1E-4	23	0.89	-0.009	17.7	32.1	1.0	0.0533	2.5	0.195	4.9	0.0309	1.0	0.21	0.0458	4.8	196	2	197	2
10189-41.1[d]	1605	5	0.00	43.0	2.8E-4	27	0.48	-0.005	15.9	31.9	1.0	0.0514	1.6	0.204	3.1	0.0312	1.0	0.33	0.0474	2.9	198	2	198	2
10189-61.1[d]	677	5	0.01	18.2	1.8E-4	46	0.32	0.001	21.2	31.8	1.0	0.0518	2.2	0.212	3.6	0.0313	1.0	0.29	0.0491	3.4	199	2	199	2
10189-54.1[d]	387	10	0.03	10.5	5.7E-4	37	1.00	-0.008	19.2	31.3	1.0	0.0512	3.0	0.186	8.2	0.0316	1.1	0.13	0.0427	8.2	201	2	202	2
10189-81.1[a, d]	254	41	0.17	6.8	3.8E-3	14	6.61	-0.120	17.4	29.9	1.1	0.0617	3.8	0.012	342.7	0.0312	1.5	0.00	0.0028	342.7	198	3	209	2
10189-27.1[e]	555	148	0.28	21.7	4.3E-5	58	0.07	0.094	4.9	22.0	1.0	0.0538	2.0	0.333	2.4	0.0455	1.0	0.42	0.0531	2.2	287	3	287	3
10189-14.1[e]	587	263	0.46	24.1	4.3E-4	21	0.75	0.136	4.0	20.8	1.0	0.0519	2.2	0.300	3.9	0.0477	1.0	0.27	0.0456	3.8	300	3	303	3
10189-20.1[e]	473	210	0.458	20.0	2.5E-4	64	0.43	0.149	4.6	20.2	1.1	0.0561	2.4	0.357	5.2	0.0492	1.2	0.22	0.0525	5.1	310	4	310	3
10189-31.1[e]	440	131	0.31	18.6	7.3E-4	17	1.27	0.078	4.9	20.0	1.0	0.0579	2.1	0.320	4.8	0.0493	1.0	0.22	0.0471	4.7	310	3	312	3
10189-54.2	305	139	0.47	13.1	1.8E-4	41	0.30	0.157	4.7	19.9	1.0	0.0556	2.6	0.366	3.5	0.0501	1.0	0.30	0.0530	3.3	315	3	**315**	**3**
10189-36.1	369	233	0.654	16.0	1.4E-4	42	0.24	0.193	4.4	19.8	1.1	0.0543	2.6	0.364	3.4	0.0504	1.1	0.34	0.0523	3.2	317	4	**317**	**4**
10189-33.1	356	186	0.541	15.3	3.8E-4	28	0.65	0.148	5.1	19.8	1.2	0.0521	2.8	0.322	4.7	0.0501	1.2	0.25	0.0466	4.6	315	4	**318**	**4**
10189-73.1	393	187	0.49	17.0	2.6E-4	41	0.46	0.144	4.6	19.8	1.1	0.0544	2.4	0.351	4.2	0.0504	1.1	0.26	0.0506	4.1	317	3	**318**	**3**
10189-25.1	394	189	0.50	17.1	6.4E-6	1418	0.01	0.163	4.7	19.8	1.0	0.0527	2.6	0.367	3.8	0.0505	1.0	0.28	0.0527	3.6	318	3	**318**	**3**
10189-59.1	287	96	0.344	12.4	2.2E-4	58	0.38	0.105	5.9	19.7	1.1	0.0549	2.7	0.360	4.8	0.0505	1.2	0.24	0.0516	4.7	318	4	**318**	**4**
10189-39.1	245	94	0.396	10.7	1.5E-4	23	0.26	0.123	6.3	19.7	1.1	0.0546	3.0	0.366	3.5	0.0506	1.1	0.33	0.0524	3.3	319	4	**319**	**4**
10189-49.1	380	157	0.427	16.5	2.8E-4	42	0.48	0.117	5.4	19.6	1.1	0.0542	2.6	0.351	4.5	0.0507	1.1	0.25	0.0501	4.4	319	4	**320**	**4**
10189-11.1	316	151	0.494	13.8	1.1E-4	19	0.18	0.157	5.2	19.7	1.1	0.0529	2.9	0.360	3.2	0.0508	1.1	0.36	0.0514	3.0	319	4	**320**	**4**
10189-22.1	414	257	0.64	18.1	3.6E-4	25	0.63	0.194	3.6	19.5	1.0	0.0556	2.2	0.353	3.7	0.0509	1.0	0.28	0.0503	3.6	320	3	**321**	**3**
10189-4.1[c]	631	442	0.724	27.8	1.8E-4	32	0.31	0.218	3.4	19.4	1.1	0.0536	2.2	0.360	3.0	0.0513	1.1	0.37	0.0510	2.8	322	4	**323**	**4**

Spot name	U (ppm)	Th (ppm)	Th/U	$^{206}Pb^{*}$ (ppm)	$^{204}Pb/^{206}Pb$	% ±	$f(206)^{204}$ %	$^{208*}Pb/^{206*}Pb$	% ±	$^{238}U/^{206}Pb$	% ±	$^{207}Pb/^{206}Pb$	% ±	$^{207*}Pb/^{235}U$	% ±	$^{206*}Pb/^{238}U$	% ±	Corr Coeff	$^{207*}Pb/^{206*}Pb$	% ±	Apparent Ages (Ma) 204 corrected $^{206}Pb/^{238}U$	$\pm^{206}Pb/^{238}U$	207 corrected $^{206}Pb/^{238}U$	$\pm^{206}Pb/^{238}U$
10189-67.1	217	92	0.44	9.6	2.4E-4	38	0.41	0.130	6.4	19.3	1.0	0.0544	3.2	0.362	4.4	0.0515	1.1	0.24	0.0509	4.3	324	3	**324**	**3**
10189-30.1	775	705	0.94	34.3	1.4E-4	33	0.24	0.310	2.3	19.3	1.0	0.0540	1.7	0.369	2.4	0.0516	1.0	0.42	0.0520	2.2	324	3	**324**	**3**
10189-38.1	463	232	0.52	20.6	1.0E-4	77	0.18	0.147	3.8	19.3	1.0	0.0551	2.0	0.382	3.1	0.0517	1.0	0.33	0.0536	3.0	325	3	**325**	**3**
10189-65.1	453	340	0.77	20.1	3.1E-5	29	0.05	0.250	3.2	19.4	1.0	0.0522	2.2	0.369	2.5	0.0516	1.0	0.42	0.0518	2.2	325	3	**325**	**3**
10189-87.1	312	149	0.49	13.8	5.2E-4	24	0.91	0.162	4.6	19.2	1.0	0.0567	2.6	0.349	4.9	0.0516	1.1	0.22	0.0490	4.8	324	3	**326**	**3**
10189-18.1	353	146	0.43	15.7	1.7E-4	47	0.30	0.152	7.7	19.3	1.1	0.0521	3.1	0.353	4.2	0.0518	1.1	0.25	0.0495	4.0	325	3	**327**	**3**
10189-58.1	668	536	0.83	29.9	1.3E-4	34	0.23	0.263	2.3	19.2	1.0	0.0527	1.6	0.364	2.4	0.0521	1.0	0.43	0.0508	2.1	327	3	**328**	**3**
10189-60.1	349	227	0.67	15.6	2.8E-4	30	0.49	0.198	3.9	19.2	1.0	0.0529	2.4	0.349	3.8	0.0519	1.0	0.27	0.0488	3.7	326	3	**328**	**3**
10189-69.1	294	110	0.39	13.2	2.3E-5	37	0.04	0.122	5.5	19.1	1.1	0.0543	2.6	0.389	2.8	0.0523	1.1	0.37	0.0540	2.6	329	3	**328**	**3**
10189-7.1[c]	879	553	0.650	40.3	1.5E-4	30	0.25	0.202	2.8	18.7	1.1	0.0535	1.7	0.378	2.5	0.0534	1.1	0.45	0.0514	2.2	335	4	336	4
10189-29.1[c]	745	418	0.58	34.2	1.2E-4	43	0.21	0.193	2.5	18.6	1.0	0.0541	1.5	0.386	2.4	0.0535	1.0	0.43	0.0523	2.1	336	3	337	3
10189-32.1[a, c]	666	126	0.20	32.2	1.4E-3	13	2.50	0.025	5.9	17.3	1.0	0.0556	2.2	0.264	9.2	0.0562	1.1	0.12	0.0341	9.1	353	4	361	4

Analytical details: Mount IP 574, K120 spot size, primary beam intensity 7 nA, 6 scans.

Error in $^{206}Pb/^{238}U$ calibration 1.1% for calibration 1 and 1.0% for calibration 2 (included).

Standard error in etandard calibration was 0.28% for calibration 1 and 0.21% for calibration 2 (not included in above errors but required when comparing data from different mounts).

09RAYJR177A; Lab#10034; Metamonzogranite; NAD 83 Zone 8 7011907 N 373965 E

10034-41.1[b]	485	134	0.286	16.4	5.6E-5	32	0.10	0.093	4.8	25.3	1.1	0.0520	2.0	0.278	2.4	0.0394	1.1	0.46	0.0512	2.1	249	3	249	3
10034-3.2[b]	1447	619	0.44	49.3	8.6E-5	18	0.15	0.148	3.0	25.2	1.0	0.0518	1.6	0.276	2.0	0.0397	1.0	0.52	0.0505	1.7	251	3	251	3
10034-21.1	402	92	0.237	13.8	5.4E-4	25	0.93	0.061	5.7	24.8	1.1	0.0532	2.2	0.250	5.3	0.0400	1.2	0.22	0.0453	5.2	253	3	**254**	**3**
10034-85.1	281	66	0.241	9.9	1.4E-4	72	0.24	0.081	7.0	24.3	1.1	0.0538	2.8	0.293	4.2	0.0410	1.1	0.27	0.0518	4.1	259	3	**259**	**3**
10034-73.1	429	124	0.299	15.1	2.7E-5	73	0.05	0.099	4.8	24.3	1.1	0.0534	2.1	0.300	2.4	0.0411	1.1	0.46	0.0530	2.2	260	3	**259**	**3**
10034-91.1	514	161	0.324	18.1	2.3E-4	27	0.40	0.100	4.5	24.3	1.1	0.0515	2.0	0.272	3.1	0.0410	1.1	0.36	0.0481	2.9	259	3	**260**	**3**
10034-57.1	540	153	0.293	19.1	1.1E-4	51	0.18	0.096	4.4	24.3	1.1	0.0524	1.9	0.289	2.7	0.0411	1.1	0.41	0.0509	2.5	260	3	**260**	**3**
10034-67.1	592	136	0.238	20.9	2.0E-4	17	0.34	0.073	6.0	24.2	1.1	0.0526	2.3	0.282	2.9	0.0411	1.1	0.39	0.0497	2.7	260	3	**260**	**3**
10034-19.1	721	252	0.361	25.5	1.5E-4	29	0.25	0.109	3.7	24.2	1.1	0.0534	1.7	0.292	2.4	0.0413	1.1	0.46	0.0513	2.2	261	3	**261**	**3**
10034-45.1	602	190	0.33	21.3	8.8E-5	109	0.15	0.093	4.9	24.2	1.0	0.0503	2.1	0.279	3.8	0.0412	1.0	0.27	0.0491	3.6	260	3	**261**	**3**
10034-29.1	424	116	0.282	15.1	5.5E-5	62	0.10	0.098	4.9	24.2	1.1	0.0523	2.1	0.293	2.6	0.0414	1.1	0.43	0.0515	2.4	261	3	**261**	**3**
10034-25.1	1818	1244	0.71	64.6	6.7E-5	40	0.12	0.233	1.8	24.1	1.0	0.0516	1.2	0.289	1.8	0.0414	1.0	0.57	0.0506	1.5	261	3	**262**	**3**
10034-34.1	658	204	0.320	23.4	1.4E-4	34	0.24	0.109	4.0	24.1	1.2	0.0523	1.8	0.287	2.6	0.0414	1.2	0.44	0.0503	2.3	261	3	**262**	**3**
10034-49.1	302	69	0.236	10.8	4.9E-5	55	0.08	0.073	6.7	24.1	1.1	0.0516	2.5	0.291	2.9	0.0415	1.1	0.39	0.0509	2.7	262	3	**262**	**3**
10034-18.1	287	53	0.191	10.2	1.9E-4	55	0.33	0.057	7.6	24.1	1.1	0.0521	2.6	0.282	4.4	0.0414	1.1	0.26	0.0493	4.2	262	3	**262**	**3**
10034-66.1	917	294	0.331	32.7	-1.6E-5	74	-0.03	0.116	3.3	24.1	1.1	0.0510	1.6	0.293	2.0	0.0416	1.1	0.57	0.0512	1.6	262	3	**263**	**3**
10034-95.1	646	206	0.329	23.0	3.6E-4	20	0.62	0.102	3.8	24.0	1.1	0.0535	1.8	0.276	3.1	0.0414	1.1	0.36	0.0483	2.9	262	3	**263**	**3**
10034-105.1	691	265	0.396	24.7	3.2E-5	227	0.06	0.129	3.2	24.0	1.1	0.0516	1.6	0.293	2.9	0.0416	1.1	0.39	0.0511	2.7	263	3	**263**	**3**
10034-13.1	484	150	0.321	17.2	3.9E-5	151	0.07	0.116	4.4	24.1	1.1	0.0485	2.2	0.274	3.0	0.0415	1.1	0.37	0.0480	2.8	262	3	**263**	**3**
10034-75.1	301	102	0.35	10.8	1.4E-4	254	0.24	0.104	6.6	23.9	1.2	0.0542	2.9	0.300	10.6	0.0417	1.3	0.13	0.0521	10.5	263	3	**263**	**3**
10034-36.1	295	76	0.265	10.6	2.0E-4	36	0.34	0.089	5.8	24.0	1.1	0.0520	2.5	0.282	3.6	0.0416	1.1	0.32	0.0492	3.4	263	3	**263**	**3**
10034-62.1	419	79	0.196	15.0	2.2E-4	27	0.38	0.057	5.9	23.9	1.1	0.0512	2.1	0.276	3.1	0.0417	1.1	0.36	0.0480	2.9	264	3	**265**	**3**
10034-62.2	338	108	0.33	12.2	8.5E-5	83	0.15	0.100	6.8	23.8	1.0	0.0548	3.0	0.310	3.7	0.0420	1.1	0.28	0.0535	3.6	265	3	**265**	**3**
10034-78.1	640	64	0.104	23.1	8.9E-5	84	0.15	0.033	6.5	23.8	1.1	0.0522	1.7	0.295	3.0	0.0420	1.1	0.37	0.0509	2.8	265	3	**265**	**3**

Spot name	U (ppm)	Th (ppm)	Th/U	$^{206}Pb^*$ (ppm)	$^{204}Pb/^{206}Pb$	% ±	$f(206)^{204}$ %	$^{208*}Pb/^{206*}Pb$	% ±	$^{238}U/^{206}Pb$	% ±	$^{207}Pb/^{206}Pb$	% ±	$^{207*}Pb/^{235}U$	% ±	$^{206*}Pb/^{238}U$	% ±	Corr Coeff	$^{207*}Pb/^{206*}Pb$	% ±	Apparent Ages (Ma) 204 corrected $^{206}Pb/^{238}U$	± $^{206}Pb/^{238}U$	Apparent Ages (Ma) 207 corrected $^{206}Pb/^{238}U$	± $^{206}Pb/^{238}U$
10034-3.1	828	329	0.411	29.9	9.4E-5	49	0.16	0.128	3.1	23.8	1.1	0.0515	1.5	0.290	2.4	0.0420	1.1	0.47	0.0501	2.1	265	3	**266**	**3**
10034-92.1	808	258	0.331	29.3	2.3E-4	29	0.40	0.106	3.5	23.6	1.2	0.0543	1.6	0.296	2.8	0.0422	1.2	0.42	0.0509	2.6	266	3	**267**	**3**
10034-17.1	670	189	0.29	24.4	1.7E-4	27	0.29	0.101	4.1	23.5	1.0	0.0529	1.8	0.295	2.5	0.0424	1.0	0.40	0.0504	2.3	268	3	**268**	**3**
10034-104.1	822	244	0.307	30.0	3.7E-5	74	0.06	0.095	3.5	23.5	1.1	0.0513	1.5	0.297	2.1	0.0425	1.1	0.54	0.0508	1.7	268	3	**268**	**3**
10034-46.1	525	155	0.305	19.2	2.2E-4	39	0.39	0.114	5.5	23.4	1.1	0.0533	1.9	0.293	3.5	0.0425	1.1	0.32	0.0500	3.3	268	3	**269**	**3**
10034-51.1[c]	989	721	0.75	37.7	9.1E-5	21	0.16	0.253	2.5	22.5	1.0	0.0536	1.7	0.320	2.1	0.0444	1.0	0.50	0.0522	1.8	280	3	280	3
10034-9.1[c]	530	140	0.273	22.4	2.8E-5	23	0.05	0.086	4.5	20.3	1.2	0.0522	1.8	0.352	2.2	0.0492	1.2	0.53	0.0518	1.8	310	4	310	4
10034-10.1[c]	457	131	0.30	20.5	5.7E-5	32	0.10	0.093	5.3	19.1	1.0	0.0537	2.2	0.382	2.5	0.0523	1.0	0.40	0.0529	2.3	329	3	329	3
10034-15.1[c]	471	241	0.53	21.5	9.8E-5	24	0.17	0.175	3.8	18.8	1.0	0.0546	2.2	0.389	2.6	0.0532	1.0	0.40	0.0531	2.3	334	3	334	3
10034-81.1[c]	524	293	0.578	25.7	6.8E-5	41	0.12	0.185	2.9	17.5	1.1	0.0526	1.7	0.405	2.2	0.0570	1.1	0.50	0.0516	1.9	357	4	358	4
10034-5.1[c]	679	229	0.349	33.3	1.2E-4	28	0.21	0.112	3.3	17.5	1.2	0.0536	1.5	0.408	2.2	0.0570	1.2	0.53	0.0518	1.8	358	4	358	4
10034-53.1[c]	860	364	0.437	42.3	6.2E-5	38	0.11	0.138	2.7	17.5	1.1	0.0548	1.4	0.425	1.9	0.0572	1.1	0.59	0.0539	1.5	359	4	359	4

Analytical details: Mount IP 574, K120 spot size, primary beam intensity 7 nA, 6 scans.

Error in $^{206}Pb/^{238}U$ calibration is 1.1% for calibration 1 and 1.0% for calibration 2 (included).

Standard error in standard calibration was 0.28% for calibration 1 and 0.21% for calibration 2 (not included in above errors but required when comparing data from different mounts).

09RAYJR178A; Lab#10185; Metagranodiorite; NAD 83 Zone 8 7006830 N 356537 E

Spot name	U (ppm)	Th (ppm)	Th/U	$^{206}Pb^*$ (ppm)	$^{204}Pb/^{206}Pb$	% ±	$f(206)^{204}$ %	$^{208*}Pb/^{206*}Pb$	% ±	$^{238}U/^{206}Pb$	% ±	$^{207}Pb/^{206}Pb$	% ±	$^{207*}Pb/^{235}U$	% ±	$^{206*}Pb/^{238}U$	% ±	Corr Coeff	$^{207*}Pb/^{206*}Pb$	% ±	Apparent Ages (Ma) 204 corrected $^{206}Pb/^{238}U$	± $^{206}Pb/^{238}U$	Apparent Ages (Ma) 207 corrected $^{206}Pb/^{238}U$	± $^{206}Pb/^{238}U$
10185-7.1[d]	1598	35	0.02	40.8	2.3E-4	29	0.39	0.001	12.3	33.5	1.0	0.0531	1.6	0.204	2.8	0.0297	1.0	0.37	0.0498	2.6	189	2	189	2
10185-31.1[d]	1456	14	0.01	37.4	1.0E-4	29	0.18	0.002	15.4	33.4	1.0	0.0505	1.6	0.202	2.1	0.0299	1.0	0.47	0.0490	1.9	190	2	190	2
10185-20.2[e]	804	246	0.316	25.5	2.8E-4	24	0.49	0.108	5.0	26.9	1.1	0.0552	2.3	0.260	3.4	0.0369	1.1	0.34	0.0510	3.2	234	3	234	3
10185-11.1	374	96	0.266	13.1	9.5E-5	24	0.16	0.097	7.0	24.5	1.1	0.0533	3.1	0.291	3.4	0.0407	1.1	0.33	0.0519	3.2	257	3	**257**	**3**
10185-12.1	789	338	0.443	27.6	1.3E-4	31	0.23	0.141	4.3	24.5	1.1	0.0533	2.2	0.289	2.8	0.0408	1.1	0.40	0.0514	2.6	258	3	**258**	**3**
10185-30.1	230	64	0.286	8.1	1.0E-4	98	0.18	0.095	9.0	24.5	1.2	0.0541	3.8	0.296	5.0	0.0408	1.2	0.25	0.0526	4.8	258	3	**258**	**3**
10185-49.1	701	341	0.502	24.5	7.2E-5	86	0.12	0.153	4.1	24.5	1.1	0.0519	2.2	0.286	3.1	0.0408	1.1	0.36	0.0508	2.9	258	3	**258**	**3**
10185-28.1	783	369	0.49	27.4	1.0E-4	38	0.17	0.169	3.2	24.5	1.1	0.0515	1.8	0.281	2.5	0.0408	1.1	0.45	0.0500	2.2	258	3	**258**	**3**
10185-25.1	522	172	0.34	18.4	1.2E-4	30	0.21	0.105	4.8	24.3	1.0	0.0508	2.3	0.278	2.8	0.0411	1.0	0.37	0.0490	2.6	260	3	**260**	**3**
10185-33.1	677	299	0.46	24.0	1.7E-4	37	0.30	0.148	3.9	24.1	1.0	0.0540	2.1	0.293	3.0	0.0413	1.0	0.34	0.0514	2.8	261	3	**261**	**3**
10185-47.1	521	175	0.35	18.4	2.3E-4	32	0.40	0.115	4.6	24.2	1.0	0.0514	2.2	0.273	3.4	0.0412	1.0	0.30	0.0480	3.3	260	3	**261**	**3**
10185-3.1	382	88	0.238	13.6	1.3E-4	78	0.22	0.078	7.1	24.0	1.1	0.0530	2.8	0.292	4.2	0.0415	1.1	0.27	0.0511	4.1	262	3	**262**	**3**
10185-13.1	532	191	0.371	19.0	2.4E-4	26	0.41	0.110	4.8	23.9	1.1	0.0557	2.2	0.300	3.2	0.0417	1.1	0.36	0.0522	3.0	263	3	**263**	**3**
10185-55.1	1075	546	0.53	38.5	-3.3E-5	59	-0.06	0.165	3.0	24.0	1.0	0.0519	1.7	0.301	2.0	0.0417	1.0	0.50	0.0524	1.7	263	3	**263**	**3**
10185-26.1	805	401	0.514	28.8	1.8E-5	145	0.03	0.177	3.3	24.0	1.1	0.0516	1.9	0.295	2.4	0.0417	1.1	0.47	0.0513	2.1	263	3	**263**	**3**
10185-9.1	783	341	0.450	28.1	2.0E-4	34	0.34	0.142	4.6	23.9	1.2	0.0540	2.4	0.295	3.4	0.0418	1.2	0.35	0.0512	3.2	264	3	**264**	**3**
10185-15.1	937	522	0.576	33.7	4.9E-5	65	0.09	0.192	2.9	23.9	1.2	0.0520	1.8	0.296	2.3	0.0418	1.2	0.52	0.0513	2.0	264	3	**264**	**3**
10185-17.1	1007	524	0.54	36.2	1.0E-4	30	0.18	0.178	2.6	23.8	1.0	0.0532	1.5	0.298	2.1	0.0419	1.0	0.49	0.0516	1.8	264	3	**264**	**3**
10185-16.1	740	364	0.508	26.6	9.6E-6	695	0.02	0.160	3.7	23.9	1.1	0.0513	2.1	0.295	3.0	0.0419	1.1	0.37	0.0511	2.8	264	3	**265**	**3**
10185-8.1	773	357	0.477	27.8	2.1E-4	45	0.36	0.147	4.4	23.8	1.1	0.0527	2.4	0.286	3.9	0.0419	1.1	0.29	0.0496	3.7	264	3	**265**	**3**
10185-22.1	817	399	0.505	29.4	1.2E-4	34	0.21	0.163	3.2	23.8	1.1	0.0523	1.8	0.292	2.5	0.0419	1.1	0.45	0.0505	2.2	265	3	**265**	**3**
10185-41.1	635	261	0.42	22.9	9.1E-5	35	0.16	0.141	4.0	23.8	1.0	0.0519	2.1	0.292	2.6	0.0420	1.0	0.40	0.0505	2.4	265	3	**265**	**3**
10185-2.1	648	223	0.36	23.4	1.9E-4	33	0.33	0.112	4.5	23.7	1.0	0.0513	2.1	0.281	3.1	0.0420	1.0	0.33	0.0485	3.0	266	3	**266**	**3**
10185-20.1	1378	452	0.339	50.1	1.3E-4	26	0.22	0.103	3.0	23.6	1.1	0.0541	1.3	0.305	2.0	0.0423	1.1	0.55	0.0522	1.7	267	3	**267**	**3**

Spot name	U (ppm)	Th (ppm)	Th/U	^{206}Pb* (ppm)	^{204}Pb/^{206}Pb	% ±	f(206)^{204} %	^{208*}Pb/^{206*}Pb	% ±	^{238}U/^{206}Pb	% ±	^{207}Pb/^{206}Pb	% ±	^{207*}Pb/^{235}U	% ±	^{206*}Pb/^{238}U	% ±	Corr Coeff	^{207*}Pb/^{206*}Pb	% ±	Apparent Ages (Ma): 204 corrected ^{206}Pb/^{238}U	Apparent Ages (Ma): 204 corrected ±^{206}Pb/^{238}U	Apparent Ages (Ma): 207 corrected ^{206}Pb/^{238}U	Apparent Ages (Ma): 207 corrected ±^{206}Pb/^{238}U
10185-36.1	1434	1050	0.757	52.5	3.0E-5	55	0.05	0.232	2.0	23.5	1.1	0.0515	1.4	0.300	1.8	0.0426	1.1	0.61	0.0511	1.5	269	3	**269**	**3**

Analytical details: Mount IP 574, K120 spot size, primary beam intensity 7 nA, 6 scans.

Error in ^{206}Pb/^{238}U calibration 1.1% for calibration 1 and 1.0% for calibration 2 (included).

Standard error in standard calibration was 0.28% for calibration 1 and 0.21% for calibration 2 (not included in above errors but required when comparing data from different mounts).

09RAYJR179A; Lab#10186; Monzogranite; NAD 83 Zone 8 6999631 N 382824 E

Spot name	U (ppm)	Th (ppm)	Th/U	^{206}Pb* (ppm)	^{204}Pb/^{206}Pb	% ±	f(206)^{204} %	^{208*}Pb/^{206*}Pb	% ±	^{238}U/^{206}Pb	% ±	^{207}Pb/^{206}Pb	% ±	^{207*}Pb/^{235}U	% ±	^{206*}Pb/^{238}U	% ±	Corr Coeff	^{207*}Pb/^{206*}Pb	% ±	204 corr. ^{206}Pb/^{238}U	±	207 corr. ^{206}Pb/^{238}U	±
10186-2.1	409	89	0.22	14.2	4.0E-5	177	0.07	0.076	6.4	24.7	1.0	0.0508	2.5	0.280	3.4	0.0404	1.0	0.30	0.0502	3.3	256	3	**256**	**3**
10186-17.1	742	216	0.301	26.1	1.1E-4	41	0.20	0.089	3.7	24.4	1.1	0.0536	1.6	0.293	2.4	0.0409	1.1	0.48	0.0519	2.1	258	3	**258**	**3**
10186-26.1	659	204	0.320	23.2	9.5E-5	48	0.17	0.105	3.9	24.3	1.1	0.0514	1.8	0.283	2.5	0.0410	1.1	0.45	0.0500	2.3	259	3	**260**	**3**
10186-7.1	964	171	0.183	34.0	4.0E-5	32	0.07	0.059	5.0	24.3	1.1	0.0507	1.7	0.284	2.1	0.0411	1.1	0.53	0.0501	1.8	260	3	**260**	**3**
10186-40.1	330	82	0.26	11.7	3.4E-4	28	0.59	0.077	6.8	24.2	1.2	0.0524	2.8	0.269	4.5	0.0411	1.2	0.27	0.0474	4.3	260	3	**261**	**3**
10186-32.1	720	165	0.236	25.4	1.2E-4	28	0.20	0.075	4.3	24.3	1.1	0.0523	1.7	0.287	2.2	0.0411	1.1	0.50	0.0506	1.9	260	3	**260**	**3**
10186-55.1	903	321	0.367	32.0	3.6E-5	82	0.06	0.127	3.2	24.2	1.1	0.0514	1.6	0.290	2.1	0.0413	1.1	0.52	0.0508	1.8	261	3	**261**	**3**
10186-38.1	1560	261	0.173	55.4	3.5E-5	76	0.06	0.057	3.4	24.2	1.1	0.0513	1.1	0.290	1.8	0.0413	1.1	0.62	0.0508	1.4	261	3	**261**	**3**
10186-23.1	997	147	0.152	35.4	3.1E-5	144	0.05	0.054	5.0	24.2	1.1	0.0499	1.6	0.282	2.4	0.0414	1.1	0.46	0.0494	2.1	261	3	**262**	**3**
10186-4.1	532	162	0.315	18.9	3.6E-5	286	0.06	0.109	5.1	24.1	1.1	0.0535	2.3	0.302	3.9	0.0414	1.1	0.29	0.0529	3.7	262	3	**261**	**3**
10186-25.1	629	117	0.19	22.4	1.6E-5	214	0.03	0.057	6.2	24.1	1.0	0.0525	2.0	0.299	2.5	0.0415	1.0	0.41	0.0523	2.3	262	3	**262**	**3**
10186-8.1	856	150	0.181	30.5	8.7E-5	47	0.15	0.057	4.3	24.0	1.1	0.0501	1.5	0.280	2.3	0.0415	1.1	0.49	0.0488	2.0	262	3	**263**	**3**
10186-9.1	607	184	0.31	21.7	1.8E-4	20	0.31	0.100	4.7	24.0	1.0	0.0535	2.1	0.292	2.6	0.0416	1.0	0.39	0.0509	2.4	263	3	**263**	**3**
10186-75.1	747	175	0.242	26.7	1.9E-4	28	0.34	0.070	5.0	24.0	1.1	0.0506	1.9	0.274	2.9	0.0416	1.1	0.39	0.0478	2.7	263	3	**264**	**3**
10186-34.1	547	129	0.24	19.6	1.7E-4	30	0.29	0.075	5.2	23.9	1.0	0.0526	2.0	0.288	2.8	0.0417	1.0	0.37	0.0502	2.6	263	3	**264**	**3**
10186-69.1	684	163	0.246	24.5	5.5E-5	68	0.10	0.078	4.7	24.0	1.1	0.0519	1.8	0.294	2.4	0.0417	1.1	0.46	0.0511	2.2	263	3	**264**	**3**
10186-42.1	1094	241	0.227	39.2	1.9E-5	131	0.03	0.074	3.4	23.9	1.1	0.0511	1.3	0.293	1.8	0.0417	1.1	0.60	0.0508	1.5	264	3	**264**	**3**
10186-14.1	1653	333	0.208	59.7	-1.0E-5	60	-0.02	0.073	2.9	23.8	1.1	0.0510	1.1	0.296	1.6	0.0420	1.1	0.71	0.0511	1.1	265	3	**266**	**3**
10186-68.1	1816	207	0.12	65.6	4.7E-5	34	0.08	0.035	4.3	23.7	1.0	0.0514	1.2	0.294	1.6	0.0421	1.0	0.62	0.0507	1.3	266	3	**266**	**3**
10186-54.1	832	164	0.204	30.2	-1.4E-5	392	-0.02	0.071	4.9	23.7	1.1	0.0518	1.8	0.303	2.6	0.0423	1.1	0.43	0.0520	2.4	267	3	**267**	**3**
10186-31.1[e]	3610	931	0.266	132.6	4.8E-5	22	0.08	0.084	1.8	23.4	1.1	0.0522	0.7	0.304	1.4	0.0428	1.1	0.81	0.0515	0.8	270	3	270	3

Analytical details: Mount IP 574, K120 spot size, primary beam intensity 7 nA, 6 scans.

Error in ^{206}Pb/^{238}U calibration 1.1% for calibration 1 and 1.0% for calibration 2 (included).

Standard error in standard calibration was 0.28% for calibration 1 and 0.21% for calibration 2 (not included in above errors but required when comparing data from different mounts).

09RAYMC123A; Lab#10190; Granodiorite; NAD 83 Zone 8 6969296 N 382738 E

Spot name	U (ppm)	Th (ppm)	Th/U	^{206}Pb* (ppm)	^{204}Pb/^{206}Pb	% ±	f(206)^{204} %	^{208*}Pb/^{206*}Pb	% ±	^{238}U/^{206}Pb	% ±	^{207}Pb/^{206}Pb	% ±	^{207*}Pb/^{235}U	% ±	^{206*}Pb/^{238}U	% ±	Corr Coeff	^{207*}Pb/^{206*}Pb	% ±	204 corr. ^{206}Pb/^{238}U	±	207 corr. ^{206}Pb/^{238}U	±
10190-101.1[a]	231	99	0.441	6.0	3.3E-3	30	5.79	0.076	11.9	31.2	1.9	0.105	5.3	0.24	29.3	0.0302	2.7	0.09	0.0570	29.2	192	5	190	4
10190-117.1[a]	243	110	0.468	6.3	2.2E-3	18	3.80	0.159	9.8	31.7	1.8	0.082	7.9	0.21	18.2	0.0304	2.0	0.11	0.0500	18.1	193	4	193	4
10190-4.1	278	147	0.548	7.6	-3.8E-4	88	-0.67	0.212	12.4	31.6	1.5	0.076	4.2	0.36	7.2	0.0319	1.6	0.22	0.0816	7.0	202	3	**195**	**3**
10190-134.1[a]	216	63	0.301	5.7	2.5E-3	33	4.25	0.098	11.9	31.2	2.2	0.082	0.8	0.19	27.5	0.0307	2.6	0.09	0.0456	27.4	195	5	196	4
10190-71.1[a]	201	66	0.338	5.5	1.3E-3	64	2.28	0.110	12.8	30.9	2.8	0.089	8.1	0.31	20.6	0.0317	3.1	0.15	0.0700	20.4	201	6	196	6
10190-115.1[a]	228	80	0.363	6.0	2.8E-3	17	4.87	0.096	10.3	31.0	2.3	0.082	3.6	0.17	20.3	0.0307	2.4	0.12	0.0402	20.2	195	5	197	4
10190-62.1[a]	151	45	0.309	3.9	4.7E-3	35	8.09	-0.030	33.1	30.9	1.5	0.084	4.5	0.05	216.2	0.0297	3.4	0.02	0.0126	216.2	189	6	197	3
10190-28.1[a]	210	79	0.389	5.5	4.0E-3	50	6.96	0.071	10.9	30.6	1.2	0.089	9.2	0.12	117.4	0.0304	3.9	0.03	0.0284	117.4	193	7	198	3
10190-31.1	281	79	0.292	7.7	7.5E-4	28	1.29	0.139	10.8	30.9	1.1	0.083	7.3	0.32	9.5	0.0320	1.2	0.12	0.0720	9.5	203	2	**198**	**3**
10190-125.1[a]	241	95	0.408	6.4	2.7E-3	16	4.63	0.130	9.7	30.7	1.1	0.082	7.4	0.18	21.4	0.0311	1.4	0.06	0.0424	21.4	197	3	199	3

Spot name	U (ppm)	Th (ppm)	Th/U	^{206}Pb* (ppm)	^{204}Pb/^{206}Pb	% ±	f(206)^{204} %	^{208*}Pb/^{206*}Pb	% ±	^{238}U/^{206}Pb	% ±	^{207}Pb/^{206}Pb	% ±	^{207*}Pb/^{235}U	% ±	^{206*}Pb/^{238}U	% ±	Corr Coeff	^{207*}Pb/^{206*}Pb	% ±	Apparent Ages (Ma) 204 corrected ^{206}Pb/^{238}U	±^{206}Pb/^{238}U	Apparent Ages (Ma) 207 corrected ^{206}Pb/^{238}U	±^{206}Pb/^{238}U
10190-68.1[a]	289	139	0.498	7.9	1.3E-3	21	2.29	0.170	9.3	30.8	1.5	0.079	6.2	0.26	10.9	0.0317	1.6	0.15	0.0596	10.8	201	3	199	3
10190-25.1[a]	279	140	0.520	7.4	3.2E-3	25	5.57	0.113	9.3	30.5	1.7	0.086	8.1	0.16	38.7	0.0310	2.3	0.06	0.0384	38.6	197	4	199	4
10190-6.1	231	81	0.363	6.4	1.2E-3	17	2.00	0.170	11.0	30.4	1.0	0.086	7.9	0.31	10.8	0.0322	1.1	0.10	0.0696	10.8	205	2	**200**	**3**
10190-119.1[a]	260	118	0.467	6.9	5.5E-3	20	9.53	0.097	8.5	29.3	2.0	0.114	3.0	0.14	58.5	0.0309	2.9	0.05	0.0321	58.4	196	6	200	4
10190-5.1[a]	431	246	0.591	11.5	3.5E-3	20	6.12	0.159	6.8	30.1	1.1	0.092	4.4	0.17	30.6	0.0312	1.7	0.06	0.0395	30.6	198	3	201	2
10190-87.1	222	77	0.358	6.2	1.0E-3	30	1.74	0.123	12.2	30.2	1.4	0.089	3.6	0.33	7.5	0.0326	1.5	0.20	0.0743	7.3	207	3	**201**	**3**
10190-67.1[a]	322	128	0.411	8.8	1.4E-3	23	2.35	0.130	9.8	30.7	1.2	0.075	3.3	0.24	9.8	0.0318	1.4	0.14	0.0556	9.7	202	3	201	3
10190-15.1[a]	384	186	0.500	10.4	2.1E-3	28	3.66	0.156	8.0	30.7	1.1	0.073	7.4	0.18	25.4	0.0314	1.5	0.06	0.0420	25.4	199	3	201	3
10190-30.2	522	25	0.049	14.4	1.1E-3	18	1.83	0.033	21.4	30.6	1.3	0.073	0.4	0.26	5.0	0.0321	1.4	0.27	0.0577	4.8	204	3	**202**	**3**
10190-39.1[a]	150	45	0.311	4.1	2.8E-3	21	4.81	0.088	14.5	29.9	2.5	0.091	10.8	0.22	27.2	0.0318	2.7	0.10	0.0500	27.1	202	5	202	5
10190-110.1[a]	206	64	0.320	5.7	2.0E-3	39	3.48	0.079	13.2	29.9	1.4	0.088	3.8	0.26	21.1	0.0323	2.0	0.09	0.0584	21.0	205	4	203	3
10190-37.1	172	54	0.324	5.0	1.1E-3	31	1.88	0.233	10.4	29.0	1.0	0.113	9.7	0.46	12.4	0.0339	1.2	0.09	0.0978	12.4	215	2	**203**	**3**
10190-24.2[a]	167	28	0.174	4.5	4.0E-3	37	6.86	0.028	13.9	29.4	1.2	0.096	9.9	0.16	68.2	0.0317	3.0	0.04	0.0371	68.2	201	6	204	3
10190-30.1[a]	202	73	0.375	5.6	2.1E-3	20	3.71	0.164	10.4	29.8	1.2	0.082	4.0	0.23	14.5	0.0323	1.4	0.10	0.0510	14.5	205	3	205	2
10190-95.1	265	122	0.475	7.5	8.8E-4	28	1.53	0.185	9.6	30.0	1.1	0.076	1.5	0.28	6.2	0.0328	1.2	0.19	0.0630	6.1	208	2	**205**	**2**
10190-61.1	266	93	0.362	7.6	7.3E-4	29	1.26	0.154	10.4	29.8	1.3	0.077	6.1	0.30	8.7	0.0331	1.3	0.15	0.0666	8.6	210	3	**206**	**3**
10190-86.1[a]	248	123	0.513	6.9	1.7E-3	22	2.93	0.170	9.5	29.9	1.1	0.075	2.3	0.22	11.8	0.0325	1.3	0.11	0.0498	11.7	206	3	206	2
10190-5.2[a]	179	48	0.279	4.9	3.0E-3	19	5.12	0.049	13.6	30.0	1.6	0.069	4.6	0.11	39.2	0.0316	1.9	0.05	0.0241	39.2	201	4	207	3
10190-56.1	358	75	0.215	10.2	5.9E-4	32	1.03	0.082	11.7	29.9	1.1	0.069	3.2	0.27	6.0	0.0331	1.1	0.19	0.0601	5.9	210	2	**207**	**2**
10190-114.1[a]	326	167	0.529	9.2	1.3E-3	21	2.20	0.174	9.1	29.9	1.5	0.068	3.5	0.22	9.6	0.0327	1.5	0.16	0.0498	9.4	208	3	208	3
10190-79.1	583	512	0.908	16.4	4.1E-4	21	0.71	0.274	5.7	30.3	1.1	0.057	2.8	0.23	4.1	0.0328	1.1	0.26	0.0513	4.0	208	2	**208**	**2**
10190-120.1	228	74	0.335	6.5	9.2E-4	28	1.59	0.079	14.2	29.9	1.1	0.067	4.0	0.24	8.8	0.0329	1.2	0.14	0.0535	8.7	209	2	**208**	**2**
10190-6.2[f]	1890	21	0.012	53.8	9.3E-5	29	0.16	0.020	10.1	30.1	1.0	0.058	2.3	0.26	2.6	0.0331	1.0	0.38	0.0565	2.4	210	2	209	2
10190-123.1	297	150	0.519	8.5	8.7E-4	19	1.50	0.162	9.7	29.5	1.1	0.068	3.6	0.26	6.4	0.0334	1.2	0.18	0.0555	6.3	212	2	**210**	**2**
10190-62.2	1024	27	0.027	29.4	1.8E-4	22	0.31	0.014	15.5	29.8	1.0	0.055	2.0	0.24	2.6	0.0334	1.0	0.39	0.0529	2.4	212	2	**211**	**2**
10190-26.1[a]	179	55	0.319	5.0	4.5E-3	27	7.85	-0.005	14.8	28.1	1.0	0.083	7.4	0.06	156.8	0.0328	2.5	0.02	0.0134	156.8	208	5	217	3
10190-106.1[a]	97	19	0.198	2.9	4.7E-3	22	8.09	0.037	19.0	26.6	2.2	0.110	5.5	0.20	43.5	0.0346	2.9	0.07	0.0413	43.4	219	6	222	5
10190-102.1[e]	494	264	0.553	15.1	2.8E-4	65	0.48	0.187	8.0	28.0	1.1	0.058	3.3	0.26	6.1	0.0355	1.1	0.18	0.0537	6.0	225	2	224	2
10190-106.2[f]	2461	3984	1.672	74.8	8.9E-5	24	0.15	0.520	2.2	28.2	1.5	0.050	1.6	0.24	2.3	0.0354	1.5	0.66	0.0492	1.7	224	3	225	3
10190-127.1[a]	234	102	0.449	7.0	3.0E-3	31	5.17	0.066	12.4	27.2	2.9	0.074	4.2	0.14	51.0	0.0349	3.3	0.07	0.0291	50.9	221	7	227	7
10190-39.2[f]	1950	290	0.154	76.8	2.6E-4	27	0.46	0.051	5.1	21.7	1.0	0.055	2.2	0.33	3.3	0.0459	1.0	0.31	0.0516	3.1	289	3	289	3
10190-125.2[c]	419	282	0.694	18.0	2.9E-4	28	0.51	0.220	5.7	19.9	1.2	0.063	2.4	0.41	3.5	0.0500	1.3	0.36	0.0588	3.3	314	4	312	4
10190-68.2[c]	1615	47	0.030	69.2	2.8E-4	15	0.49	0.004	11.1	19.9	1.1	0.056	1.3	0.35	2.1	0.0499	1.1	0.50	0.0515	1.9	314	3	314	3
10190-67.2[c]	1361	772	0.586	59.0	-1.9E-6	329	0.00	0.211	3.2	19.8	1.4	0.055	1.4	0.38	2.0	0.0505	1.4	0.72	0.0551	1.4	318	4	317	4
10190-87.2[c]	634	25	0.040	27.5	9.7E-4	23	1.69	-0.001	20.9	19.5	1.1	0.063	4.0	0.34	8.7	0.0504	1.2	0.14	0.0486	8.6	317	4	319	4
10190-123.2[c]	244	300	1.270	10.9	-5.1E-4	29	-0.89	0.461	5.3	19.4	1.4	0.066	3.1	0.53	4.2	0.0521	1.4	0.34	0.0736	4.0	327	5	319	4
10190-24.1[c]	1029	481	0.483	46.9	1.3E-4	28	0.23	0.157	4.5	18.8	1.0	0.061	2.4	0.43	2.8	0.0530	1.0	0.37	0.0586	2.6	333	3	331	3

Analytical details: Mount IP 566, K100 spot size, primary beam intensity 2 nA, 6 scans.

Error in ^{206}Pb/^{238}U calibration 1.0% (included).

Standard Error in Standard calibration was 0.31% (not included in above errors but required when comparing data from different mounts).

																			Apparent Ages (Ma)			
																			204 corrected		207 corrected	
Spot name	U (ppm)	Th (ppm)	Th/U	$^{206}Pb^*$ (ppm)	$^{204}Pb/^{206}Pb$	% ±	$f(206)^{204}$ %	$^{208*}Pb/^{206*}Pb$	% ±	$^{238}U/^{206}Pb$	% ±	$^{207}Pb/^{206}Pb$	% ±	$^{207*}Pb/^{235}U$	% ±	$^{206*}Pb/^{238}U$	% ±	Corr Coeff	$^{207*}Pb/^{206*}Pb$	% ±	$^{206}Pb/^{238}U$	$\pm ^{206}Pb/^{238}U$	$^{206}Pb/^{238}U$	$\pm ^{206}Pb/^{238}U$

Notes (see Stern, 1997):

Spot name follows the convention x-y.z; where x = sample number, y = grain number and z = spot number. Multiple analyses in an individual spot are labelled as x-y.z.z.

Superscripts next to the spot name denote individual analysis excluded from weighted mean age calculation based on the following criteria:: a = $f(206)^{204}$ > 2.0%, b = Pb loss, c = core, d = rim, e = mixed age,

f = U > 1800 ppm, g = anomlaous UO+/U+.

Uncertainties reported at 1σ and are calculated by using SQUID 2.23.08.10.21, rev. 21 Oct 2008.

Numbers in bold are values used to calculate final age.

$f206^{204}$ refers to mole percent of total 206Pb that is due to common Pb, calculated using the 204Pb-method; common Pb composition used is the surface blank (4/6: 0.05770; 7/6: 0.89500; 8/6: 2.13840).

* refers to radiogenic Pb (corrected for common Pb).

Calibration standard 6266; U = 910 ppm; Age = 559 Ma; 206Pb/238U = 0.09059.

TABLE A2. DETRITAL SHRIMP U-Pb DATA FOR SAMPLES FROM THE MCQUESTEN MAP AREA

Spot name	U (ppm)	Th (ppm)	Th/U	$^{206}Pb^*$ (ppm)	$^{204}Pb/^{206}Pb$	% ±	$f(206)^{204}$ %	$^{208*}Pb/^{206*}Pb$	% ±	$^{238}U/^{206}Pb$	% ±	$^{207}Pb/^{206}Pb$	% ±	$^{207*}Pb/^{235}U$	% ±	$^{206*}Pb/^{238}U$	% ±	Corr Coeff	$^{207*}Pb/^{206*}Pb$	% ±	Apparent Ages (Ma): 207 corrected $^{206}Pb/^{238}U$	207 corrected ±$^{206}Pb/^{238}U$	204 corrected $^{207}Pb/^{206}Pb$	204 corrected ±$^{207}Pb/^{206}Pb$
09RAYMC092A; Lab#10076; Volcanogenic sandstone; NAD 83 Zone 8 7029600 N 396916 E																								
10076-2.1	159	114	0.74	9.2	1.8E-4	63	0.32	0.232	3.8	14.9	0.83	0.0550	2.01	0.48	4.0	0.067	0.85	0.2	0.0523	3.9	**418**	**3**	300	88
10076-10.1	242	121	0.52	14.1	3.8E-4	32	0.67	0.153	3.7	14.6	0.75	0.0564	1.14	0.48	3.8	0.068	0.78	0.2	0.0508	3.8	**426**	**3**	232	87
10076-52.1	667	388	0.60	40.6	8.7E-5	33	0.15	0.188	2.1	14.1	0.72	0.0552	0.71	0.53	1.3	0.071	0.72	0.6	0.0539	1.1	**443**	**3**	367	24
10076-59.1	762	371	0.50	47.0	5.2E-5	64	0.09	0.159	2.1	13.9	0.73	0.0560	0.65	0.55	1.3	0.072	0.73	0.6	0.0553	1.1	**447**	**3**	423	24
10076-35.1	516	388	0.78	32.0	7.7E-5	134	0.13	0.257	2.0	13.8	0.80	0.0570	0.76	0.56	2.9	0.072	0.82	0.3	0.0559	2.8	**449**	**4**	449	62
10076-34.1	1039	136	0.14	80.9	2.2E-4	17	0.37	0.039	3.7	11.0	0.73	0.0588	0.61	0.70	1.4	0.091	0.73	0.5	0.0557	1.2	**561**	**4**	439	26
10076-9.1	100	106	1.09	9.5	9.7E-5	194	0.17	0.334	3.3	9.0	0.82	0.0636	1.38	0.95	4.7	0.111	0.88	0.2	0.0622	4.6	**679**	**5**	681	98
10076-45.1	65	53	0.85	7.6	2.4E-4	32	0.41	0.312	4.0	7.3	0.91	0.0761	1.53	1.37	2.4	0.136	0.92	0.4	0.0728	2.2	**817**	**7**	1008	44
10076-23.1	68	31	0.47	10.1	2.7E-4	38	0.46	0.146	4.7	5.7	0.98	0.0768	1.23	1.76	2.5	0.175	1.00	0.4	0.0730	2.3	**1040**	**10**	1014	47
10076-93.1	96	79	0.85	14.8	1.5E-4	40	0.25	0.257	2.8	5.6	0.81	0.0765	1.74	1.83	2.3	0.178	0.81	0.4	0.0744	2.1	**1059**	**8**	1053	43
10076-56.1	103	54	0.55	16.0	1.9E-4	48	0.32	0.173	3.5	5.5	0.82	0.0750	1.01	1.81	2.2	0.181	0.83	0.4	0.0724	2.0	**1077**	**9**	997	41
10076-61.1	132	80	0.63	22.1	8.4E-4	18	1.46	0.175	3.3	5.1	0.83	0.0805	0.96	1.83	3.5	0.194	0.88	0.2	0.0684	3.4	**1155**	**9**	882	71
10076-67.1	78	46	0.61	14.7	1.8E-5	200	0.03	0.193	3.3	4.6	0.83	0.0847	0.92	2.56	1.4	0.219	0.84	0.6	0.0845	1.1	**1277**	**10**	1303	21
10076-6.1	41	22	0.56	8.4	1.3E-4	241	0.23	0.182	4.6	4.2	0.95	0.0911	1.23	2.94	5.3	0.239	1.10	0.2	0.0893	5.2	**1378**	**13**	1410	99
10076-18.1	109	51	0.48	24.3	-1.2E-5	706	-0.02	0.148	3.0	3.9	0.81	0.0930	0.72	3.32	1.6	0.258	0.82	0.5	0.0932	1.4	**1481**	**12**	1491	27
10076-83.1	280	94	0.35	63.2	3.5E-5	16	0.06	0.105	2.2	3.8	0.74	0.0929	0.44	3.35	0.9	0.262	0.74	0.9	0.0925	0.5	**1505**	**11**	1477	9
10076-91.1	366	105	0.30	82.9	-3.2E-5	61	-0.06	0.085	2.4	3.8	0.83	0.0917	0.43	3.35	1.0	0.264	0.83	0.8	0.0922	0.5	**1512**	**12**	1471	10
10076-43.1	193	69	0.37	43.7	-1.2E-5	94	-0.02	0.112	2.6	3.8	0.76	0.0943	0.53	3.42	0.9	0.263	0.76	0.8	0.0944	0.6	1504	11	**1517**	**10**
10076-66.1	46	41	0.93	11.8	1.8E-4	74	0.31	0.261	3.1	3.4	0.91	0.1004	0.95	4.02	2.3	0.297	0.94	0.4	0.0980	2.1	1687	15	**1586**	**39**
10076-54.1	172	35	0.21	43.8	2.1E-5	48	0.04	0.064	3.5	3.4	0.77	0.1009	0.53	4.12	0.9	0.297	0.77	0.8	0.1006	0.6	1681	13	**1636**	**10**
10076-2.1	76	82	1.11	18.6	1.5E-5	75	0.03	0.331	2.2	3.5	0.83	0.1022	0.73	4.01	1.1	0.285	0.83	0.7	0.1020	0.8	1612	13	**1661**	**14**
10076-29.1	166	75	0.47	44.0	2.6E-5	28	0.05	0.143	2.2	3.2	0.82	0.1060	0.48	4.50	1.0	0.309	0.82	0.9	0.1056	0.5	1738	14	**1725**	**9**
10076-47.1	109	45	0.42	28.6	5.0E-5	92	0.09	0.130	2.9	3.3	0.80	0.1064	0.60	4.43	1.2	0.304	0.81	0.7	0.1057	0.8	1707	14	**1726**	**16**
10076-68.1	362	201	0.57	95.4	3.9E-5	48	0.07	0.165	1.4	3.3	0.74	0.1072	0.34	4.51	0.8	0.306	0.74	0.9	0.1066	0.4	1721	13	**1743**	**8**
10076-20.1	61	27	0.45	15.9	-2.3E-5	438	-0.04	0.141	3.7	3.3	0.87	0.1071	0.80	4.45	1.7	0.301	0.89	0.5	0.1074	1.5	1688	15	**1755**	**27**
10076-82.1	269	90	0.34	73.6	5.6E-5	20	0.10	0.102	2.1	3.1	0.75	0.1088	0.39	4.75	0.9	0.319	0.75	0.9	0.1080	0.4	1786	13	**1766**	**8**
10076-55.1	110	123	1.15	31.2	1.3E-4	28	0.22	0.340	1.7	3.0	0.97	0.1111	0.56	4.98	1.2	0.331	0.97	0.8	0.1093	0.7	1848	18	**1788**	**13**
10076-17.1	88	65	0.77	25.1	7.3E-5	52	0.13	0.219	2.3	3.0	0.82	0.1118	0.61	5.09	1.1	0.333	0.82	0.7	0.1108	0.8	1858	15	**1813**	**14**
10076-87.1	93	43	0.48	27.8	1.7E-4	32	0.30	0.132	3.1	2.9	0.83	0.1138	0.64	5.32	1.3	0.346	0.84	0.7	0.1115	0.9	1930	16	**1823**	**17**
10076-80.1	85	45	0.55	24.1	9.0E-5	93	0.16	0.161	2.8	3.0	0.83	0.1132	0.64	5.09	1.5	0.330	0.84	0.6	0.1120	1.2	1837	15	**1832**	**22**
10076-13.1	48	44	0.95	13.2	6.4E-5	165	0.11	0.285	3.1	3.1	0.93	0.1130	0.94	4.96	1.9	0.321	0.95	0.5	0.1121	1.6	1789	17	**1834**	**29**
10076-38.1	130	31	0.25	36.2	1.9E-5	45	0.03	0.076	3.6	3.1	0.80	0.1126	0.56	5.01	1.0	0.324	0.80	0.8	0.1123	0.6	1803	14	**1837**	**10**
10076-64.1	208	188	0.93	58.8	-2.3E-5	54	-0.04	0.272	1.5	3.0	0.76	0.1122	0.43	5.11	0.9	0.329	0.76	0.9	0.1125	0.5	1835	14	**1840**	**8**
10076-15.1	29	15	0.54	8.1	1.9E-4	41	0.33	0.158	4.9	3.0	1.03	0.1151	1.11	5.08	1.8	0.327	1.04	0.6	0.1126	1.5	1822	19	**1841**	**27**
10076-85.1	135	98	0.75	38.3	2.0E-5	32	0.03	0.208	2.2	3.0	0.87	0.1133	0.57	5.14	1.0	0.330	0.87	0.8	0.1130	0.6	1838	16	**1848**	**10**
10076-71.1	154	87	0.59	45.5	9.2E-5	33	0.16	0.176	2.3	2.9	0.80	0.1144	0.55	5.36	1.0	0.343	0.80	0.8	0.1132	0.7	1912	15	**1851**	**12**
10076-19.1	229	178	0.80	66.2	2.6E-5	83	0.05	0.227	2.0	3.0	0.75	0.1138	0.38	5.26	0.9	0.336	0.75	0.9	0.1134	0.5	1871	14	**1855**	**8**
10076-27.1	270	129	0.49	76.3	8.6E-6	318	0.01	0.148	1.7	3.0	0.75	0.1136	0.38	5.16	0.9	0.330	0.75	0.8	0.1135	0.5	1833	14	**1856**	**9**

Spot name	U (ppm)	Th (ppm)	Th/U	$^{206}Pb^*$ (ppm)	$^{204}Pb/^{206}Pb$	% ±	$f(206)^{204}$ %	$^{208*}Pb/^{206*}Pb$	% ±	$^{238}U/^{206}Pb$	% ±	$^{207}Pb/^{206}Pb$	% ±	$^{207*}Pb/^{235}U$	% ±	$^{206*}Pb/^{238}U$	% ±	Corr Coeff	$^{207*}Pb/^{206*}Pb$	% ±	Apparent Ages (Ma), 207 corrected: $^{206}Pb/^{238}U$	Apparent Ages (Ma), 207 corrected: $\pm ^{206}Pb/^{238}U$	Apparent Ages (Ma), 204 corrected: $^{207}Pb/^{206}Pb$	Apparent Ages (Ma), 204 corrected: $\pm ^{207}Pb/^{206}Pb$
10076-44.1	144	90	0.64	40.2	1.2E-4	26	0.22	0.191	2.1	3.1	0.78	0.1157	0.51	5.11	1.0	0.325	0.79	0.8	0.1140	0.6	1806	14	**1865**	**12**
10076-57.1	157	76	0.50	44.2	1.0E-5	588	0.02	0.146	2.6	3.1	0.80	0.1142	0.56	5.14	1.2	0.327	0.80	0.7	0.1141	0.9	1818	15	**1865**	**17**
10076-24.1	85	54	0.66	24.7	8.3E-5	63	0.14	0.182	2.8	2.9	0.84	0.1157	0.67	5.35	1.2	0.339	0.85	0.7	0.1146	0.9	1880	16	**1874**	**16**
10076-26.1	215	277	1.33	62.3	1.5E-5	35	0.03	0.387	1.2	3.0	0.76	0.1154	0.41	5.36	0.9	0.338	0.76	0.9	0.1152	0.4	1874	14	**1882**	**7**
10076-72.1	66	44	0.69	18.9	1.6E-5	360	0.03	0.209	2.9	3.0	0.86	0.1157	0.74	5.29	1.3	0.332	0.87	0.7	0.1155	1.0	1842	16	**1888**	**18**
10076-40.1	72	123	1.78	21.1	2.3E-5	97	0.04	0.514	1.7	2.9	0.85	0.1164	0.69	5.49	1.1	0.343	0.85	0.8	0.1161	0.7	1901	16	**1897**	**13**
10076-5.1	58	46	0.83	16.8	1.2E-4	62	0.21	0.247	2.7	2.9	1.17	0.1188	0.75	5.47	1.7	0.338	1.18	0.7	0.1171	1.2	1874	22	**1913**	**21**
10076-11.1	89	110	1.27	27.2	6.9E-5	71	0.12	0.368	1.7	2.8	0.82	0.1209	0.58	5.88	1.1	0.355	0.82	0.7	0.1200	0.8	1961	16	**1956**	**14**
10076-46.1	391	226	0.60	117.9	3.4E-6	235	0.01	0.176	1.3	2.8	0.73	0.1225	0.29	5.93	0.8	0.351	0.73	0.9	0.1225	0.3	1932	14	**1992**	**5**
10076-75.1	159	88	0.57	48.9	6.7E-5	35	0.12	0.164	2.0	2.8	0.78	0.1236	0.45	6.05	0.9	0.358	0.78	0.8	0.1227	0.5	1967	16	**1996**	**9**
10076-39.1	37	34	0.95	12.0	5.2E-5	65	0.09	0.297	3.1	2.7	0.97	0.1280	0.91	6.59	1.4	0.376	0.97	0.7	0.1273	1.0	2055	21	**2061**	**17**
10076-25.1	81	16	0.20	26.2	6.2E-5	35	0.11	0.060	4.4	2.7	0.83	0.1315	0.59	6.78	1.0	0.376	0.84	0.8	0.1307	0.6	2047	18	**2108**	**11**
10076-53.1	225	142	0.65	79.2	3.7E-5	28	0.06	0.185	1.6	2.4	0.76	0.1451	0.36	8.18	0.9	0.410	0.76	0.9	0.1446	0.4	2200	18	**2283**	**6**
10076-79.1	181	115	0.65	65.9	1.4E-4	23	0.23	0.191	1.8	2.4	0.79	0.1565	0.40	9.04	0.9	0.423	0.79	0.9	0.1548	0.5	2242	19	**2399**	**8**
10076-88.1	155	110	0.73	63.9	5.3E-6	397	0.01	0.213	1.4	2.1	0.77	0.1628	0.32	10.75	0.8	0.479	0.77	0.9	0.1628	0.4	2539	23	**2485**	**6**
10076-70.1	75	25	0.35	31.9	1.1E-4	37	0.18	0.094	3.8	2.0	0.89	0.1724	0.57	11.66	1.1	0.494	0.89	0.8	0.1711	0.6	2598	28	**2568**	**11**
10076-42.1	53	47	0.92	23.0	5.0E-5	33	0.09	0.258	2.3	2.0	0.89	0.1779	0.55	12.45	1.1	0.509	0.89	0.8	0.1773	0.6	2667	30	**2627**	**9**
10076-28.1	89	112	1.29	39.4	-7.8E-6	721	-0.01	0.362	1.6	1.9	0.84	0.1818	0.45	12.89	1.0	0.514	0.84	0.8	0.1819	0.6	2675	28	**2670**	**10**
10076-49.1	168	139	0.86	80.0	1.4E-4	24	0.25	0.232	1.5	1.8	0.77	0.1861	0.45	14.09	0.9	0.554	0.78	0.8	0.1843	0.5	2947	35	**2692**	**8**
10076-12.1	38	38	1.03	16.7	-1.6E-5	234	-0.03	0.291	2.7	1.9	0.98	0.1854	0.67	13.22	1.2	0.516	0.98	0.8	0.1856	0.7	2674	33	**2704**	**12**
10076-14.1	64	148	2.39	27.6	2.1E-5	237	0.04	0.674	1.6	2.0	0.92	0.1860	0.58	12.91	1.1	0.504	0.92	0.8	0.1858	0.7	2597	29	**2705**	**11**
10076-3.1	41	37	0.95	18.0	8.1E-5	67	0.14	0.271	2.5	1.9	0.93	0.1872	0.59	13.25	1.2	0.516	0.93	0.8	0.1862	0.7	2670	31	**2709**	**11**
10076-21.1	41	25	0.63	19.6	6.8E-5	30	0.12	0.166	3.1	1.8	0.94	0.2014	0.57	15.31	1.1	0.553	0.94	0.8	0.2006	0.6	2845	37	**2831**	**10**
10076-63.1	52	40	0.79	25.2	1.1E-4	96	0.19	0.205	2.9	1.8	0.96	0.2049	0.58	15.88	1.3	0.566	0.97	0.8	0.2036	0.8	2917	41	**2855**	**14**
10076-1.1	35	40	1.17	16.7	1.3E-4	42	0.23	0.309	2.5	1.8	1.08	0.2177	0.72	16.60	1.3	0.557	1.09	0.8	0.2162	0.8	2784	41	**2952**	**13**
10076-86.1	117	109	0.96	59.5	1.5E-5	156	0.03	0.268	1.6	1.7	0.82	0.2267	0.35	18.51	0.9	0.593	0.82	0.9	0.2266	0.4	2973	38	**3028**	**6**

Analytical details: Mount IP 550, K100 spot size, primary beam intensity 12 nA, 6 scans

Error in 206Pb/238U 1.0% (included)

Standard error in standard calibration was 0.16% (not included in above errors but required when comparing data from different mounts).

Notes (see Stern, 1997):

Spot name follows the convention x-y.z; where x = sample number, y = grain number and z = spot number. Multiple analyses in an individual spot are labelled as x-y.z.z.

Uncertainties reported at 1σ and are calculated by using SQUID 2.23.08.10.21, rev. 21 Oct 2008.

Numbers in bold are values used to calculate final age.

$f206^{204}$ refers to mole percent of total 206Pb that is due to common Pb, calculated using the 204Pb-method; common Pb composition used is the surface blank (4/6: 0.05770; 7/6: 0.89500; 8/6: 2.13840).

* refers to radiogenic Pb (corrected for common Pb).

Calibration standard 6266; U = 910 ppm; Age = 559 Ma; 206Pb/238U = 0.09059.

APPENDIX 3

^{40}Ar-^{39}Ar Methodology

METHODS

Mineral separates for $^{40}Ar/^{39}Ar$ were obtained using standard crushing and preparation techniques. Hand sized rock samples were crushed in a jaw crusher at the University of Ottawa and further reduced in size by hand mortar and pestle, then sieved through 500 and 250 μm screens. The 500 to 250 μm fraction was washed in water and ethanol then set to dry. Approximately 50 high quality grains free of alteration and impurities were hand picked in ethanol under a microscope. Isotopic analysis was conducted at the Geological Survey of Canada, Ottawa, Ontario and the New Mexico Institute of Mining and Technology (NMT), Socorro, U. S. A.. Corrected argon isotopic data, plateau and integrated ages for samples analysed at the GSC are listed in Table 3, and in Table 4 for samples analysed at NMT.

Samples that were analysed at the GSC were loaded into foil packets with 2 grains of Fish Canyon Tuff (FCT) sanidine (apparent age = 28.02 Ma; Renne et al., 1998) as a flux monitor and arranged radially in an aluminum canister. The samples were submitted in two separate irradiations to the research reactor at McMaster University in Hamilton, Ontario, Canada for 13.3 and 20.0 hours at 3 MWh. FCT sanidine and PP-20 hornblende (a re-preparation of standard HB3gr with the same apparent age of 1073.6 ± 5.4 Ma; Jourdan et al., 2006) were used as independent checks on the accuracy of isotopic data collection. Once irradiated, aliquots consisting of 1 – 3 grains of mica or 3 – 7 grains of hornblende were loaded into individual 1.5 mm diameter holes in a copper planchet. The planchet was loaded into the extraction line and the system evacuated. Laser step-heating of individual sample aliquots was achieved using a Merchantek MIR10 10W CO_2 laser equipped with a 2 mm x 2 mm flat-field lens. The released Ar gas was cleaned over getters for 4 minutes, and then analyzed isotopically using a Nu Instruments multicollector Noblesse mass spectrometer, equipped with a Faraday detector and three ion counters. For the analyses, a single ion counter peak-hopping mode was used for small signals, and in cases where the ^{40}Ar signal exceeded ion counting tolerance, a Faraday plus single ion counter peak-hopping routine was employed. Isotopic ratios were corrected for baselines, procedural blanks, ^{39}Ar and ^{37}Ar decay, nucleogenic interference, mass fractionation, and detector efficiency. Typical blanks are 3.1 x 10^{-16}, 3.6 x 10^{-19}, 5.4 x 10^{-19}, 1.3 x 10^{-18}, and 1.1 x 10^{-18} moles for masses 40, 39, 38, 37, and 36, respectively. Mass fractionation and detector efficiencies were determined from repeated measurements of air aliquots, whereby ^{40}Ar and ^{36}Ar signals were measured on all collectors. $^{40}Ar/^{36}Ar$ ratios were determined for each collector individually, and for each combination of collectors (e.g. ^{40}Ar on the Faraday/^{36}Ar on each ion counter). Neutron flux gradients throughout the sample canister were evaluated by analyzing the sanidine flux monitors included with each sample packet and interpolating a linear fit against calculated J-factor and sample position. The error on individual J-factor values is conservatively estimated at ± 0.6% (2σ). Nucleogenic interference corrections determined with K-glass and chrysotran were $(^{40}Ar/^{39}Ar)_K = 0.025 \pm 0.005$; $(^{38}Ar/^{39}Ar)_K = 0.011 \pm 0.010$; $(^{40}Ar/^{37}Ar)_{Ca} = 0.002 \pm 0.002$; $(^{39}Ar/^{37}Ar)_{Ca} = 0.00068 \pm 0.00004$; $(^{38}Ar/^{37}Ar)_{Ca} = 0.00003 \pm 0.00003$; and $(^{36}Ar/^{37}Ar)_{Ca} = 0.00028 \pm 0.00016$. Raw data from the mass spectrometer was imported and processed using a spreadsheet programmed with data handling macros written by M.E. Villeneuve that employ average, linear or non-linear regression protocols based on the equations of Koppers (2002). Ages were calculated using the decay constants of Steiger and Jäger (1977). Error analysis on individual steps follows numerical error analysis routines outlined in Scaillet (2000); error analysis on grouped data follows algebraic methods of

Roddick (1988).

Samples and FCT sanidine monitors that were isotopically analysed at NMT were loaded into machined aluminum discs and irradiated for 10 hours at the USGS TRIGA Reactor in Denver, Colorado, USA. After irradiaton, samples were loaded into an automated all metal extraction line. Sample grains were step-heated with a double vacuum molybdenum resistance furnace for 5 minutes. Reactive gases were removed during heating with a SAES GP-50 getter operating at 450 ^{o}C, and for 3 additional minutes with 2 SAES GP-50 getters operating at 450 ^{o}C and 20 ^{o}C. Gas was also exposed to a cold finger operating at -140 ^{o}C, and a tungsten filament operating at 2000 ^{o}C. Isotopic analyses were conducted on a Mass Analyzer Products 215-50 mass spectrometer. The determined electron multiplier sensitivity was 7.0 x 10^{-17} moles/pA. Typical total blank values were 7.0 x 10^{-16}, 0.7 x 10^{-17}, 0.2 x 10^{-17}, 0.3 x 10^{-17}, and 0.5 x 10^{-17} moles for masses 40, 39, 38, 37, and 36, respectively. J-factor uncertainty was estimated at ± 0.05% by CO_2 laser-fusion of 6 FCT sanidine grains from each of 10 radial positions around the irradiation tray. Correction factors for interfering nuclear reactions were also determined with K-glass and CaF_2: $(^{40}Ar/^{39}Ar)_K$ = 0.010 ± 0.002; $(^{36}Ar/^{37}Ar)_{Ca}$ = 0.00028 ± 0.00002; and $(^{39}Ar/^{37}Ar)_{Ca}$ = 0.00070 ± 0.00005.

REFERENCES

Jourdan, F., Verati, C., and Féraud, G., 2006, Intercalibration of the Hb3gr $^{40}Ar/^{39}Ar$ dating standard: Chemical Geology, v. 2006, p. 177-189.

Koppers, A. A. P., 2002, ArArCALC – software for $^{40}Ar/^{39}Ar$ age calculations: Computers and Geosciences, v. 28, p. 605-619.

Renne, P. R., Swisher, C. C., Deino, A. L., Karner, D. B., Owens, T. L., and DePaolo, D. J., 1998, Intercalibration of standards, absolute ages and uncertainties in $^{40}Ar/^{39}Ar$ dating: Chemical Geology, v. 145, p. 117-152.

Roddick, J. C., 1988, The assessment of errors in $^{40}Ar/^{39}Ar$ dating, *in* Radiogenic Age and Isotopic Studies, Report 2: Geological Survey of Canada, v. 88-2, p. 7–16.

Scaillet, S., 2000, Numerical error analysis in $^{40}Ar/^{39}Ar$ dating: Chemical Geology, v.162, p. 269–298.

Steiger, R., and Jäger, E., 1977, Subcommission on geochronology: Convention on the use of decay constants in geo- and cosmochronology: Earth and Planetary Science Letters, v. 36, p. 359-362.

TABLE A3. CO_2 LASER STEP HEATING $^{40}Ar/^{39}Ar$ DATA FOR SAMPLES FROM THE MCQUESTEN MAP AREA ANALYSED AT THE GEOLOGICAL SURVEY OF CANADA

ID	Power* (%)	Volume ^{39}Ar x10^{-11} cc	$^{36}Ar/^{39}Ar$	±	$^{37}Ar/^{39}Ar$	±	$^{38}Ar/^{39}Ar$	±	$^{40}Ar/^{39}Ar$	±	%^{40}Ar ATM	*$^{40}Ar/^{39}Ar$	±	f_{39}† (%)	Apparent Age Ma§	±
09RAYJR122A; Lab#9937; Ar#2846; Hornblende; J=0.00747920																
A	3.0	0.0003	0.1792	0.0402	1.982	0.441	0.351	0.036	50.771	8.268	104.3	0.000	0.000	0.4	-29.8	194.8
B	3.5	0.0003	0.0729	0.0319	3.261	0.382	0.373	0.033	45.871	6.811	47.0	24.317	11.487	0.4	301.5	131.2
C	3.9	0.0033	0.0086	0.0032	5.512	0.102	0.877	0.021	30.007	0.653	8.4	27.476	1.147	4.1	337.2	12.8
D	4.2	0.0043	0.0090	0.0025	4.887	0.083	0.890	0.020	29.287	0.517	9.1	26.632	0.889	5.4	327.7	10.0
E	4.6	0.0105	0.0006	0.0012	4.848	0.072	0.861	0.018	27.132	0.231	0.7	26.945	0.432	13.1	331.2	4.9
F	4.8	0.0090	0.0108	0.0015	5.582	0.081	1.059	0.022	30.633	0.241	10.5	27.427	0.505	11.2	336.6	5.7
G	5.5	0.0187	0.0050	0.0011	5.236	0.073	1.179	0.022	29.784	0.208	4.9	28.317	0.372	23.3	346.6	4.1
H	6.0	0.0235	0.0050	0.0010	5.500	0.073	1.050	0.020	30.342	0.158	4.9	28.856	0.338	29.2	352.6	3.8
I	6.5	0.0028	0.0023	0.0037	5.505	0.107	1.019	0.022	28.080	0.677	2.5	27.390	1.280	3.5	336.2	14.3
J	7.5	0.0014	0.0001	0.0001	6.113	0.162	0.988	0.024	27.734	1.286	0.1	28.303	2.425	1.7	346.4	27.0
K	15.0	0.0063	0.0023	0.0017	4.243	0.069	0.783	0.019	21.174	0.308	3.2	20.502	0.597	7.8	257.4	7.0
			Age (Ma)	**±**	**MSWD**	**^{39}Ar Gas %**	**Steps**									
		Plateau Age	342.8	6.9	9.8	91	8									
		Integrated Age	335.2	17.1	71.1	100	11									
09RAYJR122A; Lab#9937; Ar#2847; Biotite; J=0.00747920																
A	2.6	0.0162	0.0323	0.0005	0.110	0.007	0.146	0.011	13.202	0.122	72.3	3.656	0.188	2.9	48.7	2.5
B	2.8	0.0037	0.0182	0.0027	0.053	0.025	0.129	0.011	12.012	0.489	44.9	6.623	0.924	0.7	87.2	11.9
C	3	0.0176	0.0213	0.0007	0.022	0.005	0.112	0.011	25.308	0.137	24.9	19.014	0.234	3.2	239.9	2.8
D	3.5	0.0316	0.0086	0.0004	0.016	0.003	0.111	0.011	27.103	0.123	9.4	24.551	0.158	5.7	304.1	1.8
E	3.9	0.0368	0.0031	0.0003	0.011	0.003	0.111	0.011	27.902	0.115	3.2	26.996	0.141	6.7	331.8	1.6
F	4.2	0.0352	0.0016	0.0003	0.011	0.003	0.111	0.011	28.499	0.116	1.6	28.029	0.145	6.4	343.4	1.6
G	4.6	0.0630	0.0014	0.0002	0.014	0.002	0.111	0.011	28.667	0.078	1.5	28.249	0.092	11.4	345.8	1.0
H	5	0.0641	0.0009	0.0002	0.022	0.002	0.111	0.011	28.714	0.085	0.9	28.460	0.096	11.6	348.2	1.1
I	5.5	0.0339	0.0006	0.0003	0.018	0.003	0.111	0.011	29.013	0.144	0.7	28.823	0.168	6.2	352.2	1.9
J	6	0.0439	0.0033	0.0002	0.027	0.002	0.111	0.011	29.391	0.210	3.4	28.403	0.221	8.0	347.5	2.5
K	6.5	0.0432	0.0008	0.0002	0.037	0.003	0.112	0.011	29.192	0.113	0.8	28.969	0.132	7.8	353.8	1.5
L	15	0.1624	0.0006	0.0001	0.135	0.002	0.109	0.011	28.554	0.053	0.6	28.386	0.056	29.4	347.3	0.6
			Age (Ma)	**±**	**MSWD**	**^{39}Ar Gas %**	**Steps**									
		Plateau Age	347.7	2.8	23.0	81	7									
		Integrated Age	332.7	32.1	6849.2	100	12									
09RAYJR133A; Lab#10043; Ar#2812; Hornblende; J=0.00510080																
A	3	0.0006	0.5879	0.0134	10.864	1.458	1.299	0.027	291.344	3.202	59.6	117.622	4.506	0.3	847.9	25.9

ID	Power* (%)	Volume ^{39}Ar x10^{-11} cc	^{36}Ar/^{39}Ar	±	^{37}Ar/^{39}Ar	±	^{38}Ar/^{39}Ar	±	^{40}Ar/^{39}Ar	±	%^{40}Ar ATM	*^{40}Ar/^{39}Ar	±	f_{39}† (%)	Apparent Age Ma§	±
B	3.5	0.0006	0.2851	0.0139	14.628	1.583	0.823	0.019	136.297	2.765	61.8	52.061	4.795	0.3	424.9	34.9
C	4.2	0.0012	0.1051	0.0071	8.165	0.826	0.592	0.016	54.126	1.349	57.4	23.056	2.463	0.6	200.6	20.3
D	4.6	0.0014	0.0479	0.0076	8.320	0.807	0.913	0.020	45.143	1.419	31.4	30.989	2.644	0.7	264.8	21.0
E	5	0.0232	0.0064	0.0017	8.765	0.247	0.001	0.001	47.145	0.276	4.0	45.251	0.557	11.1	374.7	4.2
F	5.5	0.0473	0.0043	0.0014	7.960	0.217	0.001	0.001	45.182	0.167	2.8	43.913	0.444	22.7	364.6	3.3
G	6	0.0475	0.0031	0.0014	7.927	0.213	0.001	0.001	42.829	0.169	2.1	41.921	0.444	22.8	349.6	3.4
H	6.5	0.0394	0.0018	0.0013	7.085	0.188	0.001	0.001	42.117	0.188	1.3	41.590	0.419	18.9	347.1	3.2
I	7.5	0.0175	0.0027	0.0018	9.070	0.289	0.001	0.001	42.680	0.346	1.9	41.883	0.630	8.4	349.3	4.8
J	15	0.0299	0.0068	0.0015	8.305	0.233	0.001	0.001	35.262	0.195	5.7	33.243	0.484	14.3	282.6	3.8
			Age (Ma)	**±**	**MSWD**	**^{39}Ar Gas %**	**Steps**									
		Plateau Age	348.5	2.8	0.7	50	3									
		Integrated Age	344.2	26.8	324.0	100	10									
09RAYJR133A; Lab#10043, Ar#2811; Biotite; J=0.00512820																
A	2.6	0.0098	0.0347	0.0021	0.707	0.072	0.001	0.001	46.446	0.511	22.1	36.194	0.762	2.1	307.2	5.9
B	2.8	0.0076	0.0102	0.0011	1.025	0.066	0.106	0.011	44.835	0.271	6.7	41.833	0.413	1.6	350.6	3.2
C	3	0.0181	0.0043	0.0009	0.430	0.037	0.001	0.001	42.505	0.294	3.0	41.238	0.390	3.9	346.1	3.0
D	3.5	0.0140	0.0022	0.0007	0.495	0.032	0.126	0.011	38.265	0.153	1.7	37.600	0.265	3.0	318.1	2.1
E	4	0.0485	0.0018	0.0003	0.143	0.014	0.001	0.001	39.059	0.119	1.4	38.514	0.146	10.4	325.2	1.1
F	4.5	0.0642	0.0033	0.0001	0.122	0.010	0.001	0.001	39.547	0.145	2.5	38.559	0.148	13.8	325.5	1.1
G	5	0.0602	0.0009	0.0002	0.130	0.011	0.001	0.001	38.545	0.114	0.7	38.275	0.135	12.9	323.3	1.0
H	5.5	0.0643	0.0003	0.0002	0.108	0.011	0.001	0.001	38.448	0.141	0.3	38.351	0.157	13.8	323.9	1.2
I	6	0.0407	0.0005	0.0003	0.192	0.016	0.001	0.001	38.705	0.181	0.4	38.554	0.205	8.7	325.5	1.6
J	6.5	0.0369	0.0003	0.0004	0.212	0.019	0.001	0.001	38.823	0.171	0.2	38.748	0.201	7.9	327.0	1.6
K	7	0.0433	0.0002	0.0003	0.201	0.020	0.001	0.001	38.856	0.159	0.2	38.794	0.183	9.3	327.3	1.4
L	7.5	0.0277	0.0003	0.0004	0.282	0.026	0.001	0.001	38.693	0.207	0.3	38.594	0.245	6.0	325.8	1.9
M	15	0.0306	0.0040	0.0003	0.426	0.032	0.001	0.001	38.805	0.218	3.0	37.627	0.231	6.6	318.3	1.8
			Age (Ma)	**±**	**MSWD**	**^{39}Ar Gas %**	**Steps**									
		Plateau Age	325.1	2.0	4.7	83	8									
		Integrated Age	325.2	3.6	52.5	100	13									
09RAYMC115A; Lab#10062; Ar#2840; Hornblende; J=0.00497180																
A	2.6	0.0017	0.1674	0.0062	0.000	0.000	0.227	0.013	118.302	1.885	41.8	68.841	2.288	0.6	531.0	15.3
B	3	0.0014	0.0565	0.0080	1.213	1.176	0.098	0.012	50.787	1.612	32.9	34.084	2.821	0.5	282.4	21.6
C	3.5	0.0011	0.0299	0.0094	1.512	1.447	0.043	0.012	36.684	1.939	24.1	27.839	3.367	0.4	233.9	26.5
D	3.9	0.0010	0.0435	0.0110	1.641	1.601	0.035	0.012	33.578	2.098	38.3	20.730	3.836	0.4	177.0	31.2

ID	Power* (%)	Volume ^{39}Ar x10^{-11} cc	$^{36}Ar/^{39}Ar$	±	$^{37}Ar/^{39}Ar$	±	$^{38}Ar/^{39}Ar$	±	$^{40}Ar/^{39}Ar$	±	%^{40}Ar ATM	*$^{40}Ar/^{39}Ar$	±	f_{39}[†] (%)	Apparent Age Ma[§]	±
E	4.5	0.0024	0.0283	0.0046	0.711	0.728	0.068	0.011	32.274	0.935	25.9	23.909	1.628	0.9	202.6	13.1
F	5	0.0524	0.0176	0.0136	81.051	2.294	0.905	0.019	45.426	0.216	11.5	40.223	4.025	19.2	328.9	30.1
G	5.5	0.0393	0.0411	0.0174	103.864	2.957	0.912	0.019	52.367	0.295	23.2	40.236	5.158	14.4	329.0	38.6
H	6	0.0227	0.0295	0.0170	101.402	2.918	0.935	0.018	47.542	0.328	18.4	38.811	5.043	8.3	318.3	37.9
I	6.5	0.0205	0.0035	0.0012	6.305	0.231	0.639	0.015	41.933	0.168	2.4	40.910	0.393	7.5	334.0	2.9
J	7.5	0.0347	0.0341	0.0202	120.682	3.428	0.951	0.018	49.212	0.321	20.5	39.126	5.992	12.7	320.7	45.0
K	15	0.0959	0.0134	0.0206	122.789	3.452	0.943	0.019	47.257	0.291	8.4	43.300	6.093	35.1	351.8	45.0
			Age (Ma)	**±**	**MSWD**	**^{39}Ar Gas %**	**Steps**									
		Plateau Age	333.9	3.4	0.7	97	6									
		Integrated Age	329.5	30.3	123.1	100	11									
09RAYJR179A; Lab#10186, Ar#2871; Biotite; J=0.00724780																
A	2.6	0.0369	0.1704	0.0010	0.000	0.000	0.034	0.011	68.539	0.160	73.5	18.174	0.293	7.5	223.2	3.4
B	2.8	0.0124	0.0101	0.0007	0.000	0.000	0.001	0.001	18.439	0.151	16.2	15.460	0.261	2.5	191.6	3.1
C	3	0.0283	0.0044	0.0003	0.165	0.233	0.001	0.001	17.324	0.075	7.5	16.027	0.120	5.8	198.3	1.4
D	3.5	0.0531	0.0060	0.0001	0.088	0.073	0.035	0.011	17.572	0.052	10.0	15.810	0.063	10.8	195.7	0.7
E	3.9	0.0510	0.0035	0.0002	0.092	0.078	0.034	0.011	16.777	0.056	6.2	15.733	0.077	10.4	194.8	0.9
F	4.2	0.0586	0.0035	0.0001	0.080	0.068	0.033	0.011	16.905	0.051	6.0	15.884	0.058	11.9	196.6	0.7
G	4.6	0.0394	0.0031	0.0002	0.119	0.139	0.035	0.011	16.861	0.066	5.5	15.937	0.092	8.0	197.2	1.1
H	5	0.0391	0.0023	0.0002	0.000	0.000	0.034	0.011	16.576	0.068	4.1	15.893	0.096	8.0	196.7	1.1
I	5.5	0.0205	0.0022	0.0004	0.228	0.215	0.001	0.001	16.819	0.103	3.8	16.180	0.164	4.2	200.1	1.9
J	6	0.0317	0.0029	0.0002	0.000	0.000	0.001	0.001	16.733	0.069	5.1	15.881	0.095	6.5	196.6	1.1
K	6.5	0.0301	0.0030	0.0003	0.000	0.000	0.001	0.001	16.822	0.077	5.3	15.925	0.122	6.1	197.1	1.4
L	7.5	0.0421	0.0035	0.0002	0.000	0.000	0.001	0.001	16.939	0.057	6.1	15.898	0.089	8.6	196.7	1.0
M	8.5	0.0112	0.0020	0.0008	0.000	0.000	0.001	0.001	16.975	0.175	3.6	16.370	0.288	2.3	202.3	3.4
N	15	0.0372	0.0040	0.0002	0.126	0.122	0.001	0.001	17.326	0.062	6.7	16.156	0.082	7.6	199.8	1.0
			Age (Ma)	**±**	**MSWD**	**^{39}Ar Gas %**	**Steps**									
		Plateau Age	196.9	1.4	8.7	90	12									
		Integrated Age	197.0	2.2	39.1	100	14									
09RAYMC081A; Lab#10077; Ar#2881; Biotite; J=0.00721430																
A	2.6	0.0161	0.1148	0.0012	0.000	0.000	0.013	0.011	45.506	0.199	74.6	11.577	0.369	2.4	144.7	4.4
B	2.8	0.0067	0.0234	0.0012	0.827	0.620	0.001	0.001	19.673	0.235	35.2	12.751	0.417	1.0	158.8	5.0
C	3	0.0160	0.0221	0.0007	0.000	0.000	0.001	0.001	20.999	0.117	31.1	14.467	0.218	2.4	179.1	2.6
D	3.5	0.0432	0.0042	0.0001	0.000	0.000	0.003	0.011	16.153	0.059	7.7	14.906	0.069	6.4	184.3	0.8
E	3.9	0.0796	0.0020	0.0001	0.070	0.055	0.003	0.011	15.648	0.036	3.7	15.063	0.047	11.7	186.1	0.6

ID	Power* (%)	Volume ^{39}Ar x10^{-11} cc	^{36}Ar/^{39}Ar	±	^{37}Ar/^{39}Ar	±	^{38}Ar/^{39}Ar	±	^{40}Ar/^{39}Ar	±	%^{40}Ar ATM	*^{40}Ar/^{39}Ar	±	f_{39}† (%)	Apparent Age Ma§	±
F	4.2	0.0675	0.0007	0.0001	0.000	0.000	0.003	0.011	15.512	0.043	1.3	15.313	0.053	9.9	189.0	0.6
G	4.6	0.0801	0.0010	0.0001	0.070	0.052	0.003	0.011	15.596	0.037	1.8	15.308	0.046	11.8	189.0	0.5
H	5	0.0468	0.0005	0.0002	0.000	0.000	0.003	0.011	15.463	0.055	0.9	15.320	0.074	6.9	189.1	0.9
I	5.5	0.0355	0.0006	0.0002	0.158	0.196	0.001	0.001	15.602	0.058	1.1	15.423	0.086	5.2	190.3	1.0
J	6	0.0592	0.0006	0.0001	0.000	0.000	0.003	0.011	15.536	0.045	1.1	15.366	0.059	8.7	189.7	0.7
K	6.5	0.0309	0.0007	0.0002	0.181	0.149	0.003	0.011	15.423	0.078	1.3	15.220	0.105	4.6	188.0	1.2
L	7	0.0968	0.0006	0.0001	0.058	0.046	0.003	0.011	15.524	0.034	1.1	15.356	0.042	14.3	189.5	0.5
M	7.5	0.0294	0.0003	0.0003	0.190	0.166	0.002	0.011	15.404	0.079	0.6	15.306	0.109	4.3	189.0	1.3
N	8	0.0141	0.0001	0.0001	0.398	0.424	0.001	0.001	15.661	0.118	0.0	15.692	0.196	2.1	193.5	2.3
O	15	0.0575	0.0006	0.0001	0.000	0.000	0.002	0.011	15.530	0.050	1.1	15.355	0.063	8.5	189.5	0.7
			Age (Ma)	**±**	**MSWD**	**^{39}Ar Gas %**	**Steps**									
		Plateau Age	189.4	1.2	3.0	76	10									
		Integrated Age	188.3	2.1	71.1	100	15									
09RAYMC031A; Lab#10189; Ar#2875; Muscovite; J=0.00723180																
A	2.6	0.0041	0.0082	0.0020	0.102	0.058	0.001	0.001	17.527	0.561	13.9	15.095	0.806	1.8	186.9	9.5
B	2.8	0.0000	0.0001	0.0001	0.0001	0.0001	7.474	115.479	0.001	0.001	118.1	1789.544	29234.170	0.0	4753.6	16529.5
C	3	0.0000	0.4127	28.7987	0.0001	0.0001	0.001	0.001	0.001	0.001	0.0	0.001	0.001	0.0	0.0	13569.7
D	3.5	0.0004	0.0256	0.0179	0.956	0.542	0.001	0.001	15.858	5.388	47.6	8.304	7.393	0.2	105.2	91.0
E	3.9	0.0059	0.0019	0.0013	0.072	0.040	0.001	0.001	15.252	0.397	3.7	14.685	0.553	2.5	182.1	6.5
F	4.2	0.0179	0.0013	0.0005	0.000	0.000	0.000	0.001	15.429	0.137	2.4	15.053	0.203	7.7	186.4	2.4
G	4.6	0.0652	0.0002	0.0001	0.006	0.005	0.001	0.001	15.186	0.049	0.3	15.134	0.065	27.9	187.4	0.8
H	5	0.0279	0.0000	0.0000	0.000	0.000	0.000	0.011	15.295	0.091	0.0	15.295	0.131	11.9	189.3	1.5
I	5.5	0.0956	0.0002	0.0001	0.000	0.000	0.001	0.001	15.052	0.038	0.5	14.981	0.048	40.9	185.6	0.6
J	6	0.0042	0.0027	0.0022	0.000	0.000	0.001	0.001	15.926	0.555	5.1	15.121	0.860	1.8	187.2	10.1
K	15	0.0126	0.0000	0.0007	0.000	0.000	0.001	0.001	15.527	0.191	0.0	15.526	0.282	5.4	192.0	3.3
			Age (Ma)	**±**	**MSWD**	**^{39}Ar Gas %**	**Steps**									
		Plateau Age	186.5	1.4	5.1	100	11									
		Integrated Age	186.5	1.4	5.1	100	11									
09RAYJR076B; Lab#10028; Ar#2786; Muscovite; J=0.00521490																
A	2.6	0.0295	0.0015	0.0003	0.233	0.132	0.004	0.011	19.352	0.078	2.3	18.915	0.117	14.1	169.7	1.0
B	2.8	0.0098	0.0033	0.0008	0.707	0.403	0.001	0.011	21.573	0.217	4.5	20.596	0.331	4.7	184.1	2.8
C	3	0.0210	0.0004	0.0004	0.327	0.188	0.001	0.011	20.644	0.108	0.6	20.511	0.157	10.0	183.3	1.3
D	3.5	0.0082	0.0012	0.0010	0.842	0.488	0.000	0.000	20.741	0.252	1.6	20.399	0.397	3.9	182.4	3.4
E	3.9	0.0788	0.0005	0.0001	0.175	0.063	0.001	0.001	20.665	0.045	0.8	20.506	0.056	37.7	183.3	0.5

ID	Power* (%)	Volume ^{39}Ar x10^{-11} cc	^{36}Ar/^{39}Ar	±	^{37}Ar/^{39}Ar	±	^{38}Ar/^{39}Ar	±	^{40}Ar/^{39}Ar	±	%^{40}Ar ATM	*^{40}Ar/^{39}Ar	±	f_{39}† (%)	Apparent Age Ma§	±
F	4.2	0.0112	0.0010	0.0006	0.000	0.000	0.001	0.001	20.639	0.187	1.5	20.338	0.268	5.4	181.9	2.3
G	4.6	0.0136	0.0008	0.0005	0.000	0.000	0.001	0.001	20.784	0.158	1.2	20.536	0.222	6.5	183.5	1.9
H	5	0.0048	0.0024	0.0015	0.000	0.000	0.001	0.001	21.040	0.420	3.3	20.337	0.618	2.3	181.9	5.3
I	6	0.0059	0.0019	0.0012	0.000	0.000	0.001	0.001	20.812	0.343	2.7	20.242	0.501	2.8	181.1	4.3
J	15	0.0264	0.0025	0.0003	0.261	0.206	0.001	0.011	21.394	0.091	3.5	20.651	0.128	12.6	184.5	1.1
			Age (Ma)	**±**	**MSWD**	**^{39}Ar Gas %**	**Steps**									
		Plateau Age	183.4	1.1	1.1	86	9									
		Integrated Age	181.2	3.3	73.4	100	10									
<u>09RAYJR175A; Lab#9936; Ar#2849; Biotite; J=0.00747530</u>																
A	2.6	0.0254	0.1826	0.0014	0.188	0.129	0.014	0.011	65.900	0.210	81.9	11.932	0.399	5.8	154.1	4.9
B	2.8	0.0098	0.0383	0.0006	0.000	0.000	0.001	0.001	22.293	0.199	50.7	10.989	0.253	2.2	142.4	3.2
C	3	0.0151	0.0354	0.0004	0.317	0.253	0.001	0.001	23.114	0.138	45.3	12.648	0.169	3.4	163.0	2.1
D	3.5	0.0416	0.0192	0.0002	0.000	0.000	0.007	0.011	18.690	0.066	30.3	13.021	0.074	9.4	167.6	0.9
E	3.9	0.0185	0.0092	0.0005	0.258	0.322	0.001	0.001	16.050	0.102	16.9	13.341	0.177	4.2	171.5	2.2
F	4.2	0.0349	0.0072	0.0002	0.000	0.000	0.001	0.001	15.490	0.063	13.7	13.368	0.078	7.9	171.8	1.0
G	4.6	0.0341	0.0043	0.0003	0.141	0.118	0.001	0.001	14.800	0.063	8.6	13.524	0.103	7.7	173.7	1.3
H	5	0.0641	0.0048	0.0001	0.075	0.065	0.008	0.011	14.759	0.046	9.6	13.347	0.053	14.5	171.6	0.7
I	5.5	0.0528	0.0043	0.0001	0.000	0.000	0.008	0.011	14.474	0.052	8.8	13.200	0.063	12.0	169.8	0.8
J	6	0.0461	0.0039	0.0002	0.104	0.096	0.008	0.011	14.371	0.058	8.1	13.211	0.083	10.4	169.9	1.0
K	6.5	0.0133	0.0043	0.0006	0.000	0.000	0.001	0.001	14.501	0.131	8.7	13.238	0.219	3.0	170.2	2.7
L	15	0.0862	0.0043	0.0001	0.056	0.069	0.008	0.011	14.578	0.034	8.8	13.295	0.039	19.5	170.9	0.5
			Age (Ma)	**±**	**MSWD**	**^{39}Ar Gas %**	**Steps**									
		Plateau Age	170.6	1.5	16.6	92	10									
		Integrated Age	170.3	2.1	56.0	100	12									
<u>09RAYMC123A; Lab#10190; Ar#2877; Hornblende; J=0.00722300</u>																
A	3	0.0019	0.1446	0.0075	1.647	0.092	0.069	0.012	52.988	1.424	80.7	10.248	2.518	0.3	128.8	30.6
B	3.5	0.0013	0.0263	0.0092	0.802	0.118	0.045	0.012	21.095	1.907	36.8	13.335	3.308	0.2	165.9	39.3
C	3.9	0.0016	0.0137	0.0072	1.065	0.098	0.062	0.012	18.771	1.510	21.6	14.708	2.613	0.3	182.2	30.8
D	4.2	0.0012	0.0095	0.0102	1.293	0.137	0.065	0.012	17.159	2.111	16.3	14.361	3.679	0.2	178.1	43.4
E	4.6	0.0048	0.0015	0.0025	2.860	0.063	0.217	0.012	16.663	0.517	2.7	16.211	0.901	0.9	199.8	10.5
F	5	0.0156	0.0025	0.0010	3.750	0.056	0.278	0.011	16.536	0.167	4.6	15.783	0.339	2.8	194.8	4.0
G	5.5	0.0339	0.0012	0.0008	4.079	0.056	0.279	0.011	15.962	0.083	2.1	15.622	0.243	6.1	192.9	2.8
H	6	0.0918	0.0008	0.0007	4.317	0.058	0.305	0.011	16.159	0.054	1.5	15.913	0.224	16.5	196.3	2.6
I	6.5	0.0853	0.0008	0.0008	4.483	0.060	0.329	0.011	16.167	0.055	1.5	15.927	0.232	15.3	196.5	2.7

ID	Power* (%)	Volume ^{39}Ar x10^{-11} cc	$^{36}Ar/^{39}Ar$	±	$^{37}Ar/^{39}Ar$	±	$^{38}Ar/^{39}Ar$	±	$^{40}Ar/^{39}Ar$	±	$\%^{40}Ar$ ATM	$^{*40}Ar/^{39}Ar$	±	f_{39}† (%)	Apparent Age Ma§	±
J	7.5	0.1744	0.0007	0.0007	4.354	0.057	0.345	0.011	16.236	0.039	1.3	16.020	0.220	31.3	197.5	2.6
K	8.5	0.0751	0.0006	0.0008	4.471	0.060	0.332	0.012	16.079	0.058	1.2	15.888	0.233	13.5	196.0	2.7
L	10	0.0316	0.0011	0.0009	4.899	0.067	0.326	0.012	15.886	0.086	2.0	15.568	0.280	5.7	192.3	3.3
M	15	0.0390	0.0005	0.0010	5.420	0.074	0.310	0.012	16.083	0.095	0.8	15.948	0.297	7.0	196.7	3.5
			Age (Ma)	**±**	**MSWD**	**^{39}Ar Gas %**	**Steps**									
		Plateau Age	195.6	1.5	1.7	99	9									
		Integrated Age	195.5	2.1	3.0	100	13									
09RAYMC123A; Lab#10190; Ar#2876; Biotite; J=0.00722300																
A	2.6	0.2402	0.0107	0.0001	0.004	0.000	0.001	0.001	19.166	0.031	16.5	15.998	0.038	19.9	197.3	0.4
B	2.8	0.0921	0.0017	0.0001	0.001	0.001	0.001	0.001	17.049	0.115	3.0	16.537	0.119	7.6	203.6	1.4
C	3	0.1450	0.0014	0.0001	0.002	0.001	0.042	0.011	17.048	0.034	2.4	16.634	0.044	12.0	204.7	0.5
D	3.5	0.2487	0.0018	0.0001	0.003	0.001	0.042	0.011	17.109	0.029	3.1	16.584	0.034	20.6	204.1	0.4
E	3.9	0.0964	0.0022	0.0001	0.005	0.002	0.036	0.011	17.303	0.049	3.8	16.642	0.063	8.0	204.8	0.7
F	4.2	0.0784	0.0020	0.0002	0.006	0.002	0.036	0.011	17.323	0.063	3.5	16.725	0.078	6.5	205.7	0.9
G	4.6	0.0773	0.0016	0.0002	0.001	0.002	0.036	0.011	17.214	0.056	2.8	16.737	0.073	6.4	205.9	0.9
H	5	0.0545	0.0019	0.0002	0.000	0.000	0.036	0.011	17.091	0.073	3.2	16.538	0.097	4.5	203.6	1.1
I	5.5	0.0747	0.0011	0.0002	0.002	0.002	0.036	0.011	16.870	0.060	1.9	16.557	0.077	6.2	203.8	0.9
J	6	0.0303	0.0019	0.0004	0.004	0.004	0.035	0.011	16.925	0.088	3.3	16.373	0.142	2.5	201.7	1.7
K	15	0.0708	0.0014	0.0002	0.002	0.002	0.041	0.011	17.287	0.070	2.5	16.863	0.085	5.9	207.4	1.0
			Age (Ma)	**±**	**MSWD**	**^{39}Ar Gas %**	**Steps**									
		Plateau Age	204.6	1.3	8.3	80	10									
		Integrated Age	203.0	2.3	94.5	100	11									
09RAYJR078A; Lab#10029; Ar#2787; Biotite; J=0.00520920																
A	2.6	0.0635	0.0491	0.0004	0.100	0.076	0.001	0.001	22.319	0.056	65.0	7.804	0.114	10.5	71.9	1.0
B	2.8	0.0691	0.0287	0.0003	0.092	0.073	0.001	0.001	18.053	0.048	47.0	9.577	0.101	11.4	87.8	0.9
C	3	0.0647	0.0261	0.0003	0.000	0.000	0.001	0.001	17.721	0.051	43.5	10.017	0.098	10.7	91.8	0.9
D	3.5	0.0403	0.0232	0.0004	0.000	0.000	0.001	0.001	16.914	0.072	40.5	10.064	0.127	6.7	92.2	1.1
E	3.9	0.0761	0.0265	0.0003	0.000	0.000	0.001	0.001	17.776	0.045	44.0	9.947	0.098	12.6	91.1	0.9
F	4.2	0.1133	0.0295	0.0002	0.056	0.044	0.001	0.001	18.482	0.033	47.1	9.776	0.077	18.7	89.6	0.7
G	4.6	0.0357	0.0278	0.0004	0.000	0.000	0.001	0.001	17.943	0.081	45.7	9.742	0.151	5.9	89.3	1.4
H	5	0.0375	0.0283	0.0004	0.000	0.000	0.001	0.001	18.141	0.082	46.0	9.790	0.141	6.2	89.7	1.3
I	5.5	0.0359	0.0296	0.0004	0.000	0.000	0.001	0.001	18.493	0.083	47.2	9.756	0.147	5.9	89.4	1.3
J	6	0.0281	0.0280	0.0005	0.000	0.000	0.001	0.001	18.289	0.092	45.2	10.017	0.167	4.6	91.8	1.5
K	15	0.0421	0.0265	0.0004	0.151	0.117	0.001	0.001	17.275	0.074	45.3	9.453	0.140	6.9	86.7	1.3

ID	Power* (%)	Volume ^{39}Ar x10^{-11} cc	$^{36}Ar/^{39}Ar$	±	$^{37}Ar/^{39}Ar$	±	$^{38}Ar/^{39}Ar$	±	$^{40}Ar/^{39}Ar$	±	%^{40}Ar ATM	*$^{40}Ar/^{39}Ar$	±	f_{39}† (%)	Apparent Age Ma§	±
			Age (Ma)	**±**	**MSWD**	**^{39}Ar Gas %**	**Steps**									
		Plateau Age	90.0	1.2	10.8	90	10									
		Integrated Age	88.3	3.5	123.5	100	11									
09RAYJR078A; Lab#10029; Ar#2789; Muscovite; J=0.00520630																
A	2.6	0.0190	0.0054	0.0005	0.000	0.000	0.001	0.011	17.193	0.133	9.3	15.601	0.204	5.8	140.9	1.8
B	2.8	0.0907	0.0011	0.0001	0.070	0.054	0.001	0.001	16.671	0.040	2.0	16.341	0.052	27.5	147.3	0.5
C	3	0.0407	0.0008	0.0002	0.000	0.000	0.001	0.011	14.819	0.066	1.7	14.571	0.097	12.3	131.9	0.8
D	3.5	0.0355	0.0006	0.0003	0.180	0.141	0.001	0.001	16.409	0.084	1.1	16.232	0.115	10.8	146.4	1.0
E	3.9	0.0255	0.0000	0.0001	0.000	0.000	0.001	0.011	15.054	0.099	0.0	15.054	0.146	7.7	136.1	1.3
F	4.2	0.0537	0.0004	0.0002	0.119	0.093	0.001	0.001	15.234	0.058	0.8	15.117	0.074	16.3	136.7	0.7
G	4.6	0.0118	0.0019	0.0007	0.000	0.000	0.001	0.001	16.525	0.199	3.4	15.956	0.288	3.6	144.0	2.5
H	5	0.0208	0.0005	0.0004	0.000	0.000	0.000	0.000	16.810	0.118	1.0	16.649	0.164	6.3	150.0	1.4
I	5.5	0.0088	0.0026	0.0009	0.000	0.000	0.001	0.001	15.204	0.265	5.0	14.439	0.384	2.7	130.8	3.4
J	6	0.0023	0.0050	0.0036	0.000	0.000	0.001	0.001	15.044	0.993	9.7	13.577	1.462	0.7	123.2	12.8
K	15	0.0212	0.0075	0.0005	0.000	0.000	0.001	0.011	17.068	0.119	13.0	14.844	0.180	6.4	134.3	1.6
			Age (Ma)	**±**	**MSWD**	**^{39}Ar Gas %**	**Steps**									
		Integrated Age	142.0	4.1	188.6	100.0	11									
09RAYJR007A; Lab#10187; Ar#2872; Biotite; J=0.00724050																
A	2.6	0.0227	0.1156	0.0012	0.000	0.000	0.017	0.011	45.815	0.170	74.6	11.641	0.352	1.3	146.0	4.2
B	2.8	0.0171	0.0219	0.0004	0.285	0.224	0.001	0.001	16.689	0.106	38.8	10.212	0.144	1.0	128.7	1.8
C	3	0.0678	0.0126	0.0001	0.072	0.054	0.013	0.011	16.214	0.043	22.9	12.500	0.048	3.8	156.3	0.6
D	3.5	0.1028	0.0042	0.0001	0.047	0.039	0.013	0.011	14.807	0.030	8.4	13.569	0.036	5.7	169.1	0.4
E	3.9	0.1120	0.0048	0.0001	0.044	0.034	0.014	0.011	15.438	0.030	9.1	14.031	0.033	6.2	174.6	0.4
F	4.2	0.1971	0.0052	0.0001	0.000	0.000	0.014	0.011	15.766	0.020	9.7	14.231	0.030	11.0	176.9	0.4
G	4.6	0.1131	0.0034	0.0001	0.043	0.032	0.014	0.011	15.489	0.029	6.5	14.483	0.041	6.3	179.9	0.5
H	5	0.1426	0.0033	0.0001	0.034	0.025	0.014	0.011	15.447	0.027	6.4	14.461	0.030	8.0	179.7	0.4
I	5.5	0.0930	0.0015	0.0001	0.000	0.000	0.014	0.011	15.160	0.035	2.8	14.728	0.047	5.2	182.8	0.6
J	6	0.1634	0.0018	0.0000	0.030	0.022	0.015	0.011	15.199	0.026	3.5	14.668	0.029	9.1	182.1	0.3
K	6.5	0.1726	0.0015	0.0001	0.000	0.000	0.014	0.011	15.215	0.023	2.9	14.769	0.030	9.6	183.3	0.4
L	7	0.1510	0.0015	0.0001	0.000	0.000	0.014	0.011	15.401	0.025	2.9	14.958	0.032	8.4	185.5	0.4
M	7.5	0.1257	0.0017	0.0001	0.000	0.000	0.014	0.011	15.630	0.028	3.2	15.124	0.037	7.0	187.5	0.4
N	8	0.0844	0.0017	0.0001	0.000	0.000	0.014	0.011	15.854	0.038	3.3	15.338	0.050	4.7	190.0	0.6
O	8.5	0.0766	0.0015	0.0001	0.000	0.000	0.015	0.011	15.889	0.042	2.7	15.453	0.056	4.3	191.3	0.7
P	9	0.0708	0.0014	0.0001	0.069	0.062	0.014	0.011	15.574	0.046	2.7	15.154	0.062	4.0	187.8	0.7

ID	Power* (%)	Volume ^{39}Ar x10^{-11} cc	$^{36}Ar/^{39}Ar$	±	$^{37}Ar/^{39}Ar$	±	$^{38}Ar/^{39}Ar$	±	$^{40}Ar/^{39}Ar$	±	%^{40}Ar ATM	*$^{40}Ar/^{39}Ar$	±	f_{39}† (%)	Apparent Age Ma§	±
Q	9.5	0.0238	0.0014	0.0003	0.208	0.165	0.001	0.001	15.803	0.074	2.6	15.394	0.119	1.3	190.7	1.4
R	10	0.0116	0.0010	0.0006	0.000	0.000	0.001	0.001	15.984	1.186	1.8	15.693	1.197	0.7	194.2	14.0
S	15	0.0460	0.0012	0.0001	0.216	0.083	0.015	0.011	15.741	0.057	2.2	15.395	0.069	2.6	190.7	0.8
			Age (Ma)	**±**	**MSWD**	**^{39}Ar Gas %**	**Steps**									
		Integrated Age	180.1	4.0	1157.8	100.0	19									
09RAYRS030A; Lab#10035; Ar#2907; Biotite; J=0.00748580																
A	2.6	0.0659	0.1210	0.0007	0.072	0.054	0.025	0.011	44.783	0.090	79.8	9.038	0.185	23.7	118.1	2.3
B	2.8	0.0293	0.0439	0.0006	0.163	0.136	0.024	0.011	20.668	0.086	62.7	7.708	0.177	10.5	101.2	2.3
C	3	0.0311	0.0289	0.0002	0.153	0.113	0.024	0.011	18.323	0.082	46.6	9.788	0.093	11.2	127.6	1.2
D	3.5	0.0256	0.0262	0.0005	0.186	0.236	0.001	0.001	17.103	0.079	45.3	9.350	0.171	9.2	122.1	2.2
E	3.9	0.0247	0.0174	0.0003	0.386	0.163	0.001	0.001	17.128	0.083	30.1	11.979	0.106	8.9	154.9	1.3
F	4.2	0.0306	0.0138	0.0004	0.000	0.000	0.001	0.001	16.623	0.069	24.5	12.544	0.131	11.0	161.9	1.6
G	4.6	0.0200	0.0182	0.0004	0.000	0.000	0.001	0.001	16.142	0.100	33.4	10.757	0.137	7.2	139.7	1.7
H	5	0.0142	0.0161	0.0007	0.000	0.000	0.001	0.001	16.059	0.134	29.6	11.301	0.234	5.1	146.5	2.9
I	5.5	0.0112	0.0151	0.0008	0.425	0.561	0.001	0.001	16.279	0.165	27.4	11.819	0.294	4.0	153.0	3.7
J	6	0.0062	0.0127	0.0014	0.774	0.725	0.001	0.001	16.031	0.284	23.4	12.274	0.503	2.2	158.6	6.2
K	15	0.0195	0.0105	0.0003	0.245	0.285	0.001	0.001	17.538	0.103	17.6	14.444	0.135	7.0	185.2	1.6
			Age (Ma)	**±**	**MSWD**	**^{39}Ar Gas %**	**Steps**									
		Integrated Age	143.2	15.0	712.4	100.0	11									

*As measured by the laser in % of full nominal power (W).

†Fraction 39Ar as percent of total run.

§Errors are analytical only and do not reflect error in irradiation parameter J.

Isotopic ratios are corrected for analytical blank, radioactive decay, and mass discrimination.

All errors reported in this table are quoted at 2σ.

Steps shown in bold used in the calculation of the plateau age.

Inetgrated age calculated by summing isotopic measurements of all steps.

TABLE A4. FURNACE STEP HEATING ^{40}Ar/^{39}Ar DATA FOR SAMPLES FROM THE MCQUESTEN MAP AREA ANALYSED AT THE NEW MEXICO INSTITUTE OF MINING AND TECHNOLOGY

ID	Temp (°C)	^{40}Ar/^{39}Ar	^{37}Ar/^{39}Ar	^{36}Ar/^{39}Ar (x 10^{-3})	$^{39}Ar_K$ (x 10^{-15} mol)	K/Ca	^{40}Ar* (%)	^{39}Ar (%)	Age (Ma)	±2σ (Ma)
09RAYJR176A, Biotite, 2.56 mg, J=0.0024869±0.06%, D=1.00485±0.00096, NM-246AA, Lab#=60895-01										
A	750	16.11	-1.9776	16.13	-0.002	-	69.3	0.0	49.3	842.4
B	650	48.32	0.0170	28.81	20.0	29.9	82.4	14.9	170.28	0.79
C	750	48.36	0.0089	11.44	30.8	57.5	93.0	37.9	191.25	0.59
D	800	47.75	0.0076	7.656	15.66	67.2	95.3	49.6	193.30	0.67
E	850	47.96	0.0115	8.140	10.10	44.4	95.0	57.1	193.56	0.78
F	900	47.89	0.0333	10.23	7.94	15.3	93.7	63.0	190.80	0.76
G	950	47.50	0.0208	9.220	18.7	24.5	94.3	76.9	190.42	0.76
H	1000	47.20	0.0168	8.697	14.76	30.4	94.6	87.9	189.83	0.74
I	1050	46.91	0.0892	8.934	6.25	5.7	94.4	92.6	188.43	0.76
J	1100	47.11	0.5966	8.798	2.23	0.86	94.6	94.2	189.62	1.36
K	1150	49.90	1.699	15.33	1.402	0.30	91.2	95.3	193.6	2.1
L	1250	49.17	0.7357	12.77	5.27	0.69	92.5	99.2	193.28	1.00
M	1700	209.3	0.2773	544.4	1.076	1.8	23.2	100.0	205.4	7.7
Integrated age ± 2s			n=13		134.2	6.7		K2O=8.09%	188.32	0.57
Plateau ± 2s		steps C-M	n=11	MSWD=18.92	114.181	38.1 ± 24.4		85.1	191.29	1.123
09RAYJRO94A, Biotite, 1.08 mg, J=0.0024825±0.06%, D=1.0015±0.0012, NM-246AA, Lab#=60890-01										
B	650	45.70	0.0052	7.963	10.52	98.1	94.9	17.6	184.34	1.62
C	750	45.43	-0.0007	2.107	1.381	-	98.6	20.0	190.23	1.52
D	800	45.47	0.0027	1.882	6.23	187.2	98.8	30.4	190.68	0.79
E	850	45.93	0.0033	3.041	4.91	153.2	98.0	38.6	191.13	0.87
F	900	45.85	0.0021	3.188	3.39	237.9	97.9	44.3	190.66	1.05
G	950	45.65	0.0037	2.761	3.27	137.0	98.2	49.8	190.36	0.98
H	1000	45.76	0.0049	1.932	5.29	104.7	98.8	58.7	191.78	0.82
I	1050	45.58	0.0042	1.136	9.21	120.1	99.3	74.1	191.99	0.68
J	1100	45.46	0.0046	0.8781	7.99	111.9	99.4	87.5	191.83	0.66
K	1150	46.08	0.0296	3.721	3.79	17.3	97.6	93.9	190.96	0.96
L	1250	46.21	0.1042	3.852	2.81	4.9	97.6	98.6	191.36	1.25
M	1700	261.2	0.0712	712.8	0.849	7.2	19.4	100.0	213.3	8.8
Integrated age ± 2s			n=12		59.7	45.2		K2O=8.55%	190.40	0.71
Plateau ± 2s		steps C-L	n=10	MSWD=2.04	48.3	123.9 ± 70.3		80.9	191.29	0.45
09RAYJR160A, Muscovite, .75 mg, J=0.0024801±0.06%, D=1.00485±0.00096, NM-246AA, Lab#=60891-01										
E	600	109.3	0.0334	243.8	0.310	15.3	34.1	0.7	159.2	9.5
F	700	51.62	0.0109	25.71	0.806	46.9	85.3	2.4	186.9	18.8
G	740	54.23	0.0016	25.40	0.846	322.0	86.2	4.1	197.8	2.5
H	780	50.21	0.0024	10.84	1.303	209.0	93.6	6.9	198.88	1.74
I	830	47.38	0.0011	6.014	4.05	472.6	96.2	15.5	193.28	1.04
J	880	46.16	0.0009	1.400	10.27	577.7	99.1	37.2	193.85	0.64
K	910	46.06	0.0011	0.9789	6.66	472.5	99.4	51.3	193.96	0.80
L	940	45.98	0.0034	1.947	4.59	148.6	98.7	61.0	192.49	0.99
M	980	46.08	0.0051	2.417	3.86	99.1	98.5	69.1	192.31	0.90
N	1040	46.15	0.0020	2.299	4.99	253.2	98.5	79.7	192.73	0.79
O	1070	45.74	0.0006	1.268	3.93	850.2	99.2	88.0	192.31	1.08
P	1100	46.27	0.0036	2.383	2.28	140.4	98.5	92.8	193.11	1.15
Q	1140	47.67	0.0127	5.247	0.933	40.3	96.7	94.8	195.4	2.3
R	1200	51.05	0.0429	11.65	0.663	11.9	93.3	96.2	201.3	2.9
S	1650	138.2	0.1299	306.1	1.81	3.9	34.5	100.0	201.7	4.7
Integrated age ± 2s			n=15		47.3	64.2		K2O=9.77%	193.58	0.70
Plateau ± 2s		steps I-Q	n=9	MSWD=2.68	41.6	409.5 ± 270.2		87.9	193.19	0.55
09RAYMCO17A, Biotite, 1.81 mg, J=0.0024837±0.06%, D=1.00485±0.00096, NM-246AA, Lab#=60894-01										
A	650	40.98	0.0146	65.47	8.37	35.0	52.8	8.8	94.39	1.09
B	750	47.29	0.0057	12.67	17.26	89.5	92.1	26.9	185.23	0.72
C	800	46.77	0.0046	5.209	11.88	111.8	96.7	39.3	192.04	0.61
D	850	47.30	0.0062	6.490	8.54	82.9	95.9	48.3	192.65	0.74
E	900	46.88	0.0088	8.705	6.63	57.9	94.5	55.2	188.32	0.81
F	950	46.61	0.0088	9.495	10.66	58.1	94.0	66.4	186.28	0.69
G	1000	46.59	0.0091	7.353	12.22	56.0	95.3	79.2	188.74	0.69
H	1050	46.17	0.0183	5.962	7.98	27.9	96.2	87.6	188.73	0.71
I	1100	46.37	0.0674	5.009	4.29	7.6	96.8	92.1	190.71	1.01
J	1150	47.21	0.4586	7.333	2.15	1.1	95.5	94.3	191.48	1.44
K	1250	47.38	1.026	7.327	4.81	0.50	95.6	99.4	192.44	0.90
L	1700	336.2	0.4433	981.8	0.610	1.2	13.7	100.0	195.5	14.7
Integrated age ± 2s			n=12		95.4	6.7		K2O=8.15%	180.86	0.58
Plateau ± 2s		steps C-L	n=10	MSWD=32.25	69.761	57.1 ± 39.0		73.1	189.95	1.485

ID	Temp (°C)	$^{40}Ar/^{39}Ar$	$^{37}Ar/^{39}Ar$	$^{36}Ar/^{39}Ar$ (x 10^{-3})	$^{39}Ar_K$ (x 10^{-15} mol)	K/Ca	$^{40}Ar^*$ (%)	^{39}Ar (%)	Age (Ma)	±2σ (Ma)
09RAYRS005A, Biotite, 1.08 mg, J=0.0024885±0.07%, D=1.00485±0.00096, NM-246AA, Lab#=60898-01										
A	650	50.40	0.0243	85.06	1.96	21.0	50.1	2.9	110.0	2.0
B	750	45.43	0.0044	9.719	9.88	116.4	93.7	17.4	181.58	0.72
C	800	45.27	0.0030	4.034	7.56	167.8	97.4	28.5	187.72	0.70
D	850	45.74	0.0047	4.144	4.82	107.6	97.3	35.6	189.49	0.91
E	900	45.28	0.0033	3.455	4.16	155.7	97.7	41.7	188.45	0.94
F	950	45.53	0.0090	4.170	3.91	57.0	97.3	47.5	188.64	0.95
G	1000	45.21	0.0090	3.343	8.68	56.7	97.8	60.2	188.32	0.69
H	1050	45.00	0.0205	2.254	8.93	24.9	98.5	73.4	188.79	0.97
I	1100	45.41	0.0130	4.277	4.43	39.1	97.2	79.9	187.99	0.95
J	1150	45.00	0.0113	1.482	7.54	45.2	99.0	91.0	189.70	0.69
K	1250	45.43	0.0843	2.001	5.49	6.1	98.7	99.0	190.82	0.82
L	1700	357.1	0.0780	1050.5	0.654	6.5	13.1	100.0	198.5	15.7
Integrated age ± 2s			n=12		68.0	31.5		K2O=9.72%	185.66	0.60
Plateau ± 2s		steps C-L	n=10	MSWD=5.52	56.2	69.9 ± 58.0		82.6	188.88	0.69
09RAYRS141A, Biotite, 1.5 mg, J=0.0024794±0.06%, D=1.00485±0.00096, NM-246AA, Lab#=60892-01										
A	650	51.89	0.0273	102.6	5.15	18.7	41.6	7.1	94.03	1.72
B	750	45.90	0.0085	16.99	9.77	59.8	89.1	20.5	174.15	0.75
C	800	46.26	0.0089	10.88	6.19	57.1	93.0	28.9	182.90	0.89
D	850	46.32	0.0089	10.32	5.27	57.4	93.4	36.2	183.83	0.91
E	900	46.00	0.0102	8.816	4.76	50.1	94.3	42.7	184.33	0.97
F	950	46.54	0.0141	12.41	5.46	36.1	92.1	50.2	182.22	0.82
G	1000	45.78	0.0103	8.877	9.89	49.7	94.3	63.7	183.35	0.70
H	1050	45.16	0.0133	5.617	8.53	38.3	96.3	75.4	184.73	0.68
I	1100	45.13	0.0084	4.884	7.38	60.9	96.8	85.6	185.52	0.69
J	1150	45.16	0.0237	4.013	5.80	21.5	97.4	93.5	186.65	0.86
K	1250	45.55	0.0857	5.556	3.74	6.0	96.4	98.6	186.42	0.90
L	1700	250.1	0.0124	695.0	0.986	41.1	17.9	100.0	189.5	9.6
Integrated age ± 2s			n=12		72.9	31.0		K2O=7.53%	176.82	0.63
Plateau ± 2s		steps D-L	n=9	MSWD=12.11	51.826	42.3 ± 17.5		71.1	184.59	1.001
09RAYKR142A, Biotite, 1.67 mg, J=0.0024857±0.06%, D=1.00485±0.00096, NM-246AA, Lab#=60899-01										
M	650	46.55	0.0147	48.96	4.27	34.6	68.9	4.5	138.39	1.37
N	750	43.21	0.0032	2.937	20.3	158.4	98.0	26.2	180.50	0.55
O	800	43.41	0.0025	1.884	14.44	200.2	98.7	41.6	182.56	0.59
P	850	43.77	0.0051	2.906	7.70	100.3	98.0	49.8	182.80	0.68
Q	900	43.64	0.0111	3.765	3.95	45.8	97.5	54.0	181.27	0.87
R	950	43.65	0.0166	4.222	3.71	30.7	97.1	58.0	180.76	1.02
S	1000	42.97	0.0070	2.944	6.62	72.9	98.0	65.0	179.54	0.72
T	1050	43.21	0.0052	2.062	9.13	98.3	98.6	74.8	181.54	0.59
U	1100	43.24	0.0070	1.976	7.60	73.2	98.7	82.9	181.77	0.70
V	1150	43.38	0.0128	2.369	7.04	39.7	98.4	90.4	181.87	0.75
W	1250	43.68	0.0376	2.540	7.98	13.6	98.3	98.9	182.89	0.69
X	1700	213.8	0.0099	569.7	1.063	51.4	21.2	100.0	192.9	8.7
Integrated age ± 2s			n=12		93.8	55.8		K2O=8.68%	179.74	0.52
Plateau ± 2s		steps N-X	n=11	MSWD=9.65	89.556	106.7 ± 56.5		95.5	181.60	0.707
09RAYJR143A, Biotite, 2.57 mg, J=0.00249±0.07%, D=1.00485±0.00096, NM-246AA, Lab#=60897-01										
A	650	39.01	0.0147	66.82	7.12	34.7	49.4	5.6	84.47	1.13
B	750	42.01	0.0051	9.872	25.4	99.4	93.1	25.5	167.56	0.57
C	800	43.13	0.0031	3.910	18.1	165.3	97.3	39.7	179.31	0.62
D	850	43.14	0.0049	4.425	11.98	104.5	97.0	49.1	178.72	0.56
E	900	42.39	0.0103	5.854	7.76	49.5	95.9	55.1	173.95	0.69
F	950	42.29	0.0167	7.460	9.98	30.6	94.8	63.0	171.59	0.68
G	1000	42.42	0.0068	5.382	15.00	75.3	96.3	74.7	174.65	0.68
H	1050	42.52	0.0092	3.737	11.99	55.2	97.4	84.1	177.03	0.57
I	1100	43.00	0.0198	3.462	8.26	25.8	97.6	90.6	179.32	0.72
J	1150	43.13	0.0453	2.931	5.28	11.3	98.0	94.7	180.49	0.86
K	1250	43.51	0.2092	4.201	5.94	2.4	97.2	99.4	180.59	0.81
L	1700	389.6	0.0476	1167.5	0.782	10.7	11.5	100.0	190.1	14.2
Integrated age ± 2s			n=12		127.6	26.1		K2O=7.66%	170.23	0.54
Plateau ± 2s		steps C-L	n=10	MSWD=73.70	95.070	73.8 ± 50.7		74.5	177.14	1.927
09RAYJR177A, Muscovite, 1.35 mg, J=0.0024809±0.06%, D=1.00485±0.00096, NM-246AA, Lab#=60893-01										
A	600	90.13	0.0592	201.6	0.569	8.6	33.9	0.6	131.8	5.4
B	700	46.18	0.0426	28.71	1.609	12.0	81.6	2.4	161.27	1.93
C	740	43.22	0.0182	13.82	2.40	28.0	90.6	5.1	167.13	1.19
D	780	41.59	0.0135	6.465	4.23	37.9	95.4	9.8	169.36	0.97
E	830	41.54	0.0076	4.663	11.49	67.0	96.7	22.6	171.31	0.61

ID	Temp (°C)	$^{40}Ar/^{39}Ar$	$^{37}Ar/^{39}Ar$	$^{36}Ar/^{39}Ar$ ($x\ 10^{-3}$)	$^{39}Ar_K$ ($x\ 10^{-15}$ mol)	K/Ca	$^{40}Ar^*$ (%)	^{39}Ar (%)	Age (Ma)	±2σ (Ma)
F	880	40.80	0.0056	0.9683	20.8	91.5	99.3	45.7	172.73	0.61
G	910	40.56	0.0062	0.8433	12.47	82.2	99.4	59.5	171.93	0.57
H	940	40.13	0.0070	1.284	8.31	73.0	99.1	68.7	169.62	0.65
I	980	39.90	0.0140	2.188	6.04	36.4	98.4	75.4	167.63	0.71
J	1040	39.69	0.0074	2.964	7.14	68.6	97.8	83.4	165.81	0.69
K	1070	38.93	0.0034	1.764	5.65	151.3	98.7	89.7	164.18	0.74
L	1100	39.26	0.0058	4.409	2.29	87.6	96.7	92.2	162.30	1.05
M	1140	39.61	0.0125	2.961	1.263	40.8	97.8	93.6	165.52	1.75
N	1200	39.37	0.0158	4.078	1.160	32.3	96.9	94.9	163.16	1.83
O	1650	64.93	0.0072	79.60	4.60	70.6	63.8	100.0	176.39	1.83
Integrated age ± 2s			n=15		90.0	58.9		K2O=10.32%	169.65	0.48
Plateau ± 2s		steps C-N	n=12	MSWD=74.03	83.231	76.7 ± 35.2		92.5	168.92	1.933
09RAYRSO12A, Biotite, 2.2 mg, J=0.0024893±0.06%, D=1.00485±0.00096, NM-246AA, Lab#=60896-01										
A	650	44.12	0.0104	88.76	9.52	49.0	40.5	7.2	78.59	1.39
B	750	45.13	0.0056	39.07	22.3	90.7	74.4	24.1	144.82	0.82
C	800	46.01	0.0066	23.45	13.78	77.4	84.9	34.6	167.43	0.75
D	850	46.37	0.0100	20.12	10.01	51.1	87.2	42.2	172.95	0.84
E	900	46.18	0.0134	25.65	8.92	38.1	83.6	48.9	165.47	0.80
F	950	45.68	0.0324	25.35	11.74	15.8	83.6	57.8	163.81	0.79
G	1000	45.63	0.0236	26.56	19.8	21.6	82.8	72.8	162.14	0.78
H	1050	45.46	0.0980	27.13	13.58	5.2	82.4	83.1	160.75	0.77
I	1100	45.64	0.0281	23.24	10.05	18.2	85.0	90.8	166.20	0.79
J	1150	46.49	0.0366	17.04	6.44	13.9	89.2	95.6	177.14	0.85
K	1250	46.94	0.4654	12.54	3.51	1.1	92.2	98.3	184.58	1.06
L	1700	150.3	0.1187	362.4	2.23	4.3	28.7	100.0	184.3	5.1
Integrated age ± 2s			n=12		131.8	13.1		K2O=9.25%	156.95	0.69
Plateau ± 2s		steps C-I	n=7	MSWD=98.49	87.836	31.7 ± 25.0		66.6	165.42	2.957

Isotopic ratios corrected for blank, radioactive decay, and mass discrimination, not corrected for interfering reactions.
Errors quoted for individual analyses include analytical error only, without interfering reaction or J uncertainties.
Integrated age calculated by summing isotopic measurements of all steps.
Integrated age error calculated by quadratically combining errors of isotopic measurements of all steps.
Plateau age is inverse-variance-weighted mean of selected steps.
Plateau age error is inverse-variance-weighted mean error (Taylor, 1982) times root MSWD where MSWD>1.
Plateau error is weighted error of Taylor (1982).
Decay constants and isotopic abundances after Steiger and Jäger (1977).
X preceding sample ID denotes analyses excluded from plateau age calculations.
Weight percent K_2O calculated from ^{39}Ar signal, sample weight, and instrument sensitivity.
Ages calculated relative to FC-2 Fish Canyon Tuff sanidine interlaboratory standard at 28.02 Ma
Decay Constant (LambdaK (total)) = 5.543e-10/a
Correction factors:
$(^{39}Ar/^{37}Ar)_{Ca}$ = 0.0007 ± 5e-05
$(^{36}Ar/^{37}Ar)_{Ca}$ = 0.00028 ± 2e-05
$(^{38}Ar/^{39}Ar)_K$ = 0.013
$(^{40}Ar/^{39}Ar)_K$ = 0.01 ± 0.002

APPENDIX 4

(U-Th)/He Methodology

METHODS

To provide constraint on the low-temperature thermochronological evolution of the McQuesten map area, eleven samples of zircon separates were analysed for (U-Th)/He thermochronology. Heavy mineral separates for these samples had been previously obtained for U-Pb SIMS dating using standard GSC techniques outlined in Appendix 1. Zircon picking and helium analysis were conducted at Dalhousie University in Halifax, Nova Scotia. Five zircon crystals from each rock sample were hand picked under a high power (160x) stereoscopic microscope based on morphology, clarity, homogeneity, and lack of inclusions and cracks. Cross-polarized light was useful for screening out inclusions, however the majority of zircon crystals contained some degree of inclusions which was later confirmed by SEM imaging. To avoid excessive uncertainty in the alpha correction (Reiners, 2005) larger grains were preferentially selected, with a minimum crystallographic axis length of 60 μm in any direction. Crystals with a symmetrical and idealized tetrahedral prism morphology with symmetric pyramidal terminations were carefully selected so the surface area to volume ratio could be computed as accurately as possible. Grains were photographed and measured using Pax-It! software. Individual zircons were loaded into a 1-mm platinum foil tube with crimped edges and sealed. Several grains of Durango apatite were also loaded into three separate Pt tubes. Individual Pt packets were loaded into a stainless steel planchet holder for He isotopic analysis. ^{4}He extraction was conducted in a vacuum line by heating the Pt packet to 1300 ± 25 ^{o}C for 30 minutes with a Quantronix model 117 Nd:YAG laser operated in continuous mode at 1064 nm. The gas was purified over getters and measured with a Pfeiffer Prisma 200 quadrupole mass spectrometer by isotope dilution using 99.999% ^{3}He as a spike. The heating cycle was repeated until the re-extract quantity of ^{4}He was less than 1% of the total gas; this usually occurs after one or two repetitions, however some grains required three additional steps to degas. Four grains (09RAYJR179A-2, 09RAYJR094A-4, 09RAYJR178-2, and 09RAYJR177A-1) yielded re-extracts that were still a few percent of the total gas after the third repetition. Data from one grain (08RAY004-3) was lost during helium extraction due to a power failure. Hot blanks were run with empty Pt packets with each batch, and cold blanks were run before each grain. Absolute ^{4}He blank values ranged between 0.65 to 1.62 fmol, or 0.01 to 0.38% of the total ^{4}He extracted from the sample. Analytical uncertainty of He gas extracted is 1.47 to 1.78% at the 1σ confidence level.

The most common method for measurement of U and Th concentration for the purpose of (U-Th)/He dating is by dissolution of the grains in their Pt packets, followed by quantitative analysis using isotope dilution inductively coupled plasma mass-spectrometry (ICP-MS). For the purpose of this study, U and Th analyses were conducted using the laser ablation ICP-MS laboratory at the GSC. This method circumvents problems commonly associated with isotope dilution ICP-MS, such as zircon pressure digestion, host packet interferences, and the need for accurately measured isotope spikes of known atomic abundances. Individual zircon grains were removed from their packets, mounted on an epoxy mount and polished to expose the inner grain in the same way as for U-Pb SIMS analysis. Four grains that had undergone He extraction were lost during this process (08RAY003-1; 09RAYJR122A-1; 09RAYJR177A-2; and 09RAYJR179A-4). The three aliquots of Durango apatite grains and the GSC zircon standard BR6266 were also added to the mount. The mount was mapped and imaged for back-scatter electron and cathodoluminescence using a Zeiss EVO scanning electron microscope at the GSC in Ottawa. Concentrations of U and Th were measured on an Agilent 7700x ICP-MS connected to a Photon Machines Analyte 193 excimer laser. Laser transects were taken with a spot size of 21 μm at a rate between 1 and 3 μm, depending on the length of the grain, both parallel and perpendicular to the long-axis of the zircon. NIST glass was used as a calibration standard. For the purpose of measuring concentrations of standards, a spot size of either 28, 34 or 52 μm was used. Bulk U and Th concentrations and the alpha correction were calculated with the HeFTy computer program (Ketcham, 2005). Estimated 2σ uncertainty for zircon He ages is 8% (Reiners et al., 2004), based on accuracy and reproducibility of U and Th concentrations measured on Durango apatite and BR6266 zircon combined with the error of He analyses.

REFERENCES

Ketcham, R. A., 2005, Forward and inverse modeling of low-temperature thermochronometry data, *in* Reiners, P. W., and Ehlers, T. A., eds., Low Temperature Thermochronology: Techniques, Interpretations, and Applications: Reviews in Mineralogy and Geochemistry, v. 58, p. 275-314.

Reiners, P. W., 2005, Zircon (U-Th)/He Thermochronometry, *in* Reiners, P.W., and Ehlers, T.A., eds., Low Temperature Thermochronology: Techniques, Interpretations, and Applications: Reviews in Mineralogy and Geochemistry, v. 58, p. 151-179.

Reiners, P. W., Spell, T. L., Nicolescu, S., and Zanetti, K. A., 2004, Zircon (U-Th)/He thermochronometry: He diffusion and comparisons with $^{40}Ar/^{39}Ar$ dating: Geochimica et Cosmochimica Acta, v. 68, p. 1857-1887.